

# UC Berkeley

## UC Berkeley Electronic Theses and Dissertations

### Title

Influencing cell fate decisions using physical and chemical cues

### Permalink

<https://escholarship.org/uc/item/0bq39484>

### Author

Sia, Junren

### Publication Date

2016

Peer reviewed|Thesis/dissertation

Influencing cell fate decisions using physical and chemical cues

by

Junren Sia

A dissertation submitted in partial satisfaction of the requirements for the degree of

Joint Doctor of Philosophy  
with the University of California, San Francisco

in

Bioengineering

in the

Graduate Division

of the

University of California, Berkeley

Committee in charge:

Professor Song Li, Chair  
Professor Valerie Weaver  
Professor Jeremy Thorner

Summer 2016



## **Abstract**

### Influencing cell fate decisions using physical and chemical cues

By

Junren Sia

Joint Doctor of Philosophy with University of California, San Francisco in Bioengineering

University of California, Berkeley

Professor Song Li, Chair

Directed genetic reprogramming of cells from one identity to another offers tremendous potential in regenerative medicine, disease modelling and drug testing. However, its application is limited by the low efficiency at which it occurs, and existing methods to improve efficiency mostly utilize additional molecular biology and biochemical manipulations. This thesis explored an alternative paradigm for improving reprogramming efficiency: presentation of physical cues. To this end, I first showed that simply agitating an adherent culture with an orbital shaker enhanced its efficiency of reprogramming to induced pluripotent stem cells (iPSCs). I further demonstrated that convective mixing of the culture medium by orbital agitation blunted the upregulation of CDK inhibitor p57/Kip2 that was caused by the culture becoming overconfluent, which in turn enhanced the efficiency of reprogramming to iPSCs. Next, I showed that culturing reprogramming cells on solid supports scored with microgrooves enhanced their reprogramming into cardiomyocytes. I demonstrated that the microgrooves caused upregulation of the activity of the transcription factor megakaryoblastic leukemia-1 (Mkl1) / myocardin-related transcription factor A (Mrtf-a) and also enhanced organization of sarcomeric structure, with both effects contributing to better reprogramming efficiency. In addition to physical cues, I also explored whether treatment with only small molecules could reprogram fibroblasts into skeletal muscle cells. Indeed, I found that an optimized basal medium (10% FBS in DMEM with 50  $\mu\text{g}/\text{ml}$  of ascorbic acid and 50  $\text{ng}/\text{ml}$  of basic fibroblast growth factor (bFGF)) containing just 2 small molecules— 616452 [an inhibitor of the protein kinase activity of the transforming growth factor-beta (TGF- $\beta$ ) type I receptor (R1)] and forskolin (a plant diterpene that stimulates adenylyl cyclase and elevates the intracellular level of 3',5'-cyclic-AMP)—was sufficient to achieve reprogramming at high efficiency. In summary, this thesis described how both physical and chemical cues can contribute to enhancing the reprogramming of cell identity.

# Contents

Biography .....	iii
Education .....	iii
Fellowship .....	iii
Publications .....	iii
Presentations .....	iii
List of Tables .....	iv
List of Figures .....	v
Chapter 1: Introduction .....	1
Chapter 2: Dynamic Culture Improves Cell Reprogramming Efficiency .....	4
2.1 Introduction .....	4
2.2 Materials and Methods.....	5
2.2.1 Fibroblast isolation, cell culture and reprogramming .....	5
2.2.2 Immunofluorescence staining and microscopy .....	6
2.2.3 Quantification of reprogramming efficiency .....	6
2.2.4 Reverse transcription-quantitative polymerase chain Reaction (RT-qPCR) .....	6
2.2.5 Western blotting analysis .....	7
2.2.6 Measurement of viscosity, shear stress and mixing rate .....	8
2.2.7 siRNA transfection .....	8
2.3 Results .....	9
2.3.1 Dynamic culture improved reprogramming efficiency.....	9
2.3.2 Time course study revealed the optimal period for dynamic culture .....	13
2.3.3 Dynamic culture ameliorated negative effect of over-confluence on reprogramming .....	13
2.3.4 Mixing rather than shear stress conferred the beneficial effect of dynamic culture .	15
2.3.5 Effect of dynamic culture on mechanosensitive proteins YAP and $\beta$ -catenin .....	16
2.3.6 Effect of dynamic culture on reprogramming efficiency was mediated by p57 expression level.....	18
2.3.7 Dynamic culture synergize with small molecules to improve reprogramming efficiency .....	20
2.4 Discussion.....	21
Chapter 3: Effect of Biophysical Cues on Reprogramming to Cardiomyocytes.....	23
3.1 Introduction .....	23
3.2 Materials and Methods.....	24
3.2.1 Cell culture and reprogramming.....	24
3.2.2 Fabrication of stretching device .....	24
3.2.3 Polyacrylamide gels fabrication .....	24
3.2.4 Microgroove membrane fabrication .....	25
3.2.5 Immunostaining, imaging, flow cytometry and quantification .....	25
3.2.6 Real time quantitative polymerase chain reaction.....	26
3.3 Results .....	27
3.3.1 Microgroove improved yield of cardiomyocyte like cells.....	27
3.3.2 Microgroove improved the yield of functional cardiomyocytes .....	31

3.3.3 Cytoskeletal drugs treatment suggested effect of microgroove was mediated by Mkl1 .....	34
3.3.4 Overexpressing Mkl1 and treatment with valproic acid recapitulated the effect of microgroove in the early stage .....	37
3.4 Discussion.....	39
Chapter 4: Direct Reprogramming from Dermal Fibroblasts to Skeletal Muscle Cells .....	42
4.1 Introduction .....	42
4.2 Materials and Methods.....	43
4.2.1 Cell culture and screening for candidates .....	43
4.2.2 Immunostaining, imaging and quantification.....	44
4.2.3 Flow activated cell sorting .....	44
4.2.4 Real time quantitative polymerase chain reaction.....	44
4.2.5 Microarray analysis .....	45
4.2.6 Skeletal muscle cells purification.....	45
4.2.7 In vivo transplantation.....	45
4.2.8 Statistical analysis .....	46
4.3 Results .....	46
4.3.1 Induction of skeletal muscle cells by chemical cocktail.....	46
4.3.2 Skeletal muscle cells were directly reprogrammed and did not pass through a pluripotent state .....	48
4.3.3 Lineage tracing indicated that skeletal muscle cells were reprogrammed from fibroblasts .....	49
4.3.4 Microgrooved substrate allowed easy purification of skeletal muscle cells.....	52
4.3.5 Reprogrammed skeletal muscle cells engrafted in vivo .....	52
4.4 Discussion.....	54
Conclusion and Future Directions.....	56
References .....	57
Appendix A.....	67
Appendix B .....	69

## Biography

### Education

Doctor of Philosophy in Bioengineering University of California, Berkeley, California	5/2012 to 8/2016
Masters of Science in Industrial Engineering and Operations Research University of California, Berkeley, California	8/2010 to 5/2012
Bachelor of Engineering in Biomedical Engineering Duke University, Durham, North Carolina	8/2006 to 5/2009

### Fellowship

Agency for Science, Technology and Research National Science Scholarship	2010 to 2015
--	--------------

### Publications

**Sia, J.**, Yu, P., Srivastava, D., & Li, S. (2016). Effect of biophysical cues on reprogramming to cardiomyocytes. *Biomaterials*, *103*, 1-11.

**Sia, J.**, Sun, R., Chu, J., & Li, S. (2016). Dynamic culture improves cell reprogramming efficiency. *Biomaterials*, *92*, 36-45.

Yang, Y., Kulangara, K., **Sia, J.**, Wang, L., & Leong, K. W. (2011). Engineering of a microfluidic cell culture platform embedded with nanoscale features. *Lab on a chip*, *11*(9), 1638-1646.

### Presentations

**Sia, J.**, Yu, P., Srivastava, D., & Li, S. The Effects of Physical Cues on Reprogramming of Fibroblasts into Induced Cardiomyocytes. BMES, Tampa, FL, USA, 2015 (Oral)

**Sia, J.**, Sun, R., Chu, J., & Li, S. Effect of Dynamic Culture on Reprogramming to Pluripotency. ISSCR, Stockholm, Sweden, 2015 (Poster)

## List of Tables

Table 2.1 Primers used for RT-qPCR. ....	7
Table 2.2 Antibodies information for immunofluorescence and Western blotting.....	8
Table 2.3 Cell cycle time of iPSCs derived under static and dynamic culture. ....	11
Table 3.1 Primer information. ....	26
Table 4.1 Information on small molecules. ....	43
Table 4.2 Information on candidate screen for enhancing efficiency.....	43
Table 4.3 Information on antibodies used.....	44
Table 4.4 Primer information.....	45

## List of Figures

Figure 2.3 Characterization of iPSCs on day 28. ....	12
Figure 2.4 Dynamic culture did not induce double stranded break. ....	13
Figure 2.5 Time course for dynamic culture. ....	14
Figure 2.6 Effects of cell seeding density. ....	14
Figure 2.7 Effect of mixing and shear stress on reprogramming efficiency. ....	16
Figure 2.8 Effect of dynamic culture on mechano-sensitive proteins. ....	17
Figure 2.9 Effect of static and dynamic culture on cell cycle. ....	19
Figure 2.10 Dynamic culture synergized with 616452 to improve reprogramming efficiency. ....	20
Figure 3.1 Schematics of experiments. ....	27
Figure 3.2 Screen for physical cues that may affect efficiency of reprogramming to cardiomyocytes. ....	28
Figure 3.3 Quantification of cells on different substrates. ....	29
Figure 3.4 Alignment of cells on microgrooved substrate. ....	29
Figure 3.5 Early characterization of reprogrammed tail tip fibroblasts on flat and grooved surface. ....	29
Figure 3.6 Reprogramming of tail tip fibroblasts with optimized culture. ....	32
Figure 3.7 Reprogramming of cardiac fibroblasts with optimized culture. ....	34
Figure 3.8 Effect of actin cytoskeletal drugs on reprogramming efficiency. ....	34
Figure 3.9 Effect of cytoskeletal drugs on localization of Mkl1. ....	35
Figure 3.10. Effect of microgroove on localization of Mkl1. ....	36
Figure 3.11 Mkl1 localization for static and stretched reprogramming TTF. ....	37
Figure 3.12 Mkl1 overexpression and valproic acid treatment recapitulated the early effect of microgroove. ....	38
Figure 3.13 Microgroove enhanced organization of sarcomeric structure. ....	39
Figure 4.1 Emergence of clusters of skeletal muscle cells. ....	47
Figure 4.2 Screening for optimal small molecule combinations and basal medium. ....	48
Figure 4.3 Time course PCR. ....	49
Figure 4.4 mRNA microarray analysis on fibroblasts in 6F medium on day 2. ....	50
Figure 4.5 Skeletal muscle cells were derived from fibroblast population. ....	51
Figure 4.6 Myoblasts and dermal fibroblasts treated with 6, F and 6F together. ....	52
Figure 4.7 Purification of skeletal muscle cells with microgrooved substrate. ....	54
Figure 4.8 Maturation and engraftment potential of reprogrammed skeletal muscle cells. ....	55

## Chapter 1: Introduction

Today, we know that the forced expression of key lineage-associated transcription factors can remodel the transcription network of the target cell to phenotypically transdifferentiate it into another cell type. This concept was first demonstrated in 1987 when the overexpression of the skeletal muscle factor, MyoD, in fibroblast cell lines caused their transdifferentiation into myofibers [1]. Many years later, it was shown that the forced expression of C/EBP $\alpha$  / C/EBP $\beta$  in differentiated B cells led to their rapid reprogramming into macrophages [2]. The next prominent milestone was reached in 2006 when Takahashi and Yamanaka demonstrated that the overexpression of Oct4, Sox2, Klf4 and Myc could reprogram fibroblasts into induced pluripotent stem cells (iPSCs) [3]. Since then, there have been many studies demonstrating the reprogramming of fibroblasts to other cell types, such as cardiomyocytes [4], neurons [5] and hepatocytes [6]. Needless to say, the therapeutic potential of these discoveries is tremendous. Fibroblasts expanded from a patient's skin biopsy can be reprogrammed into iPSCs and subsequently differentiated into target cell types for transplantation, disease modelling or drug testing. The delivery of the reprogramming factors to injured or diseased sites *in situ* can, in principle, also directly reprogram reactive or fibrotic cells into the desired cell types, as has been demonstrated in mouse models for heart ischemia [7] and central nervous system injury [8].

There are, however, inherent limitations to these technologies. These constraints include the following: (1) the efficiency of reprogramming is low; (2) there are phenotypic disparities between reprogrammed and endogenous cells; (3) there is the potential for off-target effects, such as unregulated growth that might lead to tumorigenicity. To address low efficiency, much work has been undertaken, but almost all of these approaches involve either additional genetic manipulations through overexpression or knocking down of more candidates such as transcription factors, signaling proteins, microRNAs and chromatin regulators, or the use of small molecules that interfere with the activities of enzymes involved in signaling cascades or chromatin structure regulation. The long term effects of these methods need to be fully characterized and potential off-target effects excluded before they can be deemed safe for therapeutic use.

This thesis explored an alternative paradigm for improving reprogramming efficiency: physical stimulation of the cells undergoing reprogramming. In doing so, I sought to avoid additional direct interference with the cells' genetic and biochemical pathways while allowing the cells to regulate their functions in response to the physical cues applied, with the desired outcome of enhancing their reprogramming process. To this end, I showed that simply agitating the reprogramming cells on an orbital shaker, as well as culturing them on a grooved substrate, could significantly improve the efficiency of their reprogramming to iPSCs and cardiomyocytes, respectively. I provided some insights into the underlying mechanisms, which could have broad implications for understanding how mechanotransduction can affect lineage reprogramming.

Transcription factors can effectively modulate the expression of many genes at once and thus their activities can bring about widespread changes in the cell's transcriptome. Many transcription factors implicated in organ development and lineage specification have been well studied. In seeking to reprogram fibroblasts into another cell type, researchers typically start off by overexpressing a pool of candidate factors which they know, from previous works, are critical in the development of the target cell type, and then seek to narrow the pool down. By utilizing transcription factors, researchers can capitalize on their potency and also the wealth of existing knowledge on their functions. For these reasons, the first published successful reprogramming to the various cell types were all achieved by the overexpression of transcription factors, with different cocktails of factors identified for different cell types.

Recently however, multiple studies have been published describing that reprogramming can be achieved simply via the exogenous administration of small molecules. This approach has successfully converted fibroblasts into iPSCs [9,10], cardiomyocytes [11,12], neurons [13], astrocytes [14] and neural stem cells [15]. The key benefit of this approach is that it obviates the need for genetic manipulation, and is thus safer and more convenient. Reprogramming to other target cell types using only small molecules remains to be achieved.

In Chapter 2, I showed that fibroblasts overexpressing Oct4, Sox2, Klf4 and Myc reprogrammed to iPSCs more efficiently when subjected to dynamic culture on an orbital shaker. The effect of dynamic culture on the cells was two-fold: (i) it exerted hydrodynamic shear stress on the adherent cells; (ii) it mixed the culture medium convectively. Manipulating the viscosity of the culture medium suggested that the improved efficiency was mainly attributed to convective mixing rather than hydrodynamic shear stress. Temporal studies demonstrated that the enhancement of reprogramming efficiency required the orbital agitation in the middle, but not in the early or late phase of reprogramming. I went on to show how the enhancing effect of dynamic culture was mediated by down-regulation of p57 / Kip2 / CDKN1C (a known inhibitor of several classes of the cyclin-dependent protein kinases that drive mammalian cell cycle progression), and that dynamic culture synergized with small molecules treatment to further enhance reprogramming efficiency.

In Chapter 3, I studied the effects of periodic mechanical stretch, substrate stiffness and microgrooved substrate on the yield of reprogramming from fibroblasts to cardiomyocytes. Subjecting reprogramming fibroblasts to periodic mechanical stretch and different substrate stiffness did not improve reprogramming yield. On the other hand, culturing the cells on microgrooved substrates enhanced the expression of cardiomyocyte genes by day 2 and improved the yield of partially reprogrammed cells. By combining a microgrooved substrate with an existing optimized culture protocol, I also improved the yield of fully reprogrammed cardiomyocytes with striated cardiac troponin T staining and spontaneous contractile activity. I demonstrated that the microgrooves caused upregulation of the activity of the transcription factor Mkl1 (megakaryoblastic leukemia-1), also known as myocardin-related transcription factor A (Mrtf-a), and enhanced the organization of sarcomeric structure, with both effects ultimately leading to better reprogramming efficiency.

In Chapter 4, I reported the iterative screening of small molecules to identify candidates that can reprogram dermal fibroblasts into skeletal muscle cells. I found 2 chemicals, in combination with an optimized basal medium, which could efficiently induce skeletal muscle cells from dermal fibroblasts. I used FACS to deplete muscle progenitors and stem cells and selected for fibroblasts, and showed that skeletal muscle cells could be derived from such a starting population with the reprogramming medium. The reprogrammed population consisted of both progenitors and differentiated myocytes, and could fuse into mature beating myotubes when cultured in differentiation medium and, when injected into mice *in vivo*, successfully engrafted.

## Chapter 2: Dynamic Culture Improves Cell Reprogramming Efficiency

### 2.1 Introduction

The forced expression of the transcription factors Oct4, Klf4, c-Myc, and Sox2 (OSKM) reprograms somatic cells into induced pluripotent stem cells (iPSCs)[3,16]. iPSCs possess similar pluripotent characteristics to embryonic stem cells, thus providing a readily available source of pluripotent stem cells for disease modeling and regenerative medicine applications. To force the overexpression of OSKM for achieving reprogramming, exogenous genetic constructs could be delivered and integrated into the host's chromosomes through viral transduction[3]. Non-viral approaches such as transfection of plasmids, synthetic mRNA and proteins could also be used to increase the levels of OSKM for reprogramming[17]. However, all these approaches result in different levels of OSKM being expressed in different cells due to the stochastic nature of transduction and transfection. This variegated expression levels could complicate mechanistic studies with bulk culture. To address this issue, transgenic mouse models have been developed[18,19]. These mice are genetically engineered to contain a doxycycline-inducible cassette encoding OSKM as well as a reverse tetracycline-dependent transactivator cassette so that treatment with doxycycline would force the expression of OSKM[18,19]. Fibroblasts isolated from these mice exhibit homogenous level of OSKM expression upon doxycycline treatment so that read outs obtained from bulk cell culture are more reflective of general occurrences instead of possibly a few dominant events. In my studies, I have used fibroblasts isolated from such a transgenic mouse[19].

The efficiency of reprogramming is relatively low, ranging between 0.1% and 10% for most somatic cell types using the different methods for achieving OSKM overexpression[20]. To date, extensive work has been done to improve efficiency through further genetic manipulations[21–24]. For instance, controlled depletion of Mbd3, a core member of the Mbd3/NuRD (nucleosome remodelling and deacetylation) repressor complex, by 50% to 80% level together with OSKM transduction in naive pluripotency promoting conditions resulted in deterministic and synchronized iPSCs reprogramming[25]. Another work showed that fibroblasts from p53 null mice reprogrammed to iPSCs at 10% efficiency with just overexpression of Oct4, Klf4 and Sox2[26]. Besides genetic manipulations, reprogramming efficiency has been shown to be improved by treatment with small molecules [27–31]. For instance, it was shown that treating OSKM transduced MEFs with 2 mM of valproic acid, a HDAC inhibitor, for 1 week resulted in a 100 fold improvement in reprogramming efficiency[32]. Vitamin C, a natural compound, could also enhance iPSC generation by alleviating cell senescence, accelerating gene expression changes and promoting the transition of pre-iPSC colonies to a fully reprogrammed state[33].

Manipulating the biophysical environment of the cells can also improve reprogramming efficiency. Culturing fibroblasts on microtopography can modulate their epigenetic states to improve reprogramming efficiency by as much as 4 folds[34]. Subjecting the culture to hypoxic condition can also improve efficiency, although the underlying mechanism is not yet elucidated[35]. By using a cell suspension culture, higher yield of iPSCs can be obtained over

time[36]. Culturing fibroblasts on soft hydrogel can also improve efficiency by promoting mesenchymal to epithelial transition during the early phase of reprogramming[37]. Such biophysical approaches demonstrate the potential of adopting this paradigm in improving reprogramming efficiency. However, in most cases, the underlying mechanisms are not well understood.

In this work, I demonstrated that agitating an adherent reprogramming culture (henceforth termed as dynamic culture) on an orbital shaker significantly increased the yield of iPSC colonies. Manipulating the viscosity of the culture medium suggested that the improved efficiency is mainly attributed to convective mixing rather than hydrodynamic shear stress. Temporal studies indicated that the enhancement of reprogramming efficiency required the dynamic culture in the middle but not early phase of reprogramming. In the early phase, fibroblasts had a high proliferation rate, but as the culture became over-confluent by the middle phase, expression of p57 was upregulated to inhibit cell proliferation and consequently, the reprogramming process. Subjecting the over confluent culture to orbital shaking from this point on prevented the upregulation of p57, thus improving reprogramming efficiency. Seeding cells at low densities to avoid over-confluency resulted in a lower efficiency, and optimal reprogramming efficiency was attained at a high seeding density with dynamic culture. These findings established dynamic culture as a new and simply implementable biophysical approach to improving reprogramming efficiency, and provided insights into its underlying mechanisms.

## **2.2 Materials and Methods**

### **2.2.1 Fibroblast isolation, cell culture and reprogramming**

Skin fibroblasts were derived from transgenic mice that carried doxycycline-inducible OSKM genes (stock no 011011, Jackson Lab). The four reprogramming factors, OSKM, were expressed from the collagen type 1 gene locus upon induction with doxycycline[38]. 1 day post-partum mice were sacrificed by decapitation with a pair of sharp scissors. The skin was peeled off and floated on 0.05% freshly thawed trypsin overnight and the dermis was separated from the epidermis next day. The dermis was cut up and digested in 200U/ml collagenase II and 0.1% Trypsin at 37 °C for 30 minutes. The digesting mixture was mixed with fetal bovine serum (FBS) to quench the digestion enzyme activity and spun down. The pellet was plated on gelatin coated dish and expanded for 2 days in MEF medium (DMEM with 10% FBS and 1% penicillin/streptomycin). Thereafter, the culture was trypsinized, passed through a 40 µm filter and frozen down into aliquots in a medium containing 10% dimethyl sulfoxide (DMSO) and 90% FBS.

For cell reprogramming experiment, fibroblasts were seeded into 6 well plates in MEF medium. Unless otherwise stated, cells were seeded at a density of 3000 cells/cm<sup>2</sup>. The next day, medium was replaced with reprogramming medium (Knockout™ DMEM, 10% Knockout Serum Replacement™, 5% FBS, 1% penicillin/streptomycin, 1% Glutamax, 1000 U/ml LIF and 2µg/ml doxycycline) to induce the expression of OSKM.

For dynamic culture, the culture plates were placed on an orbital shaker in the incubator and, unless noted otherwise, agitated at 100 rounds per minute (rpm). At the indicated times, doxycycline was removed from the reprogramming medium to stop the exogenous expression

of OSKM, with all other medium components retained. For all experiments, media was changed once every 2-3 days.

Reprogrammed iPSC colonies with three dimensional dome-like morphology and clear boundary were picked on day 20 and expanded in reprogramming medium for 4 passages. To form embryoid bodies (EBs), the iPSCs were suspended in 20  $\mu$ l hanging drops at 2000 cells per drop for 3 days in EB medium (same as reprogramming medium but with LIF removed). The embryoid bodies were then plated on gelatin coated plate and cultured for an additional 9 days in EB medium to allow further spontaneous differentiation before fixation and staining.

To measure cell doubling time,  $10^4$  doxycycline independent iPSCs reprogrammed in static and dynamic culture at passage 4 were seeded into each well of 6 well plate. Cells were counted 72 hours later. Population averaged doubling time,  $t_d$ , was calculated from the following equation:  $t_d = \frac{72 \log 2}{\log\left(\frac{\text{count}}{10000}\right)}$ .

$$t_d = \frac{72 \log 2}{\log\left(\frac{\text{count}}{10000}\right)}$$

### 2.2.2 Immunofluorescence staining and microscopy

For immunostaining, cells were fixed in 4% paraformaldehyde for 15 minutes, and permeabilized with 0.5% Triton-X 100 for 15 minutes. Cells were stained with the respective primary and secondary antibodies, and imaged with a Zeiss AxioObserver epi-fluorescent microscope. Refer to table 2.2 for list of primary antibodies. Secondary antibodies were Alexa Fluor 488 or Alexa Fluor 546 (ThermoFisher Scientific).

To determine cell proliferation rate, EDU staining was performed by using Click-iT<sup>®</sup> EdU Alexa Fluor<sup>®</sup> 488 Imaging Kit (ThermoFisher Scientific). Samples were pulsed with 10  $\mu$ M EDU for 30 minutes. Subsequent steps were performed according to manufacturer's instructions.

### 2.2.3 Quantification of reprogramming efficiency

At the indicated time, culture was fixed and immunostained for iPSC markers Nanog and SSEA1. Stained samples were kept in phosphate buffered saline (PBS) and loaded onto ImageXpress Micro High-Content Analysis System (Molecular Devices) for automated whole well imaging at 4X magnification. The images were stitched using the MetaXpress Analysis Software (Molecular Devices) and loaded in Photoshop for colony counting. A transparent layer was created and positive colonies were marked and covered with a circular brush. The layer was then saved as a separate image and the number of circular marks were counted using ImageJ. Reprogramming efficiency was obtained by dividing the number of Nanog+ positive colonies by the total number of cells seeded at the beginning of the experiments.

For flow cytometry analysis, the culture was first treated with 500U/ml collagenase II dissolved in plain Knockout<sup>™</sup> DMEM for 15 minutes to partially digest the ECM, followed by trypsin treatment. The detached cells was triturated with progressively smaller needles to obtain a single cell suspension before incubation with StainAlive<sup>™</sup> SSEA1 antibody (Stemgent) for 30 minutes. The suspension was spun down and washed with PBS two times before being analyzed with Guava (Merck Millipore).

### 2.2.4 Reverse transcription-quantitative polymerase chain Reaction (RT-qPCR)

At the indicated time, culture was lysed with Trizol (ThermoFisher Scientific) and RNA was extracted following the manufacturer's instruction. RNA concentration was quantified with

Nanodrop 1000 (Thermo Scientific) and equal amount was loaded for cDNA synthesis using Maxima First Strand cDNA Synthesis Kit (ThermoFisher Scientific). cDNA was then loaded into 96 well PCR plate with primers and Maxima SYBR Green qPCR Master Mix (ThermoFisher Scientific). Primer information is listed in table 2.1. Thermal cycling and data acquisition was performed on iQ5 system (Biorad). GAPDH used as housekeeping gene for normalization. Data was analyzed with  $\Delta\Delta C_t$  method.

**Table 2.1** Primers used for RT-qPCR

	<b>Forward</b>	<b>Reverse</b>
p21cip1	GCAGAATAAAAGGTGCCACAGG	GACAACGGCACACTTTGCTC
p27kip1	GTTTCAGACGGTCCCCGAA	TCTTAATTCGGAGCTGTTTACGTC
p57	CGAGGAGCAGGACGAGAATC	GAAGAAGTCGTTCCGATTGGC
p16ink4a	CATCTGGAGCAGCATGGAGTC	ATCATCATCACCTGAATCGGGG
GAPDH forward	TTGAGGTCAATGAAGGGGTC	TCGTCCCGTAGACAAAATGG

### 2.2.5 Western blotting analysis

To determine p57 expression, cells were lysed with a lysis buffer containing 20 mM Tris-HCl, 150 mM NaCl, 1% Triton X-100, 0.1% SDS and 10 mM NaF along with protease inhibitors (phenylmethyl sulphonyl fluoride,  $\text{Na}_3\text{VO}_4$  and leupeptin). Lysates were centrifuged and the supernatants removed and quantified by Direct Detect<sup>®</sup> Infrared Spectrometer (Merck Millipore). For analysis of YAP/TAZ and  $\beta$ -Catenin localization, nuclear and cytoplasmic lysates were prepared with NucBuster<sup>™</sup> Protein Extraction Kit (Merck Millipore) according to the manufacturer's instructions.

Equal amounts of proteins were separated with SDS-PAGE and then transferred to polyvinylidene fluoride membranes. Membranes were blocked in either denatured 5% BSA (when staining for phosphorylated proteins) or 3% non-fat milk and then incubated with primary antibodies. Refer to table 2.1 for list of antibodies. Next, membranes were incubated with HRP-conjugated IgG secondary antibodies (Santa Cruz Biotechnologies) for one hour. Protein bands were visualized by using Western Lightning Plus-Enhanced Chemiluminescence Substrate (Perkin Elmer Life & Analytical Sciences).

**Table 2.2** Antibodies information for immunofluorescence and Western blotting

Antibody	Company	Catalogue no.	Purpose
Alpha-fetoprotein	R&D	MAB 1368	Immunofluorescence
Sox17	R&D	MAB 1924	Immunofluorescence
Cardiac troponin T	ThermoFisher Scientific	MS 295P0	Immunofluorescence
Smooth muscle actin	Abcam	ab 32575	Immunofluorescence
Nanog	Abcam	ab 70482	Immunofluorescence
SSEA	Santa Cruz Biotech	sc-21702	Immunofluorescence
Sox2	EMD Millipore	ab 5603	Immunofluorescence
Oct4	Santa Cruz Biotech	sc-5279	Immunofluorescence
$\gamma$ H2AX	Biolegend	613401	Immunofluorescence
Yap	Santa Cruz Biotech	sc-101199	Western Blot
B-catenin	Cell Signaling	8480P	Western Blot
p57	Santa Cruz Biotech	sc-1037	Western Blot
H3	Abcam	ab 1791	Western Blot
GAPDH	Santa Cruz Biotech	sc-32233	Western Blot

### 2.2.6 Measurement of viscosity, shear stress and mixing rate

Dextran was added to manipulate the viscosity of the culture medium. Measured amount of dextran was sterilized by incubation in boiling water bath for 30 minutes. The viscosity of medium with and without dextran at 37°C was measured with rheometer (MCR300, Anton Paar, Ashland, VA). 50 mm parallel plate at a gap height of 0.5 mm was used. A humidity chamber was placed around the sample to prevent dehydration. The lower plate temperature was regulated with a Peltier heating element connected to a recirculating water bath. Medium was sheared at different rates and the torque measurement was used to calculate viscosity by the equation  $\eta = \frac{2Mh}{\pi\Omega R^4}$ , where M is torque, h is distance between plates,  $\Omega$  is rate of rotation and R is radius of plate.

The average shear stress  $\tau$  at the bottom of the culture dishes on the orbital shaker was determined by the equation  $\tau = R\sqrt{\rho\eta(2\pi f)^3}$ , where R is the radius of the dish,  $\rho$  is fluid density,  $\eta$  is dynamic viscosity and f is orbiting frequency [39].

To measure mixing rate, a spot of blue dye (3  $\mu$ l) was added to the medium and the time taken for the spot to become completely homogenous with the medium recorded.

### 2.2.7 siRNA transfection

800 pmol of siRNA in 1ml DMEM and 20 $\mu$ l Lipofectamin 2000 (Invitrogen) in 1ml DMEM were incubated separately for 5 minutes and then mixed and incubated together for another 20 minutes at room temperature. 500 $\mu$ l of the siRNA-lipid complex was added to the reprogramming medium in each well (total of 4 wells), and the medium was replaced after 6 hrs. Transfection was performed every 48 hours for a total of 5 times. The following siRNAs were used: p57 siRNA (pool of 37621A-C, Santa Cruz Biotechnology); control siRNA (D-001810-10-20, Dharmacon)

## 2.3 Results

### 2.3.1 Dynamic culture improved reprogramming efficiency

I utilized neonatal skin fibroblasts with doxycycline-inducible OSKM transgenes for our experiments[19]. The cells were seeded at 3000 cell/cm<sup>2</sup> and reprogramming was induced the next day. Orbital shaking was started one day after. Doxycycline was withdrawn on day 16 and Nanog+ colonies were counted on day 20 (Fig. 2.1A). Dynamic culture significantly increased the reprogramming efficiency by 2 folds (Fig. 2.1B, 2.1C). I also ran flow cytometry analysis for SSEA1, a surface marker of iPSCs, to quantify efficiency at individual cell level. Consistently, the percentage of SSEA1+ cells was increased by 3 folds for dynamic culture (Fig. 2.1D).

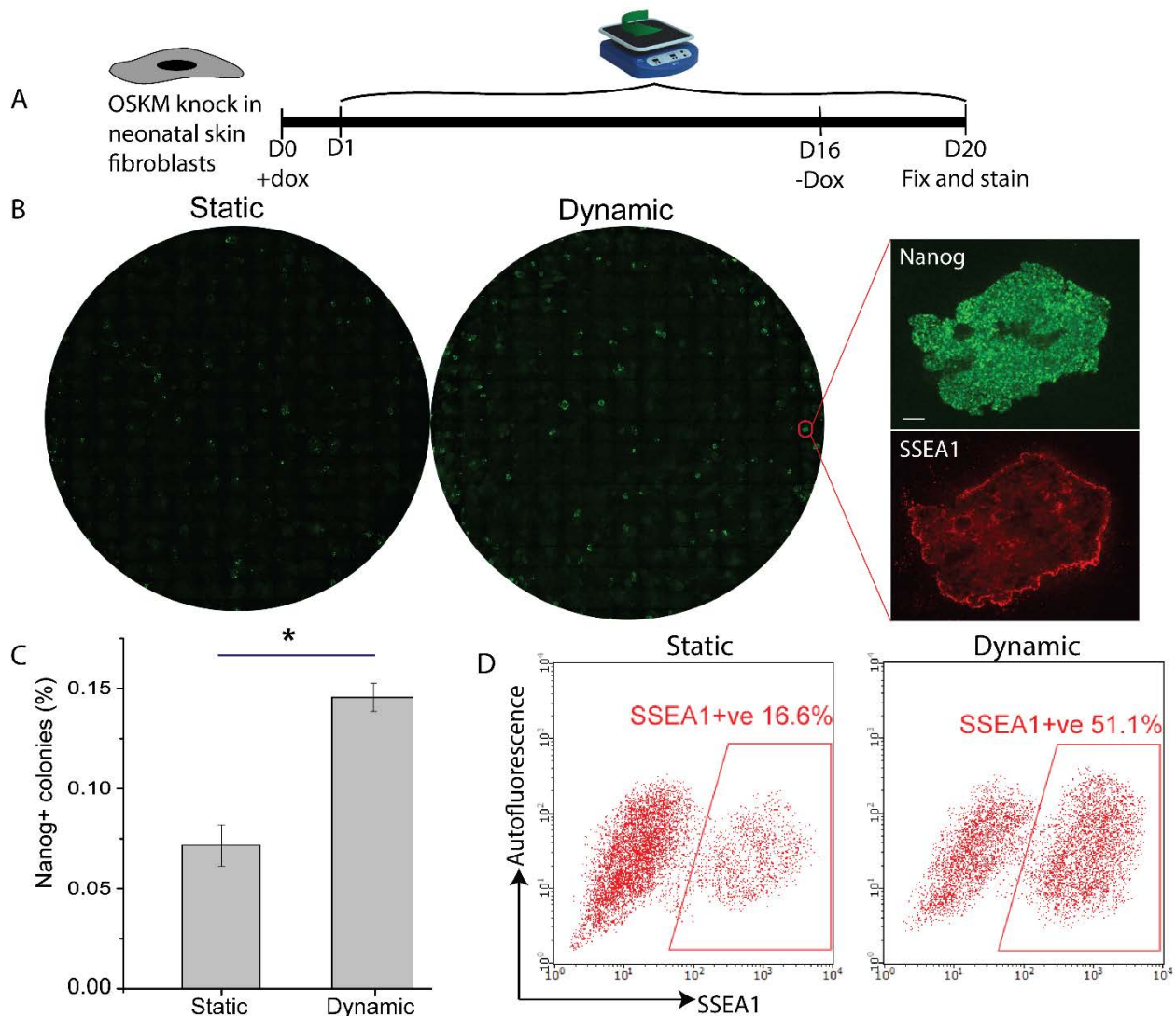
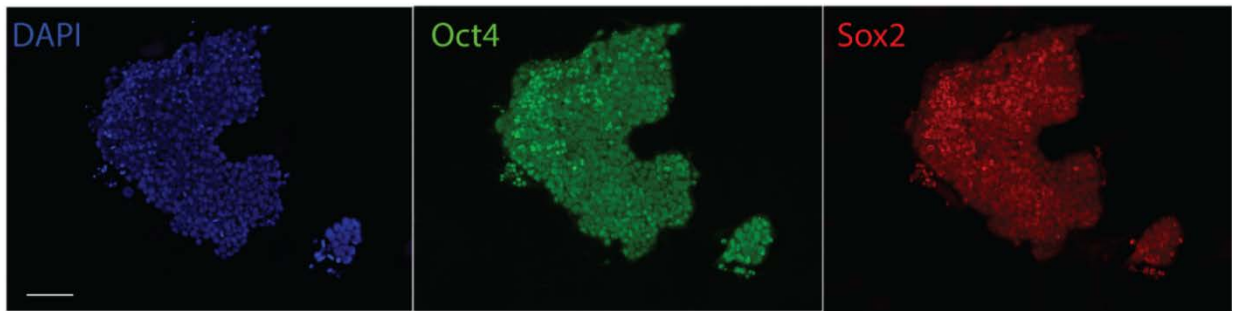


**Figure 2.1 Effect of dynamic culture on cell reprogramming efficiency. A)** Schematics of experiment. Doxycycline was added from day 0 to 16. Dynamic culture was applied from day 1 onwards. **B)** Whole well image of Nanog+ colonies. Scale bar denotes 100  $\mu$ m. **C)** Quantification of reprogramming efficiencies. Efficiency was calculated by normalizing number of Nanog+ colonies by number of cells seeded. (\* $p$ <0.05,  $n$ =6.) **D)** Percentage of SSEA1+ cells quantified by flow cytometry.

iPSCs colonies obtained under dynamic culture were picked on day 20, expanded for 4 passages and then stained for Oct4 and Sox2 (Fig. 2.2A). Embryoid bodies formed with the expanded iPSCs were allowed to spontaneously differentiate. Differentiated cells stained positive for markers from the 3 germ layers (Fig. 2.2B), indicating that the iPSCs obtained under dynamic culture were pluripotent. I also compared the doubling times for iPSCs derived under dynamic and static culture, and found them to be similar (Table 2.3). To assess the long term self-renewal and pluripotency of the iPSCs obtained under dynamic culture, I cultured them for a total of 28 days after picking. After 28 days, they stained positive for pluripotency markers Nanog, SSEA1 and Oct4 (Fig 2.3A) and formed 3 germ layers upon spontaneous differentiation (Fig 2.3B), indicating that they maintained their self-renewal capability and pluripotency long term.

A



B

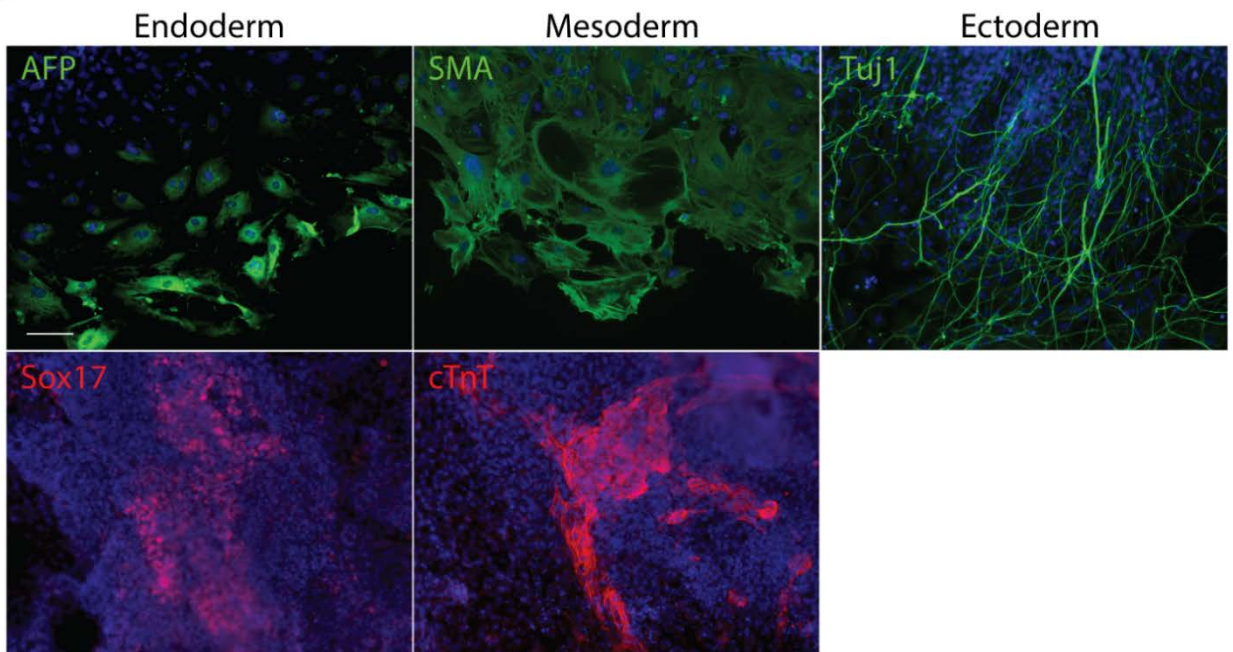


**Figure 2.2 Characterization of the pluripotency of iPSCs. A)** Picked iPSC colonies were stained for Oct4 and Sox2. **B)** iPSCs derived under dynamic culture were used to form EBs and allowed to spontaneously differentiate. Differentiated cells were stained for markers from the 3 germ layers. AFP is alpha fetoprotein, SMA is  $\alpha$ -smooth muscle actin and cTnT is cardiac troponin T. Scale bars denote 100  $\mu$ m.

**Table 2.3** Cell cycle time of iPSCs derived under static and dynamic culture.

	Static		Dynamic	
	Cell count	$t_d$ (hrs)	Cell count	$t_d$ (hrs)
	261000	15.3	256000	15.4
	245000	15.6	245000	15.6
	231000	15.9	285000	14.9
Average	246000	15.6	262000	15.3

Doubling times between the two conditions were not statistically significant according to t-test ( $p=0.33$ ).

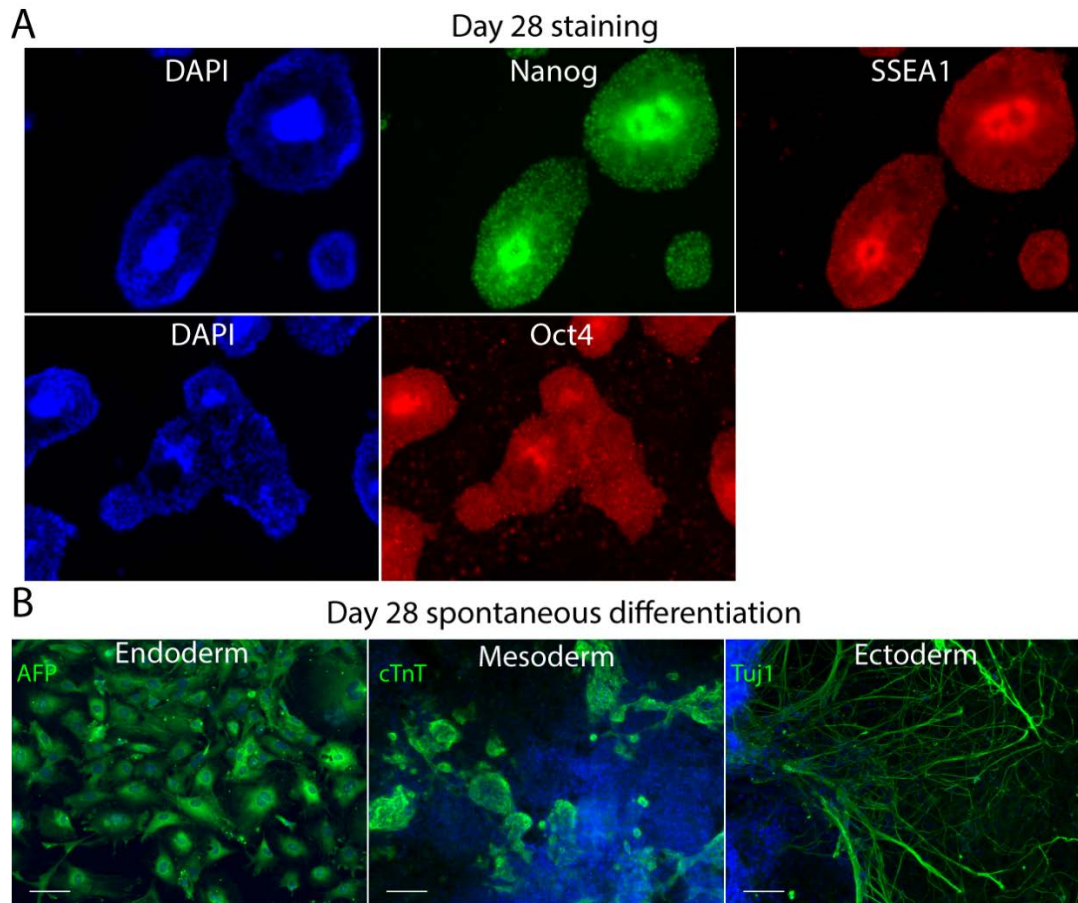


**Figure 2.3 Characterization of iPSCs on day 28.** **A)** Picked iPSC colonies from dynamic culture were cultured for 28 days and stained for pluripotency markers. **B)** iPSCs from A were subjected to EB formation and spontaneous differentiation. 3 germ layers were formed.

To assess if mechanical shear stress exerted on cells by dynamic culture could cause chromosomal aberrations through, for instance, inducing DNA double-stranded break, I stained the reprogramming culture with antibody targeting  $\gamma$ H2AX. H2AX is a variant of the histone H2A family, which in response to DNA double-strand breaks becomes phosphorylated into the form known as  $\gamma$ H2AX[40]. On day 8, I observed no positive staining in nascent colonies in both dynamic and static culture (Fig. 2.4A). On day 20, I observed some staining for  $\gamma$ H2AX in reprogrammed Nanog positive colonies in both dynamic and static culture (Fig. 2.4B). This positive staining could be attributed to a higher basal level of  $\gamma$ H2AX in iPSCs, as has been reported[41]. More importantly, the intensity of  $\gamma$ H2AX staining was not significantly different between dynamic and static culture (Fig 2.4B), indicating that dynamic culture did not cause additional double stranded breaks.

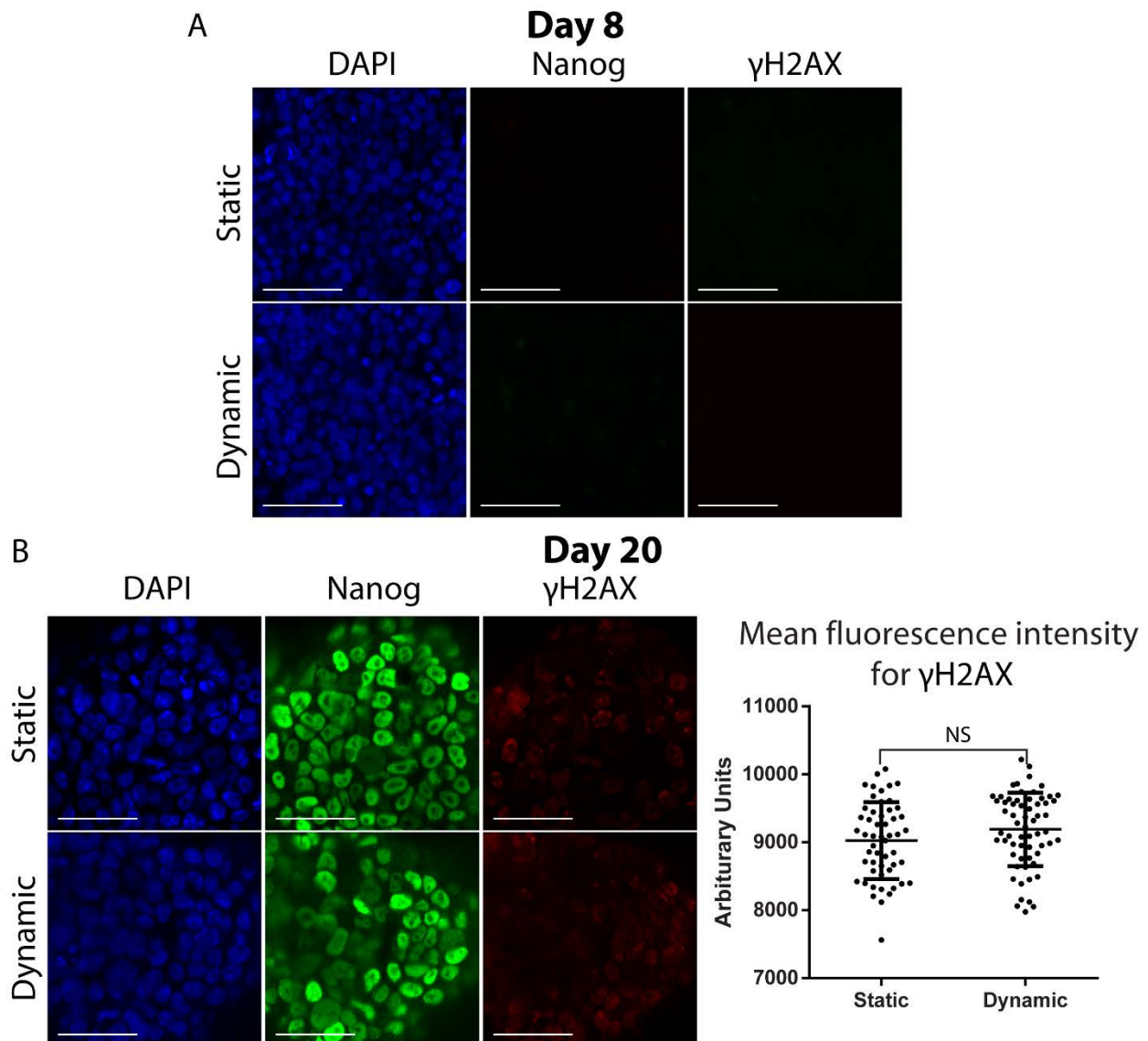


**Figure 2.4 Dynamic culture did not induce double stranded break.** **A)** Reprogramming culture under dynamic and static conditions were fixed and stained for Nanog and  $\gamma$ H2AX on day 8. Nascent colonies were imaged. Scale bar denotes 100  $\mu$ m. **B)** Reprogrammed culture was fixed and stained on day 20. Images are shown on the left. Scale bar denotes 100  $\mu$ m. Scatter plot of  $\gamma$ H2AX intensity is shown on the right.

### 2.3.2 Time course study revealed the optimal period for dynamic culture

I next sought to establish the optimal period of dynamic culture to improve reprogramming efficiency. Applying shaking during the early phase (D2-D6) inhibited reprogramming, and during the late phase (D12-D20) resulted in no significant change. The greatest improvement was obtained when shaking was applied from day 6 onwards (Fig. 2.5). Close examination of cell culture showed that day 6 was when the reprogramming culture became confluent. I therefore hypothesized that from this time point onwards, the confluence of the cells had a negative effect on reprogramming, and that dynamic culture ameliorated some of these effects to improve reprogramming efficiency.

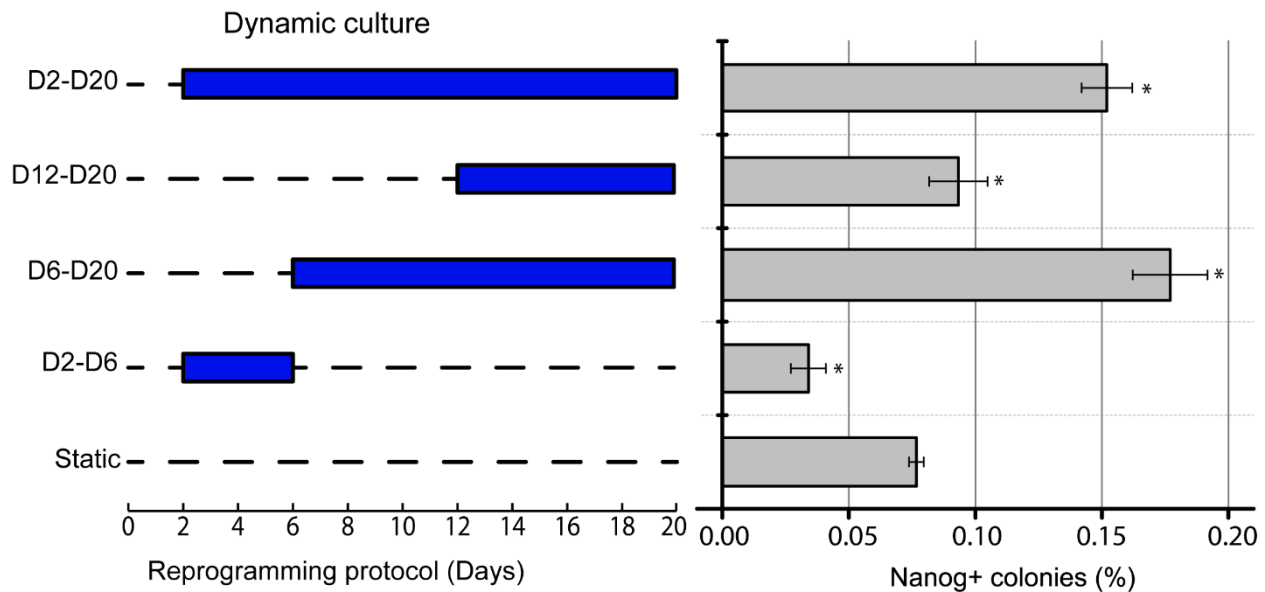


**Figure 2.5 Time course for dynamic culture.** Orbital shaking was applied at different time points as indicated by the graph on the left, with the corresponding reprogramming efficiency indicated on the right. (\* $p < 0.05$ ,  $n = 3$ .)

### 2.3.3 Dynamic culture ameliorated negative effect of over-confluence on reprogramming

First I sought to establish the effect of cell density on reprogramming. I seeded cells at 3000, 5000 and 7000/cm<sup>2</sup> and added doxycycline for 16 days and fixed cells on day 20. Reprogramming efficiency dropped significantly as seeding density increased (Fig. 2.6A). I then determined whether the negative effect of higher seeding density on reprogramming efficiency was manifested only after the culture became confluent. I replated the reprogramming culture at day 6 to a lower density (10000/cm<sup>2</sup>) to see if reprogramming efficiency was improved. Indeed, after being relieved of their confluent niche, reprogramming efficiency of the cells was significantly improved to the same level for all 3 initial seeding densities (Fig. 2.6A). To rule out the possibility that reseeding in itself affects reprogramming efficiency, I also trypsinized and reseeded all of the cells without adjusting the cell density. As a result, reprogramming efficiency was comparatively much lower (Fig. 2.6A). Therefore, I concluded that the negative effect of higher seeding densities on reprogramming manifested after the density of the culture has grown beyond a certain threshold.

Next, I tested if dynamic culture applied post-confluence could then rescue reprogramming efficiency at the three high seeding densities. Simply, I started orbital shaking

from day 6 onwards for the different cell densities and quantified Nanog+ colonies at the end. Indeed, reprogramming efficiencies were significantly improved for all three seeding densities (Fig. 2.6B).

I then asked the question: At a sufficiently low seeding density, would reprogramming efficiency be higher and dynamic culture not have any effect anymore? To answer this, I seeded cells at 500 and 1000/cm<sup>2</sup>, induced them with doxycycline at day 0 and applied orbital shaking from day 6 onwards. Results showed that dynamic culture did not affect reprogramming efficiency at these low densities (Fig. 2.6C). Additionally, the efficiencies were several folds lower than high density dynamic culture. One explanation is that cell-cell communications such as juxtacrine signaling important for reprogramming might take place less effectively at lower seeding densities[42].

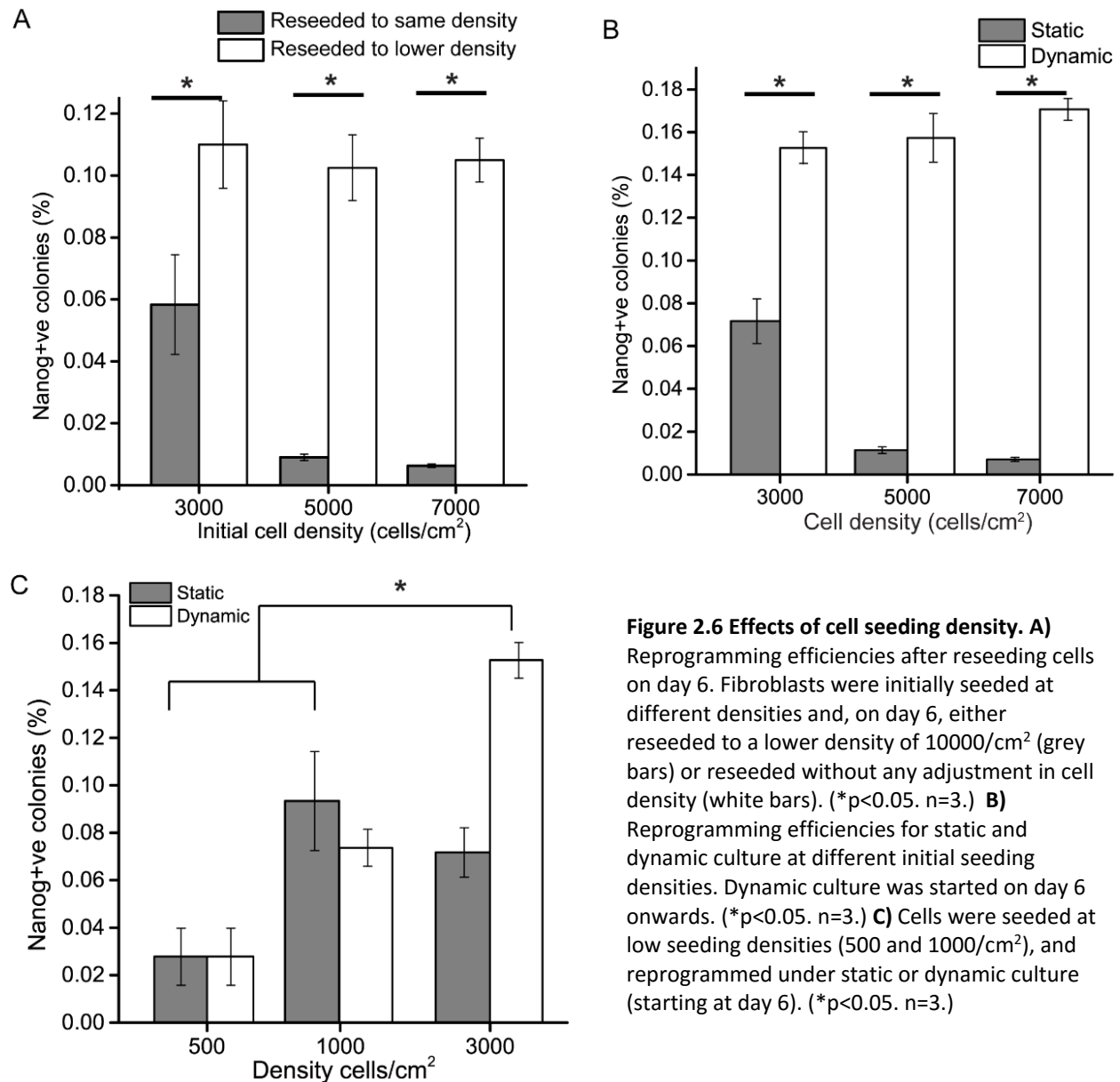


**Figure 2.6 Effects of cell seeding density. A)** Reprogramming efficiencies after reseeding cells on day 6. Fibroblasts were initially seeded at different densities and, on day 6, either reseeded to a lower density of 10000/cm<sup>2</sup> (grey bars) or reseeded without any adjustment in cell density (white bars). (\*p<0.05. n=3.) **B)** Reprogramming efficiencies for static and dynamic culture at different initial seeding densities. Dynamic culture was started on day 6 onwards. (\*p<0.05. n=3.) **C)** Cells were seeded at low seeding densities (500 and 1000/cm<sup>2</sup>), and reprogrammed under static or dynamic culture (starting at day 6). (\*p<0.05. n=3.)

### **2.3.4 Mixing rather than shear stress conferred the beneficial effect of dynamic culture**

Cells subjected to dynamic culture experience both convective mixing and hydrodynamic shear stress compared to static culture. Convective mixing could enhance the transport of cytokines, nutrients and metabolic products to regulate cell signaling, and oscillatory hydrodynamic shear stress can trigger various mechanotransduction pathways in cells, some of which could directly or indirectly affect the reprogramming process. I thus sought to find out which of these two phenomena contributed to the beneficial effect of dynamic culture.

Our approach was to use dextran to adjust the viscosity of the medium so that I could apply similar magnitude of shear stress with different rates of mixing. By increasing viscosity, I obtained the same magnitude of shear stress at a lower frequency of orbit. I added 1% high molecular weight dextran (5 million to 60 million Da.) to the culture medium to increase the viscosity of the medium from 0.912 mPa.s to 4.21 mPa.s, as measured by rheometry (Fig. 2.7A). Addition of dextran did not alter the Newtonian property of the medium as viscosity remained constant across different shear rates (Fig. 2.7A). To ensure that dextran in itself did not significantly affect the reprogramming process, I reprogrammed cells seeded at 1000/cm<sup>2</sup> with and without dextran under static condition, and I observed a similar reprogramming efficiency (Fig. 2.7B). The size and morphology of the colonies were indistinguishable between the two conditions (Data not shown).

I then reprogrammed cells seeded at 3000/cm<sup>2</sup> statically and dynamically at 60 rpm and 100 rpm, with and without dextran (Fig. 2.7C). Under static condition, the reprogramming efficiency was slightly lower for dextran medium than no-dextran medium (Fig. 2.7C), although this was not observed for cells seeded at 1000/cm<sup>2</sup> (Fig. 2.7B). At these two rotation rates, shear stress exerted by dextran medium at 60 rpm (DM 60) and no-dextran medium at 100 rpm (NDM 100) is both equivalent to 3.2 dyne/cm<sup>2</sup> according to equation 2 (Materials and Methods). On the other hand, rate of convective mixing is lower for DM 60 than NDM 100 as the higher viscosity and lower rate of agitation would lead to less bulk motion of the medium. I confirmed this by measuring the time it took for a spot of blue dye to mix completely for DM 60 and NDM 100. DM 60 took 311 seconds, while NDM 100 took 21 seconds, a difference of 15 folds. If shear stress is the dominant attributable factor, I would expect efficiencies to be similar between these 2 conditions. If mixing is the dominant factor, efficiency would be lower for DM 60. The results showed that the reprogramming efficiency was significantly lower for DM 60, indicating that mixing is the dominant factor (Fig. 2.7C). At 100 rpm, reprogramming efficiency was similar for the media with and without dextran, even though shear stress was different (7.0 dyne/cm<sup>2</sup> for dextran and 3.2 dyne/cm<sup>2</sup> for no-dextran). This suggests that at 100 rpm, the rate of mixing is sufficiently high even for a medium with higher viscosity to enhance reprogramming efficiency.

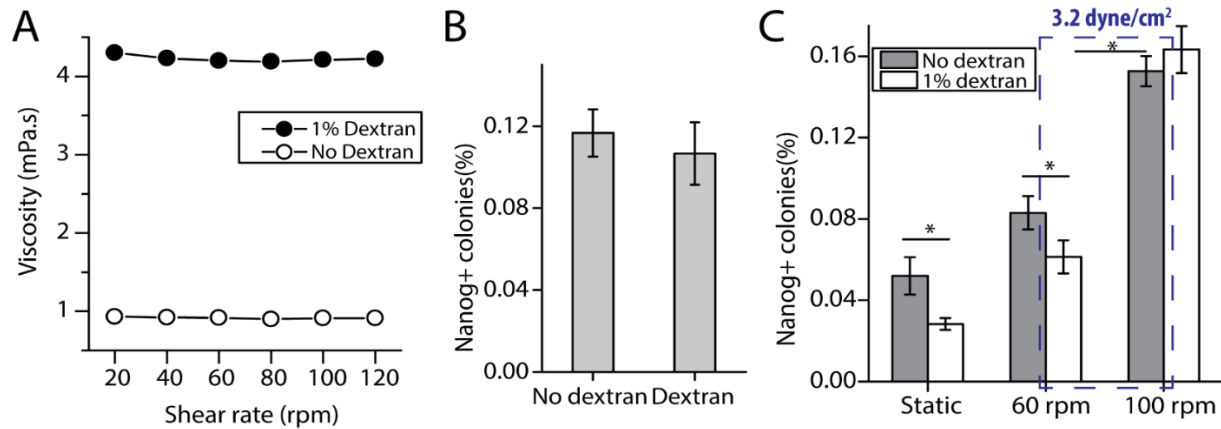


**Figure 2.7 Effect of mixing and shear stress on reprogramming efficiency.** **A)** Rheometer measurement of viscosity against shear rate for media with and without 1% dextran. **B)** Reprogramming efficiencies for media with and without dextran. Fibroblasts were seeded at 1000/cm<sup>2</sup> and reprogrammed under static culture condition. **C)** Reprogramming efficiency for fibroblasts seeded at 3000/cm<sup>2</sup> for various conditions. Dotted box indicates the two experimental conditions with the same magnitude of shear stress but different mixing rate. (\*p<0.05. n=3)

### 2.3.5 Effect of dynamic culture on mechanosensitive proteins YAP and $\beta$ -catenin

To explore the underlying mechanisms of how dynamic culture enhanced reprogramming, I examined the effects of dynamic culture on mechanosensitive signaling molecules YAP and  $\beta$ -Catenin. YAP is a transcriptional coactivator in the Hippo pathway and plays crucial roles in embryonic stem cell self-renewal and iPSCs reprogramming[43]. It translocates to the cytosol and becomes inactivated when cell density become too high, but can be reactivated by mechanical cues[44].  $\beta$ -catenin is a transcriptional coactivator in the Wnt pathway, and its activation and translocation into nucleus are critical in the later stage of reprogramming [45][46].  $\beta$ -catenin itself has also been found to be responsive to shear stress [47]. Importantly, both proteins have been implicated in contact inhibition and cell cycle arrest [48][49][50].

I started dynamic culture on day 6 for 48 hours before fixing and staining. I observed two main categories of cells in the reprogramming culture as described in previous literature: Emerging colonies and refractory cells (Fig 2.8A-B). Confocal image showed that localization of YAP and  $\beta$ -catenin was indistinguishable between the static and dynamic culture for both categories of cells (Fig. 2.8A-B). In addition, I performed Western blotting analysis of the bulk nuclear and cytoplasmic fractions and the results substantiated this observation (Fig. 5C). As an interesting side note, YAP was restricted to the cytoplasm for the emerging colonies, but showed both cytoplasm and nuclear localization in refractory cells (Fig. 2.8A-B).

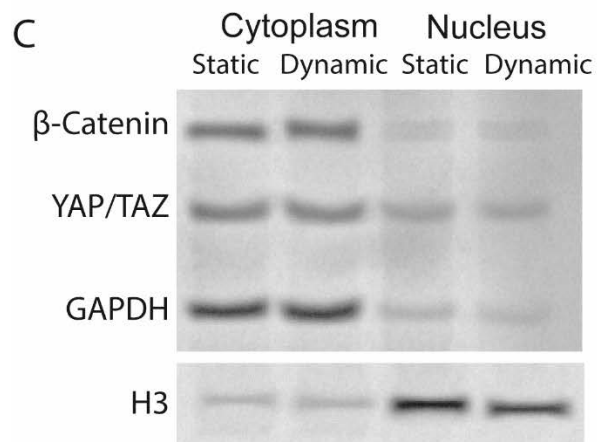
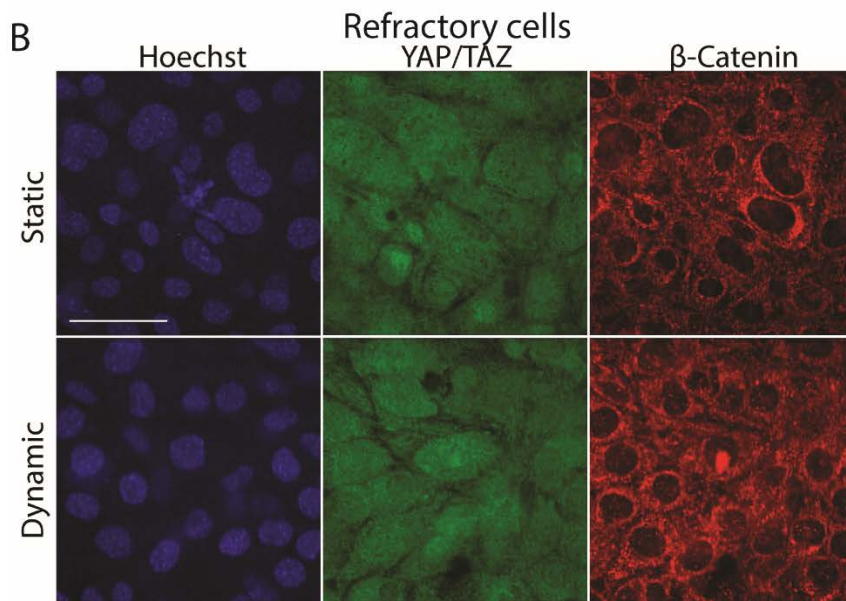
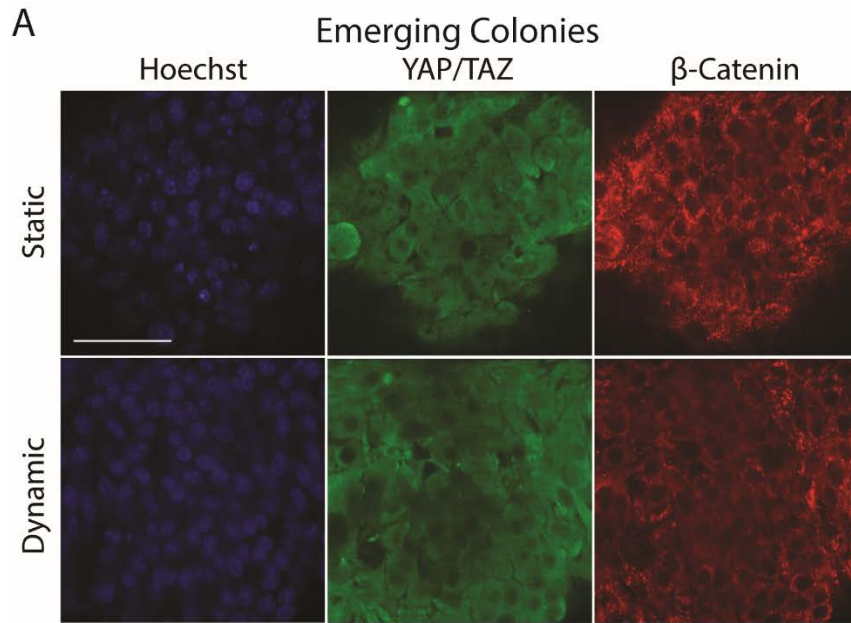


**Figure 2.8 Effect of dynamic culture on mechano-sensitive proteins. A-B)** Confocal microscope images for emerging colonies and refractory cells on day 8 for static and dynamic culture. Dynamic culture has been applied for 48 hrs. Scale bar denotes 100  $\mu$ m. **C)** Western blotting analysis of cytoplasmic and nuclear fractions for samples in A and B.

### 2.3.6 Effect of dynamic culture on reprogramming efficiency was mediated by p57 expression level

I further explored other pathways that may be regulated by dynamic culture. I know that a high proliferation rate is required for reprogramming [51], and that proliferation rate is inhibited when density becomes too high [52]. Therefore, I measured the transcript level of cyclin dependent kinase inhibitors (CDKi) from the Cip/Kip (p21, p57, p27) and Ink4 (p16) family for the static and dynamic culture on days 4 and 8 with RT-qPCR. For the dynamic culture sample, orbital shaking was applied from day 6 onwards. Of all the CDKis, mRNA level of p57 was upregulated 2-fold for the static culture from day 4 to day 8, but not so for the dynamic culture (Fig. 2.9A). Protein level as measured by Western blot also confirmed this observation (Fig. 2.9B).

I then further determined whether cell proliferation rate for static culture was lower. Specifically, I examined cells that are poised to undergo reprogramming. Expression level of Thy1 can be used as an early negative marker of reprogramming. Cells negative for this marker after four-factor induction are poised to undergo successful reprogramming [53]. Cells on day 8 were pulsed with EDU for 30 minutes before being fixed, stained and subjected to flow cytometry. The Thy1- fraction showed a lower proportion of EDU staining for static culture, implying that proliferation rate was indeed inhibited (Fig. 2.9C).

I next examined what caused p57 expression to be upregulated from day 4 to day 8. I hypothesized that the overconfluency of the culture from day 6 onwards promoted cell cycle arrest and upregulation of p57. I carried out 2 experiments to test this hypothesis. In the first experiment, on day 4 and day 8, I quantified p57 expression level of reprogramming cultures that were initially seeded at 1000 and 3000 cells/cm<sup>2</sup>, and observed upregulation of p57 for 3000 cells/cm<sup>2</sup> but not 1000 cells/cm<sup>2</sup> (Fig. 2.9D). This is in line with the observation that culture seeded at 1000 cells/cm<sup>2</sup> did not become confluent until day 12 or so, whereas culture seeded at 3000 cells/cm<sup>2</sup> became confluent from day 6 onwards. In the second experiment, I trypsinized and reseeded either a portion of the reprogramming cells on day 6 to a lower density or all of the cells to the same density as before. Cells seeded to a lower density did not upregulate p57 while those seeded to the same density did. Results from both experiments indicated that the upregulation of p57 in reprogramming cells was caused by the culture becoming over confluent.

Overconfluence of the culture led to upregulation of p57, and dynamic culture prevented it. Therefore, I hypothesize that the effect of dynamic culture on reprogramming efficiency was mediated through p57 regulation. To test this hypothesis, I performed siRNA knockdown of p57 in the static reprogramming culture to see if I could recapitulate the effect of dynamic culture. I transfected static reprogramming culture from day 6 onwards with either p57 siRNA or non-targeting control every 48 hours until day 14. 48 hours after the first transfection, I quantified p57 expression by RT-qPCR and confirmed that p57 transcript level was knockdown by about 50% (Fig 2.9F), which was the same extent of downregulation by dynamic culture (Fig 2.9A). By day 20, the reprogramming efficiency for the static culture with p57 siRNA knockdown was improved to the same level as that for dynamic culture (Fig 2.9G), indicating that downregulation of p57 with siRNA knockdown recapitulated the effect of dynamic culture.

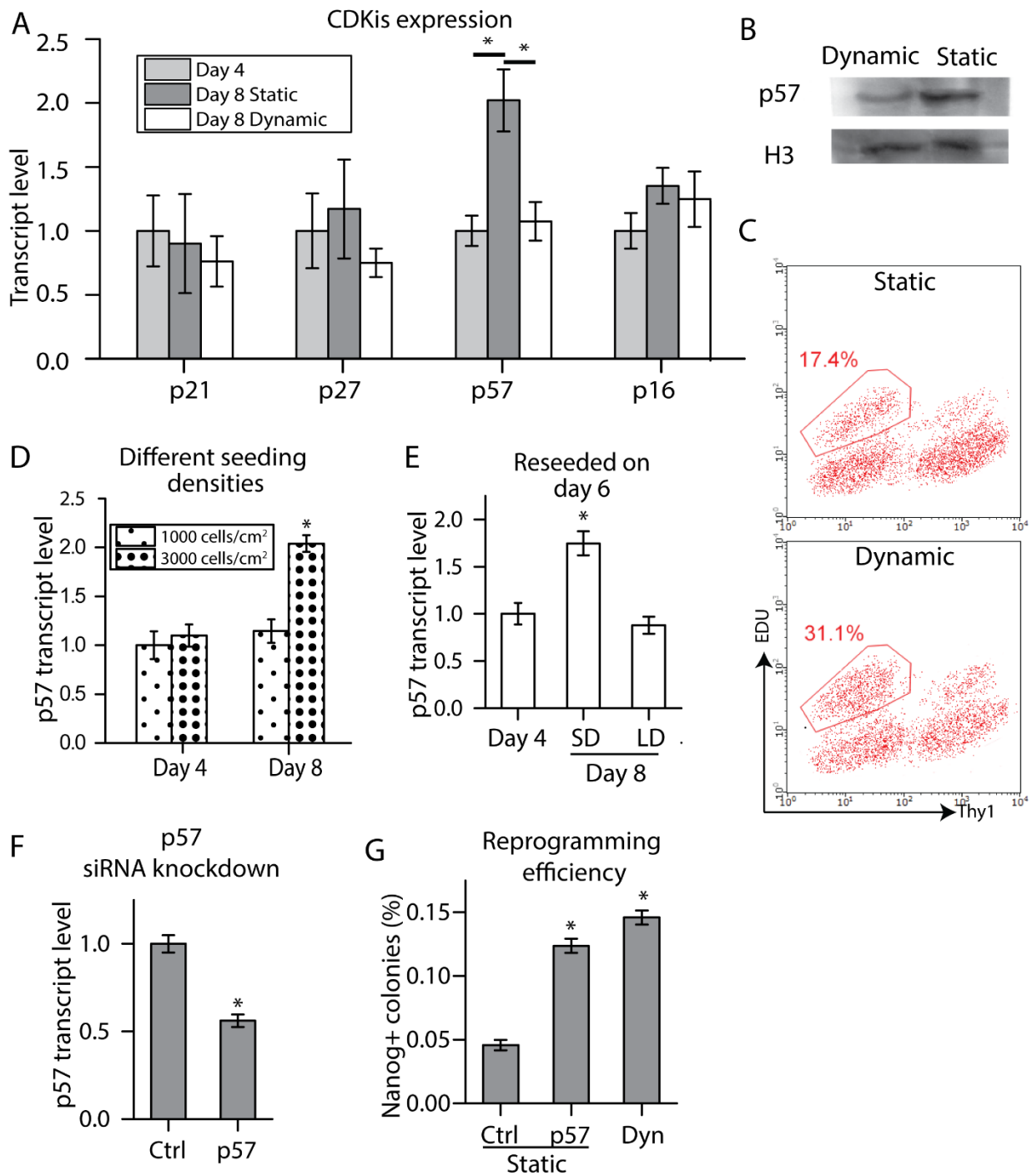


**Figure 2.9 Effect of static and dynamic culture on cell cycle.** **A)** RT-qPCR for various Cyclin Dependent Kinase Inhibitors. (\* $p < 0.05$ ,  $n = 3$ .) **B)** Western blot for p57 to verify A) at protein level. **C)** Flow cytometry for EDU staining on day 8. **D)** p57 expression of static reprogramming cultures over time at different seeding densities. (\* $p < 0.05$ , compared to 3000 cells/cm<sup>2</sup>, Day 4,  $n = 3$ .) **E)** Reprogramming culture initially seeded at 3000 cells/cm<sup>2</sup> was reseeded to lower density (LD) of 10000 cells/cm<sup>2</sup> or same density (SD) on day 6 and RT-qPCR was performed on day 8. (\* $p < 0.05$ , compared to Day 4,  $n = 3$ .) **F)** p57 siRNA was transfected into reprogramming culture on day 6 and RT-qPCR was performed on day 8. (\* $p < 0.05$ ,  $n = 3$ .) **G)** Reprogramming efficiency of cultures transfected with p57 siRNA. (\* $p < 0.05$ , compared to static, non-targeting control,  $n = 3$ .)

### 2.3.7 Dynamic culture synergized with small molecules to improve reprogramming efficiency

Addition of small molecules to the reprogramming media can improve reprogramming efficiency (reviewed in [54]). In particular, valproic acid, a HDAC inhibitor, and 616452, an Alk5 inhibitor, have been reported to improve efficiency significantly by at least several folds[55–57]. The exact mechanisms by which these chemicals improved reprogramming efficiency were not elucidated. I hypothesized that if these chemicals act via biological pathways that are orthogonal to p57 regulation, dynamic culture will have an additive or synergistic effect with them. I added 2 mM of valproic acid and 1  $\mu$ M of 616452 to the reprogramming media for the first 16 days during the doxycycline induction phase, and withdrew the chemicals together with doxycycline from day 16 onwards. Dynamic culture was started from day 6 onwards. Dynamic culture alone without any chemicals added improved efficiency by 2.5 folds (Fig 2.10A, B). Valproic acid improved efficiency by 4.5 folds under both static and dynamic culture (Fig 2.10A, B). 616452 improved efficiency by 3 folds under static culture, but by 7 folds under dynamic culture (Fig 2.10A, B). Therefore, dynamic culture did not have any synergistic effect with valproic acid, but synergized with 616452 to improve efficiency multiplicatively.

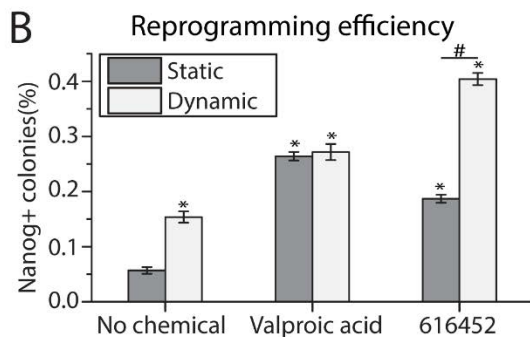
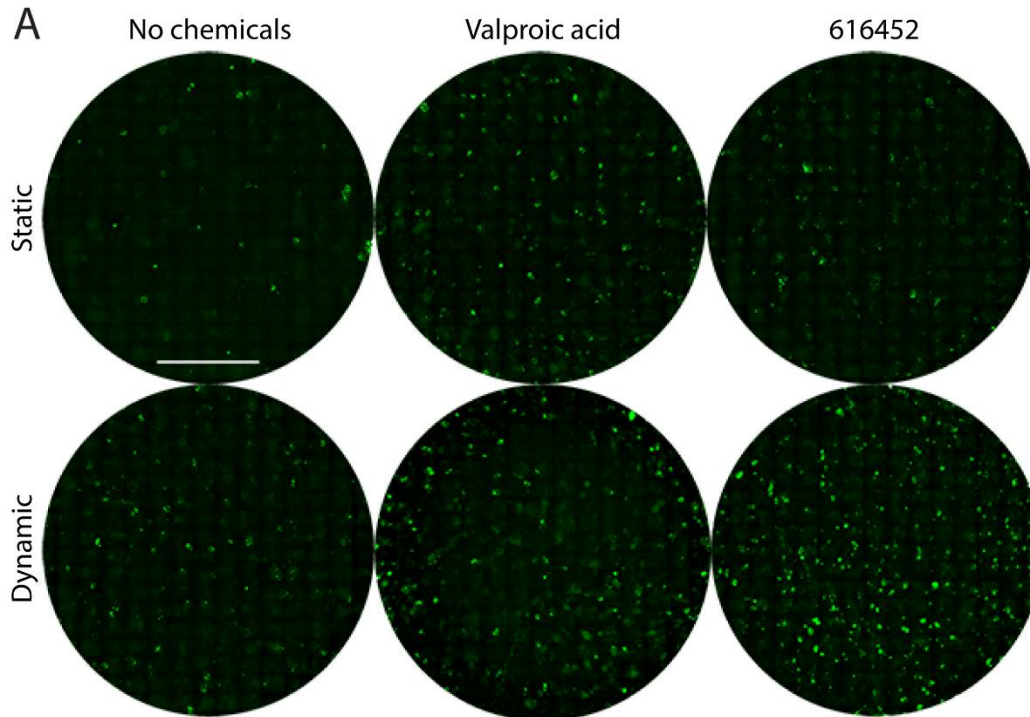


**Figure 2.10 Dynamic culture synergized with 616452 to improve reprogramming efficiency. A)** Representative whole well images of reprogrammed culture stained with Nanog. Scale bar denotes 10 mm. **B)** Quantification of Nanog positive colonies for different treatments. (\* $p < 0.05$ , compared to static with no chemicals.  $n = 3$ . # $p < 0.05$ .)

## 2.4 Discussion

Previous works have demonstrated the importance of cell proliferation on reprogramming[58][51][59][60] although the underlying reasons have not been elucidated yet. One possibility is that the extensive nuclear changes occurring during cell division allow the epigenome to be modified for the core-transcriptional circuitry of pluripotency to be established. For instance, it has been suggested that the large-scale remodeling of three dimensional chromatin architecture occurring during a brief period in early G1 phase may provide a window of opportunity to influence cellular identity in response to extracellular cues[61]. Another possibility is that the chromatin is in a less condensed state immediately following DNA replication, and this allows the Yamanaka factors to form transcription complexes at otherwise inaccessible pluripotency genes loci and subsequently turn on their expression[62]. During the initial phase of reprogramming, all cells undergo a dramatic increase in proliferation rate[63], and the culture would inevitably become over-confluent at some point. I demonstrate that this causes an upregulation of p57 and inhibits reprogramming through the inhibition of cell proliferation. By subjecting the culture to orbital shaking, upregulation of p57 is prevented and reprogramming efficiency is dramatically improved. Expression level of p57 has been directly implicated in reprogramming efficiency[64]. Reseeding the culture to a lower density upon reaching confluency could also improve efficiency, but not to the same extent as dynamic culture(Fig 2.6A-B), suggesting that the process of reseeding in itself is detrimental, as has been described before[65].

One question is then whether low seeding density could avoid over-confluency and thus obviate the need for dynamic culture in improving reprogramming efficiency. However, I demonstrated that this is not the case as reprogramming efficiency for sparsely seeded cells cultured statically is lower than more densely seeded cells cultured dynamically. Previous work has shown that E-cadherin mediated cell to cell contact is critical for reprogramming [42]. This and perhaps other juxtacrine signaling critical to reprogramming cannot occur effectively when seeding density is low. Under static condition, increasing seeding density allow such signaling processes to take place but also introduces the problem of over-confluency and inhibition of cell proliferation through upregulation of p57. Applying dynamic culture to sufficiently densely seeded culture mitigated the upregulation of p57, thus allowing optimal reprogramming efficiency to be obtained. Reprogramming efficiency was not improved by dynamic culture for sparsely seeded cells(Fig 2.6C). Confluency was never reached for 500 cells/cm<sup>2</sup>, thus explaining why dynamic culture did not improve efficiency at this seeding density since it exerted its beneficial effect only post confluence. Confluency was reached for 1000/cm<sup>2</sup> typically after day 12 and by then, cells probably have undergone sufficient number of divisions to be reprogrammed successfully.

To decouple the effect of convective mixing from hydrodynamic shear stress, I applied similar shear stress at different shear rates by adjusting the viscosity of the medium with dextran. Our results suggest that the beneficial property of dynamic culture is mainly attributed to mixing. However, the highest shear stress applied for all the experimental conditions was 7 dyne/cm<sup>2</sup>, which might not be high enough to stimulate the mechanotransduction pathways that affect reprogramming. Improving the transport rate of solutes through convective mixing

has two effects: first, more efficient removal of metabolic wastes and inhibitory cytokines from the cells; secondly, more efficient supply of nutrients to the cells. Either or both of these could contribute to maintaining cell proliferation rate post-confluence and improving successful reprogramming outcome.

In general, apart from direct cell to cell contact[66], contact inhibition could possibly be mediated by the local buildup or depletion of soluble factors[67], in which case dynamic culture could abolish these local gradients simply by bulk mixing. It will be interesting to study if this effect of dynamic culture on cell proliferation via p57 regulation manifests beyond the reprogramming context. If so, dynamic culture can be broadly applied to the expansion of adherent cell culture for regenerative medicine purposes.

I compared the effect of dynamic culture to small molecules boosters of reprogramming and test for synergistic effects between the two. Dynamic culture did not synergize with valproic acid, suggesting that both of them could be acting along related pathways to improve efficiency. For instance, it has been reported that valproic acid prevented senescence in reprogramming cells possibly by downregulating p16 and p21 expression[55]. The functions of p57, p16 and p21 overlap to some degree in that they all inhibit the activity of Cyclin Dependent Kinases 4 and 6[68–70]. Thus, by downregulating p16 and p21, valproic acid could be inducing the same effect as downregulation of p57 by dynamic culture. On the other hand, dynamic culture synergized with 616452 to improve reprogramming efficiency. This suggested that p57 upregulation still posed as a barrier to reprogramming in 616452 treated culture, and dynamic culture helped remove this barrier. In fact, it was noted that 616452 treatment resulted in higher cell number during the starting phase of reprogramming, thus possibly exacerbating overconfluency and p57 upregulation[56]. Thus, dynamic culture could be mitigating this undesirable side effect, thus further enhancing the effect of 616452 treatment on reprogramming efficiency.

In conclusion, over confluency in reprogramming cultures inhibit cell proliferation and subsequently reprogramming efficiency. Dynamic culture could ameliorate this heretofore unaddressed phenomenon to easily and effectively improve reprogramming efficiency.

## Chapter 3: Effect of Biophysical Cues on Reprogramming to Cardiomyocytes

### 3.1 Introduction

Fibroblasts were first demonstrated to be capable of being reprogrammed into cardiomyocytes by the forced expression of three transcription factors: Gata4, Mef2c and Tbx5[4]. However, the efficiency of this process is low and only about 0.01%-0.1% of the starting population become beating cardiomyocytes. Since this possibility was demonstrated about 5 years ago, much effort has been undertaken to improve the efficiency of this process, as reviewed in ref [71]. These approaches can be broadly classified into addition of miRNAs[72–74], small molecules[75], proteins[76] and modification of transcription factors[77–80]. More recently, it has also been shown that the addition of fibroblast growth factor (FGF) 2, FGF10 and vascular endothelial growth factor (VEGF) to serum free culture media significantly increased the yield of beating cardiomyocytes[81], demonstrating that culture conditions could also affect reprogramming efficiency.

Cells sense and respond to physical cues in their environment. In the previous chapter, I have described some biophysical approaches demonstrated to improve efficiency of reprogramming to iPSCs. For reprogramming to other somatic cell types, literature demonstrating the enhancing effect of biophysical cues is scarce, with only one work showing that microtopography can enhance reprogramming to neurons[82].

Nevertheless, various physical cues have been amply demonstrated to have positive effects on the development of cardiomyocytes. Mechanical stretching improved the maturation of cardiomyocytes that were differentiated from mesenchymal stem cells [83]. Softer substrates favored the maturation of neonatal cardiomyocytes in terms of sarcomere assembly, calcium transients and gene expression[84,85]. Microgrooves have been found to enhance the differentiation and maturation of cardiomyocytes[86–88] from stem cells.

Therefore, the effects of physical cues on cell reprogramming and on cardiomyocyte development have been separately established, and this work studied the effects of several biophysical cues on direct reprogramming from fibroblasts to cardiomyocytes.

I screened the effect of cyclical mechanical stretch, substrate stiffness and microgroove on efficiency of reprogramming from fibroblasts to cardiomyocytes, and found an enhancement in the induction of cardiomyocyte-like cells with microgroove. Long term culture on microgroove combined with an optimized culture protocol[81] further increased the yield of completely-reprogrammed beating cells compared to flat surface. I also showed how microgroove improved reprogramming to cardiomyocyte by regulating Mkl1 activity and also enhancing organization of sarcomeric structure. This work established how topographical cues can affect reprogramming to cardiomyocytes and provided insights into the underlying mechanisms.

## 3.2 Materials and Methods

### 3.2.1 Cell culture and reprogramming

To obtain tail tip fibroblasts, neonates of  $\alpha$ MHC-GFP transgenic mouse[4] were sacrificed by decapitation and the tail tips excised. Tail tips were digested with 2 mg/ml collagenase for 30 minutes and plated for explant culture. After a week, cells were frozen down into aliquots. To obtain Thy1+/GFP- cardiac fibroblasts, hearts from neonates were digested with 2 mg/ml collagenase and cultured for 3 days in growth media. Cells were then passed through a 40  $\mu$ m cell strainer and incubated with APC conjugated anti-Thy1 antibody (eBioscience, 17-0909-41) before sorting with BD Bioscience Influx Sorter.

To make Gata4, Mef2c, Tbx5 and Mkl1 retroviruses, Platinum E cells were transfected with pMX plasmids encoding these genes using Fugene 6 overnight. Media was replaced the next day, collected after 24 hours and passed through a .45  $\mu$ m syringe filter. This virus containing media was used within the same day to transduce seeded fibroblasts.

For reprogramming experiments, fibroblasts were seeded onto tissue culture plates and then transduced with virus overnight. Transduced fibroblasts were then reseeded onto the various substrates, which have been prepared as described below, at 10000 cells/cm<sup>2</sup>. Media was changed to DMEM/M199, 10% FBS, 1% NEAA, 1% Pen/Strep (reprogramming media) and replaced every 3 days.

For optimized culture to obtain beating cells[81], transduced fibroblasts were cultured in reprogramming media for the first 2 weeks. For the next 2 weeks, media was switched to StemPro-34 SF medium (GIBCO) with 1X GlutaMAX (GIBCO), 1% Pen/Strep, 50  $\mu$ g/ml ascorbic acid (Sigma Aldrich), 5 ng/ml recombinant human VEGF (R&D Systems), 10 ng/ml recombinant human bFGF ( R&D Systems), and 50 ng/ml recombinant human FGF10 (R&D Systems).

### 3.2.2 Fabrication of stretching device

Refer to Appendix A

### 3.2.3 Polyacrylamide gels fabrication

Protocol for fabricating hydrogel substrate was adapted from previously published work[89]. 22 mm by 22 mm coverslips were soaked in 2N NaOH for 20 mins, rinsed in DI water and dried by N<sub>2</sub>. Coverslips were then treated for 5 mins in a 1% (v/v) methacryloxypropyltrimethoxysilane (Gelest), 94% (v/v) methanol (MeOH), 5% (v/v) water solution with glacial acetic acid added to a final concentration of 1mM. Thereafter, coverslips were rinsed thoroughly in methanol before being oven baked at 110°C for 30 minutes. Polyacrylamide gel solutions were prepared with varying concentrations of acrylamide and Bis acrylamide to vary rigidity. *N*-acryloyl-6-aminocaproic acid (ACA, TCI) monomer was added to a final concentration of 100 mM. Rigidities for the various formulations were confirmed by rheometry (Appendix B). Ammonium persulfate (Biorad) and TEMED (Sigma Aldrich) were added to the gel solutions to a final concentration of 0.1% and mixed briefly. 25  $\mu$ l of the polymerizing solutions were quickly placed on a Gel Slick™ (Lonza) treated glass slide before the silanized coverslips were placed on top. The gels were allowed to polymerize for 2 hours before being peeled off from the glass slide. The gels were sterilized in 70% ethanol for 15

minutes and rehydrated in MES buffer (0.1 M 2-(*N*-morpholino) ethanesulfonic acid, pH 6.2). Then, the carboxyl groups of the ACA were activated with 0.2 M EDC and 0.5 M NHS (ThermoFisher Scientific) in MES buffer for 30 min at room temperature. Gels were then washed quickly with PBS before being reacted with 0.25 mg/ml Matrigel diluted in PBS overnight at 4°C. Cells were seeded the next day.

### **3.2.4 Microgroove membrane fabrication**

SU 8 mold was fabricated with standard photolithographic technique, as previously described[86]. Briefly, SU 8 photoresist (Microchem) was spin-coated onto a silicon wafer and polymerized by exposure to UV through a patterned chrome mask. The unpolymerized photoresist was subsequently washed away in developer solution. PDMS was spin coated over the SU 8 mold and cured. Cured membrane was washed with 70% ethanol, oven dried overnight and then oxygen plasma treated. Immediately afterwards, membrane was coated with 0.25 mg/ml Matrigel for 30 minutes before cell seeding.

### **3.2.5 Immunostaining, imaging, flow cytometry and quantification**

For immunostaining, cells were fixed in 4% paraformaldehyde and permeabilized with 0.5% Triton-X 100, both for 15 minutes. Cells were then incubated with Phalloidin (ThermoFisher Scientific), anti-cardiac troponin T (MS-295-P, Thermo Scientific) or anti-Mkl1 (sc-21558, Santa Cruz) antibodies overnight at 4°C. Secondary antibody (Alexafluor 546, ThermoFisher Scientific) were added for at least 1 hour before the nuclei were stained with Hoechst. Imaging was performed on a Zeiss AxioObserver epi-fluorescent microscope.

To quantify reprogramming efficiency at day 10, samples were trypsinized and analyzed for number of GFP+ cells using Guava. This number was then normalized by the number of cells seeded to give reprogramming yield. For quantification of cTnT+ cells by flow cytometry, samples were trypsinized and fixed with 4% PFA for 15 minutes. Samples were then permeabilized and blocked concurrently with 0.4% saponin and 5% donkey serum diluted in PBS. Anti-GFP (GFP-1010, Aves Labs) and anti-cardiac troponin T (MS-295-P, Thermo Scientific) antibodies were added followed by secondary antibodies (Alexafluor 546, ThermoFisher Scientific & F-1005, Aves Lab). In between every steps, cells were spun down and washed with PBS once.

For quantification of cTnT+ cells by imaging, plates containing stained adherent cells were loaded onto ImageXpress Micro High-Content Analysis System (IXM, Molecular Devices) for automated whole well imaging at 10X magnification. The images were then loaded in Photoshop (Adobe) for manual counting. A transparent layer was created and positive cells were marked and covered with a circular brush. The layer was then saved as a separate image and the number of circular marks were counted using ImageJ.

For quantification of beating cells, I first stained cells with Rhod2-AM (Abcam) to visualize spontaneous calcium transient. The culture plate were then loaded into IXM and viewed under 10X magnification frame by frame through Cy3 filter to identify cells with calcium flux and spontaneous contraction. When necessary, objective was changed to 20X and filter to phase contrast to confirm sighting of spontaneous contraction.

For quantification of Mkl1 nuclear intensity, 20X images of Mkl1 staining and the corresponding nuclear staining with Hoechst were acquired with fluorescent microscope. The images were analyzed with CellProfiler [90] using a custom designed pipeline to measure the intensity of Mkl1 staining integrated over the nuclear region as demarcated by Hoechst staining for each cell.

### 3.2.6 Real time quantitative polymerase chain reaction

At the indicated time, culture was lysed with Trizol (ThermoFisher Scientific) and RNA was extracted following the manufacturer's instruction. RNA concentration was quantified with Nanodrop 1000 (Thermo Scientific) and equal amount was loaded for cDNA synthesis using Maxima First Strand cDNA Synthesis Kit (ThermoFisher Scientific). cDNA was then loaded into 96 well PCR plate with primers and Maxima SYBR Green qPCR Master Mix (ThermoFisher Scientific). Thermal cycling and data acquisition was performed on iQ5 system (Biorad). GAPDH was used as housekeeping gene. Data was analyzed with  $\Delta\Delta C_t$  method. Primer information is listed in table 3.1. To measure endogenous expression of Gata4, Mef2c and Tbx5, primers were designed to include the 5' UTR of the genes. To measure viral expression of Gata4, Mef2c and Tbx5, primers were designed to include the psi packaging signal of the viral vector.

**Table 3.1** Primer information

	<b>Forward</b>	<b>Reverse</b>
Endogenous Gata4	CTGGCCAGGACTGCCG	TGCTTTCTGCCTGCTACACA
Endogenous Mef2c	GGGGGTTTCTCTTCAAAGCCA	CAATGCTTTTGTGGCACCAGT
EndogenousTbx5	AATCCCCAGCACAAACTCCA	CGAGGTTCTATTCTCGCTCTG
Viral Gata4	GCCGCCACGTGAAG	CTTTGGTACATGGCAGTCTAGAGG
Viral Mef2c	CCATCCTCTAGACTGCCGGA	GTCACCTGTCTGTTACGCTCA
Viral Tbx5	GGGTGGACCATCCTCTAGACT	GGCCAAAGCCCTCATCTGTA
Total Gata4	GCTCCATGTCCCAGACATTC	ATGCATAGCCTTGTGGGGAC
Total Mef2c	CAGTTGGGAGACCGTACCAC	GGAGTGGAATTCGTTCCGGT
Total Tbx5	TGGACCCGTTGGACACATTA	GGAAGACGTGGGTGCAAAC
Mkl1	CATGAAGGTGGCAGAGCTGA	ACTTGGTCTTGGTAGGCACG
Tnnt2	GTGTGCAGTCCCTGTTTCTAGA	GCTTGGGTTTGGTGTCTCT
Nkx 2.5	ATTTTACCCGGGAGCCTACG	CAGCGCGCACAGCTCTTTT
Actn2	AATCAGATAGAGCCCGGCG	AGTGAACGTCTTCTCTGCTG
Hand2	CACCAGCTACATCGCCTACC	TCTCATTAGCTCTTTCTTCTCT
Desmin	CAGAGGCTCAAGGCCAAACTA	AGGGATTTCGATTCTGCGCTC
Col1a1	CGATGGATTCCCGTTCGAGT	GAGGCCTCGGTGGACATTAG
Postn	AGGTGGCGATGGTCACTTAT	ACGGCCTTCTCTTGATCGTC
Snai1	CACACGCTGCCTTGTGTCT	GGTCAGCAAAAGCACGGTT
Gapdh	TTGAGGTCAATGAAGGGGTC	TCGTCCCGTAGACAAAATGG

### 3.3 Results

#### 3.3.1 Microgroove improved yield of cardiomyocyte like cells

I sought to investigate how different biophysical factors may affect the efficiency of reprogramming. I studied the effects of cyclical uniaxial stretch, substrate stiffness and microgroove. In order to quantify conversion of fibroblasts into cardiomyocytes conveniently, I utilized a  $\alpha$ MHC promoter-driven EGFP transgenic mice ( $\alpha$ MHC-GFP), in which only cardiomyocytes expressed the green fluorescent protein (GFP) [4]. I transduced neonatal tail tip fibroblasts (TTF) obtained from the  $\alpha$ MHC-GFP transgenic mouse with retroviruses encoding Gata4, Mef2c and Tbx5 (GMT) overnight, and reseeded the transduced cells on the different surfaces the next day (Fig 3.1). After 10 days of culture, I analyzed the cells with flow cytometry to quantify the number of  $\alpha$ MHC-GFP+ cells. This number was normalized by the initial number of cells seeded to give the reprogramming yield.

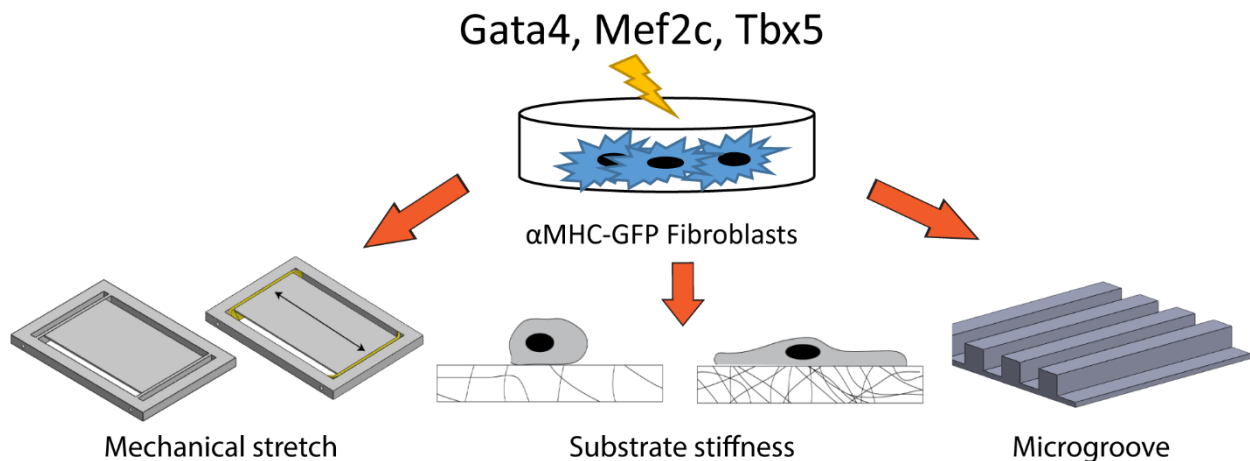


**Figure 3.1 Schematics of experiments.** TTF from  $\alpha$ MHC-GFP mice were transduced with GMT overnight before seeding onto the various substrates. Flow cytometry was performed on day 10 to quantify GFP+ cells.

For mechanical stretching, TTF stretched at both frequencies gradually re-orientated such that by day 10, almost all cells were perpendicular to the direction of stretch (Fig 3.2A). This showed that the magnitude of stretch (10%) was large enough to stimulate a cytoskeletal response. As a result of cyclical stretch, efficiency was significantly lowered for 1 Hz frequency (Fig 3.2B).

For different substrate stiffness, TTF cultured on glass and 1 kPa substrate were the most and least spread out respectively. TTF on 21 kPa and 62 kPa were moderately spread out and indistinguishable from each other morphologically (Fig 3.2C). TTF attached equally well on all the stiffness substrates (Fig 3.3A). Yield of GFP+ cells was not significantly different for the different stiffness (Fig 3.2D).

For microgroove, cells aligned in the direction of the groove and exhibited an elongated morphology (Fig 3.2E, Fig 3.4). TTF attached equally well on the flat and grooved substrates after seeding (Fig 3.3B), but proliferated slightly less quickly on the grooved substrate (Fig 3.3C). Yield of GFP+ cells was about 50% higher for the various dimensions of groove tested compared to flat surface (Fig 3.2F).

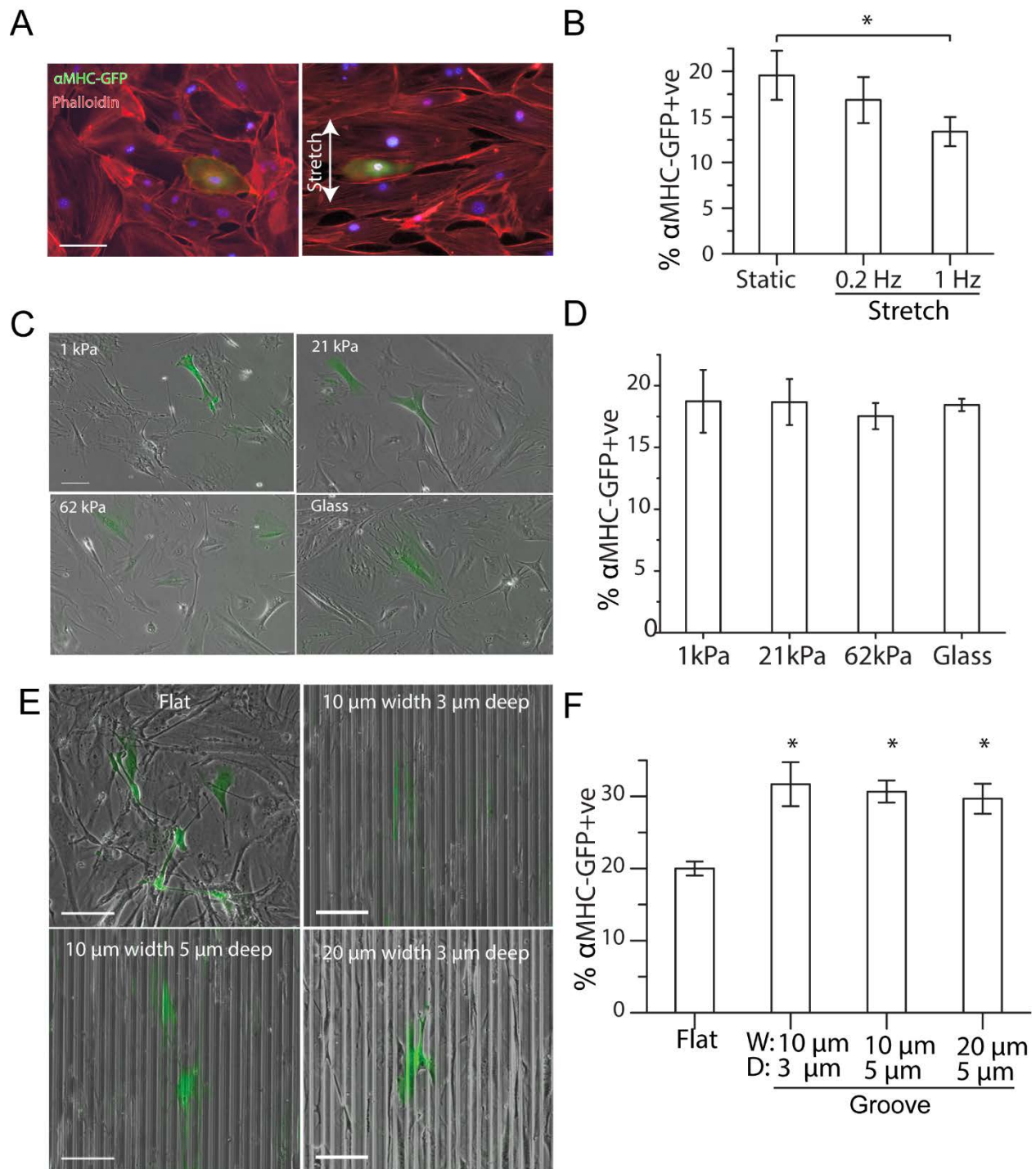


**Figure 3.2 Screen for physical cues that may affect efficiency of reprogramming to cardiomyocytes. A)** Transduced TTF with and without cyclical stretch fixed and stained on day 10. Scale bar denotes 50  $\mu\text{m}$ . **B)** Yield of GFP+ cells, normalized by initial number of cells seeded, quantified on day 10 after stretching at various frequencies. (\* $p < 0.005$ , Bonferroni test, compared to static.  $n = 5$ .) **C)** Phase contrast images of TTFs on various stiffness on day 10. GFP signal was overlaid. Scale bar denotes 100  $\mu\text{m}$ . **D)** Yield of GFP+ TTF cultured on various stiffness on day 10. ( $n = 5$ ) **E)** Phase contrast images of TTFs on various topographies on day 10. Scale bar denotes 100  $\mu\text{m}$ . **F)** Yield of GFP+ TTF cultured on various topographies on day 10. (\* $p < 0.001$ , Bonferroni test.  $n = 4$ )

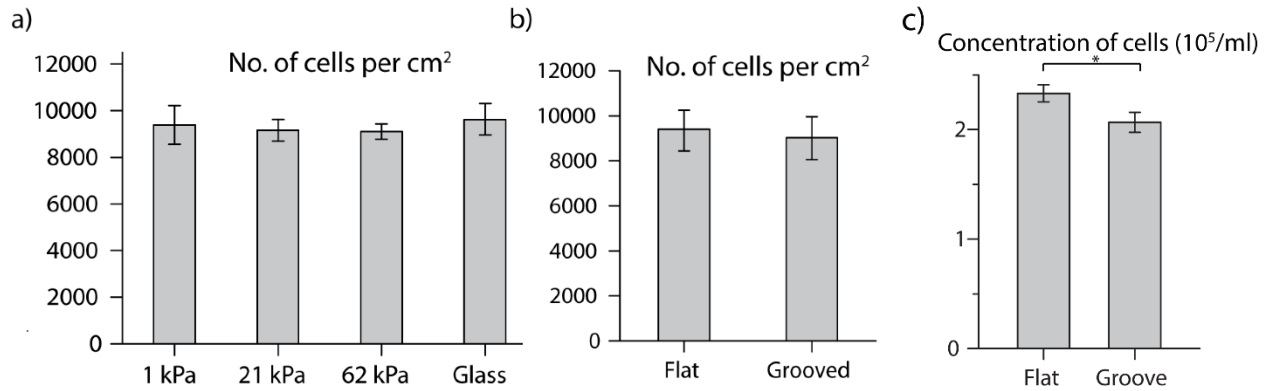


**Figure 3.3 Quantification of cells on different substrates. A)** Attachment of GMT transduced tail tip fibroblasts on different stiffness substrate. **B)** Attachment of GMT transduced tail tip fibroblasts on flat and grooved surface. In both cases, cells were seeded at 10000/cm<sup>2</sup>. After 8 hours, samples were washed to remove unattached cells, fixed and stained with Hoechst. Images of nuclei were acquired at 10X magnification and quantified with ImageJ software. n=3. **C)** Concentration of GMT transduced tail tip fibroblasts on flat and grooved surface on day 10 as quantified by flow cytometry. (\*p<0.05. n=3)

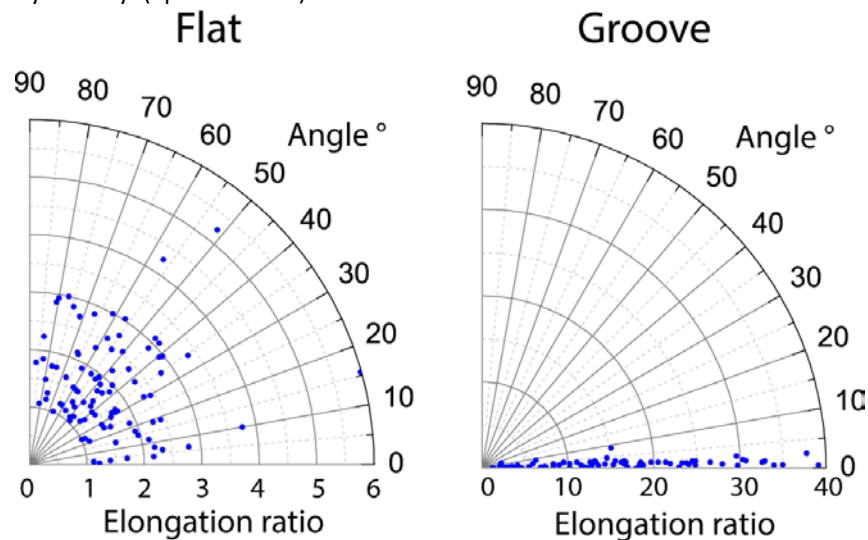


**Figure 3.4 Alignment of cells on microgrooved substrate.** TTF were cultured on flat and grooved surface for 2 days before CellTracker™ Orange was added to fluorescently label the cells. Fluorescent images were acquired with microscope and analyzed with ImageJ. Elongation ratio was calculated by fitting an ellipse over the cell and dividing the length of major axis by that of the minor axis.

To further characterize the GFP+ cells, I stained the cells for cardiac troponin T (cTnT), a specific sarcomeric marker of differentiated mature cardiomyocytes[91], and performed flow cytometry. I observed that the culture from grooved surface also had higher population of cTnT+ cells at day 10 (Fig 3.5A). I also tracked the yield of GFP+ cells over time and observed that a difference emerged between the flat and grooved culture by day 4 (Fig 3.5B). I performed RT-qPCR on reprogramming cultures at day 2 while the GFP+ population size was similar (Fig 3.5B) between the two surfaces so that any differences in transcript level would not be an artifact of difference in population size. After two days of culture on microgroove, some cardiomyocyte genes (Gata4, Mef2c, Tbx5, Nkx2.5, Hand2, Actn, Tnnt2) were already significantly upregulated on the grooved surface compared to flat (Fig 3.5C), indicating that

microgroove regulated the reprogramming process from an early stage onwards. Using primers that targeted the endogenously and virally expressed mRNA separately, I attributed the upregulation of Gata4, Mef2c and Tbx5 to the endogenous genes (Fig 3.5D-E), so as to rule out the possibility that microgroove was somehow enhancing the expression of viral transgenes. Previous works have shown that downregulating fibroblast signature could improve efficiency of reprogramming to cardiomyocytes [73–75] and that microgroove could downregulate the expression of fibroblast genes in reprogramming to pluripotent stem cells [92]. However, the expression level of fibroblast genes (Col1a1, Postn, Snai1) was not significantly different between the flat and grooved surface for GMT transduced TTF, indicating that grooved surface did not downregulate these fibroblast genes and that this effect may be context dependent.

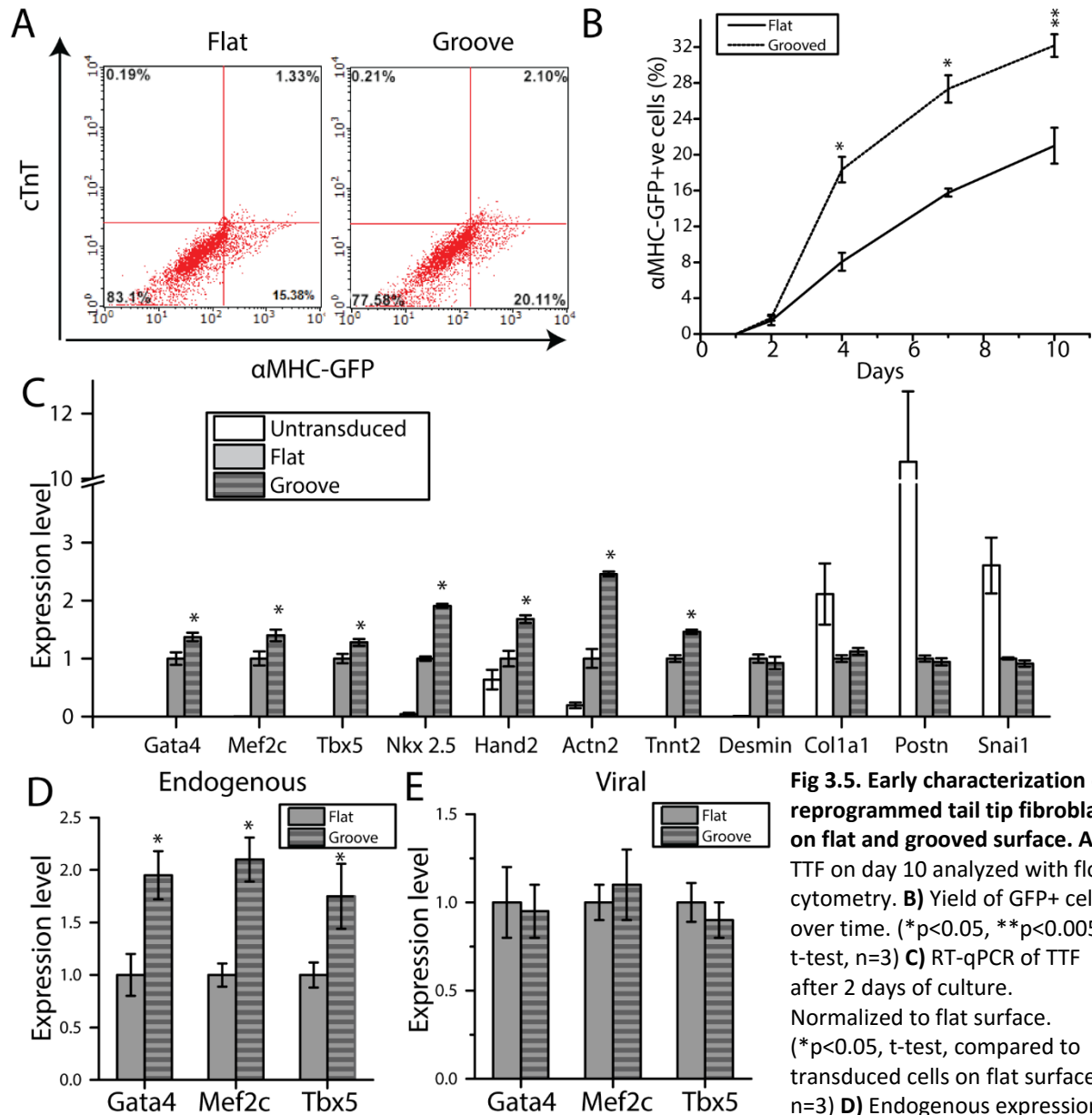


**Fig 3.5. Early characterization of reprogrammed tail tip fibroblasts on flat and grooved surface. A)** TTF on day 10 analyzed with flow cytometry. **B)** Yield of GFP+ cells over time. (\* $p < 0.05$ , \*\* $p < 0.005$ , t-test,  $n = 3$ ) **C)** RT-qPCR of TTF after 2 days of culture. Normalized to flat surface. (\* $p < 0.05$ , t-test, compared to transduced cells on flat surface.  $n = 3$ ) **D)** Endogenous expression of GMT. (\* $p < 0.05$ , t-test,  $n = 3$ ) **E)** Viral expression of GMT. ( $n = 3$ ).

### 3.3.2 Microgroove improved the yield of functional cardiomyocytes

I continued the culture of GMT transduced TTF for up to 1 month and still did not observe any beating cells on flat and grooved surface, suggesting that although the  $\alpha$ MHC promoter was activated in these cells, they were only partially reprogrammed and not functional. To attempt to achieve complete reprogramming, I employed an optimized culture protocol published recently [81]. In this protocol, reprogramming cells were cultured in DMEM/M199/serum medium for the first 2 weeks and then in a serum-free medium supplemented with FGF2, FGF10 and VEGF for the next 2 weeks (Fig 3.6A). With this protocol, I still did not observe any beating cells from TTF. Staining with Rhod-2-AM also did not reveal any spontaneous calcium transient. However, I observed distinctly cTnT+ cells by immunofluorescent staining (Fig 3.6B, 3.6D), although this cTnT signal was diffused and did not show the striated pattern that would be observed for properly assembled sarcomeres in functional cardiomyocytes. Nevertheless, microgrooved surface increased the number of cTnT+ cells by close to 1 fold (Fig 3.6C).

Previous works have demonstrated that cardiac fibroblasts were more amenable to reprogramming into cardiomyocytes than tail tip fibroblasts[4,81], so I performed the same experiment using cardiac fibroblast (CF) as the starting cells. More specifically, I used the Thy1+/GFP- population isolated from digested neonatal heart using FACs (Fig 3.7A) to prevent contamination by resident cardiac progenitors and cardiomyocytes. After transducing them with GMT and culturing them for 1 month with optimized culture protocol, the number of cTnT+ and contracting cells was about one fold higher on the grooved surface (Fig 3.7B-D). cTnT immunostaining revealed striated patterns in many of the cells (Fig 3.7F), indicating formation of sarcomeric structures. Some of these reprogrammed cells exhibited calcium transient (Fig 3.7E) and also contracted spontaneously. This increase over the flat surface was higher than the half fold increase in cTnT+ cells measured on day 10 (Fig 3.5A), suggesting that the beneficial effect of microgroove on reprogramming was cumulative over the longer duration of culture.

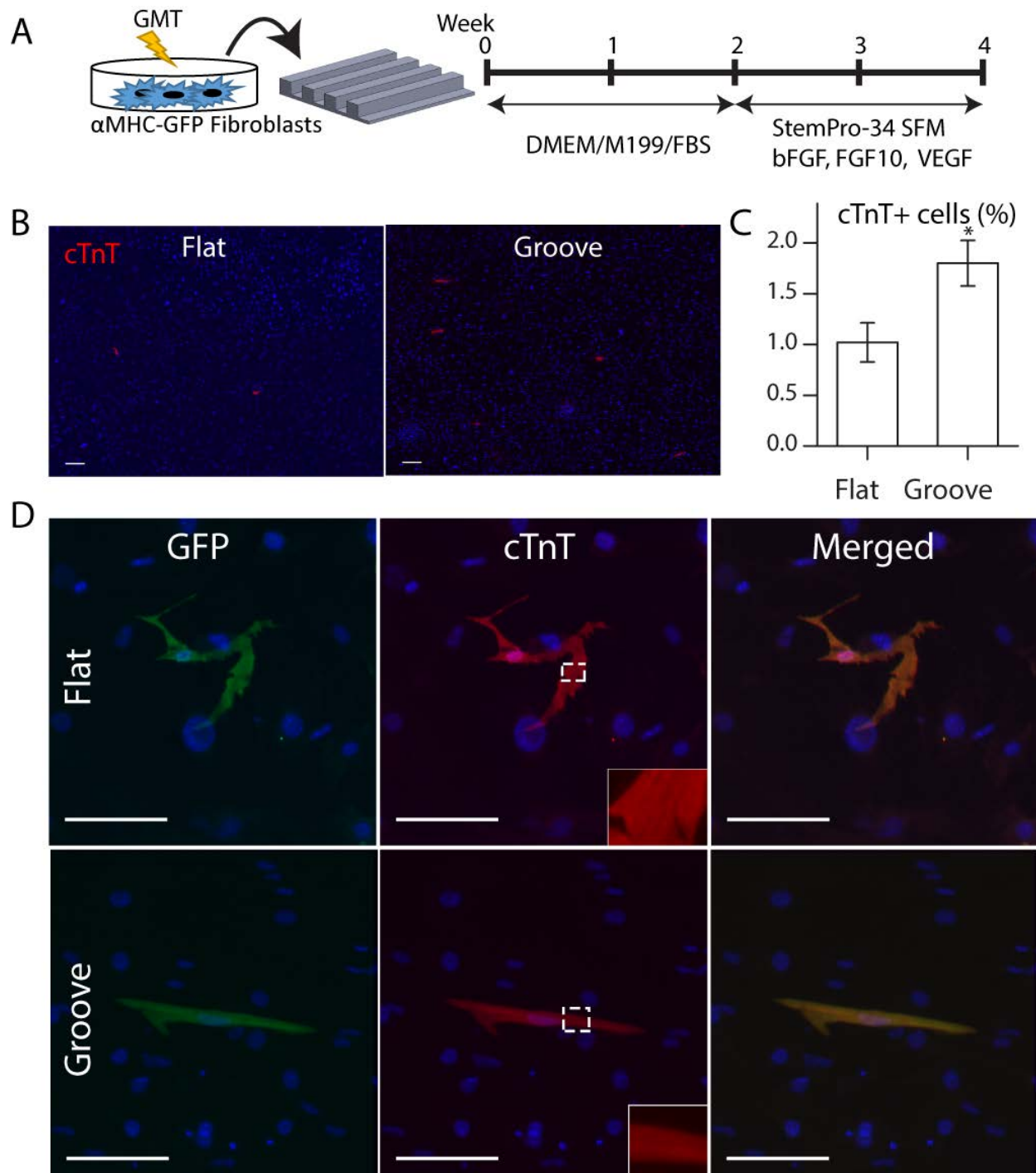


**Figure 3.6 Reprogramming of tail tip fibroblasts with optimized culture.** **A)** Schematics of optimized culture for enhancing complete reprogramming. Transduced fibroblasts were seeded on substrates and cultured for 2 weeks in reprogramming media and then 2 more weeks in serum-free medium supplemented with FGF2, FGF10 and VEGF **B)** Representative low magnification view of cTnT staining for flat and groove samples after optimized culture of transduced TTF. Scale bar denotes 100  $\mu$ m. **C)** Quantification of cTnT+ cells on flat and grooved surface. (\* $p < 0.001$ ,  $n = 5$ ) **D)** cTnT staining on flat and groove surface after optimized culture. Scale bar denotes 100  $\mu$ m.

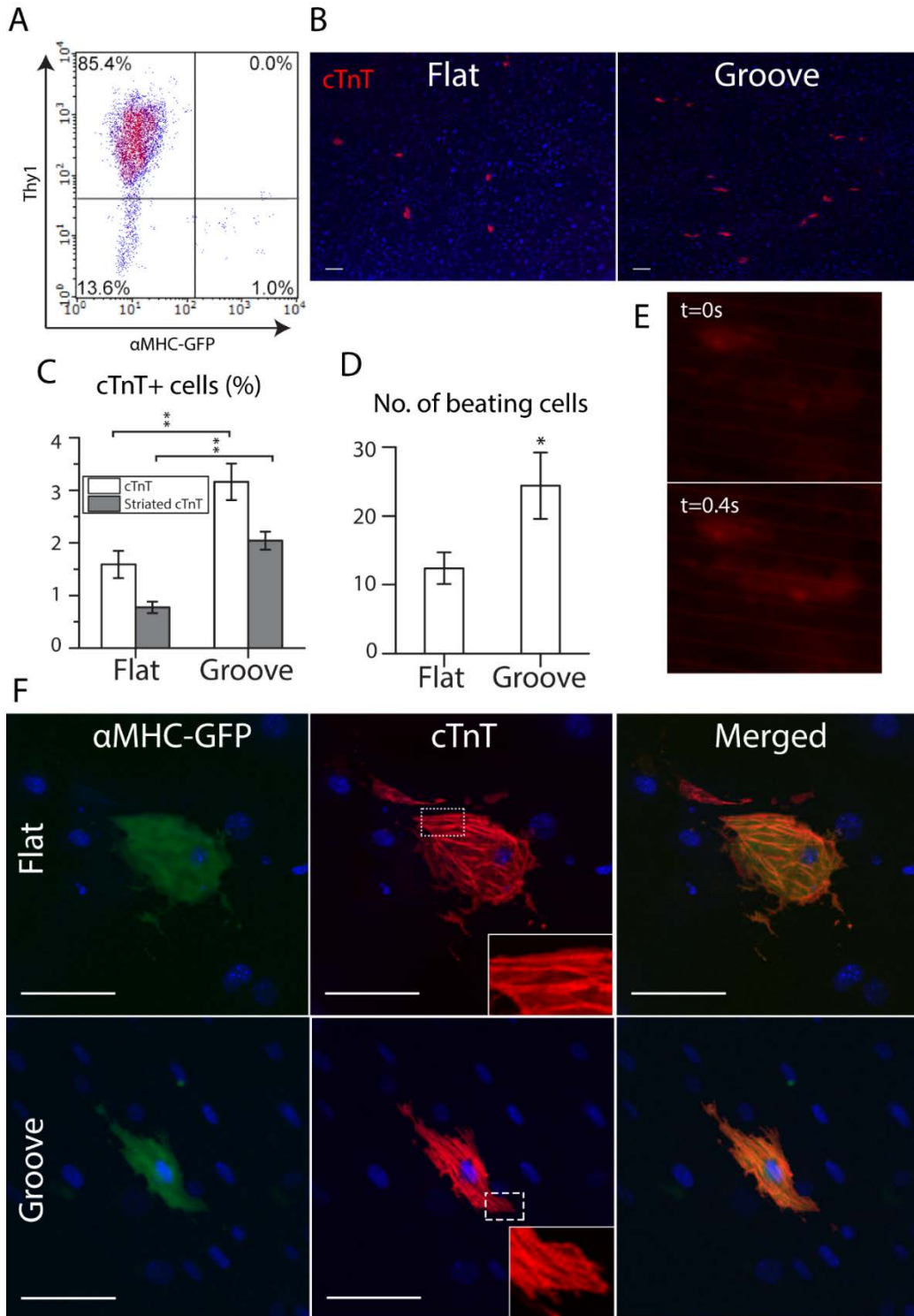
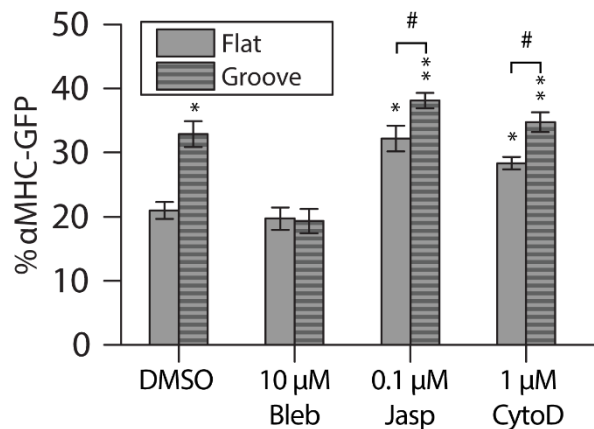


**Figure 3.7 Reprogramming of cardiac fibroblasts with optimized culture. A)** FACS plot of Thy1+/GFP- cells isolated from digested hearts of neonatal  $\alpha$ MHC-GFP mice. **B)** Representative low magnification view of cTnT staining for flat and groove samples after optimized culture of transduced CF. Scale bar denotes 100  $\mu$ m. **C)** Quantification of cells with cTnT expression and with cTnT that displayed striation. (\*\* $p < 0.001$ ,  $n = 5$ ) **D)** Quantification of beating cells per well of a 12 well plate. (\* $p < 0.005$ ,  $n = 5$ ) **E)** Still image captures of oscillating calcium transients visualized through Rhod2 AM staining. **F)** cTnT staining on flat and groove surface after optimized culture. Scale bar denotes 100  $\mu$ m.

### 3.3.3 Cytoskeletal drugs treatment suggested effect of microgroove was mediated by Mkl1

The actin cytoskeleton forms an interconnected network for the transmission of mechanical signals from the cell surface to sites where they are transduced into biochemical responses[93,94]. A critical component of the actin cytoskeletal network is myosin II, which crosslinks actin fibres end to end and pulls them together, thus generating tension for the effective transmission of mechanical forces[95]. I initially hypothesized that the structural continuity of the actin network and activity of myosin II were critical for the cells' response to the microgrooved substrate by transmitting the passive mechanical signals from the substrate to biochemical nodes within the cell. I sought to test this hypothesis by treating the GMT transduced TTF with drugs affecting the polymerization of actin and the activity of myosin II.

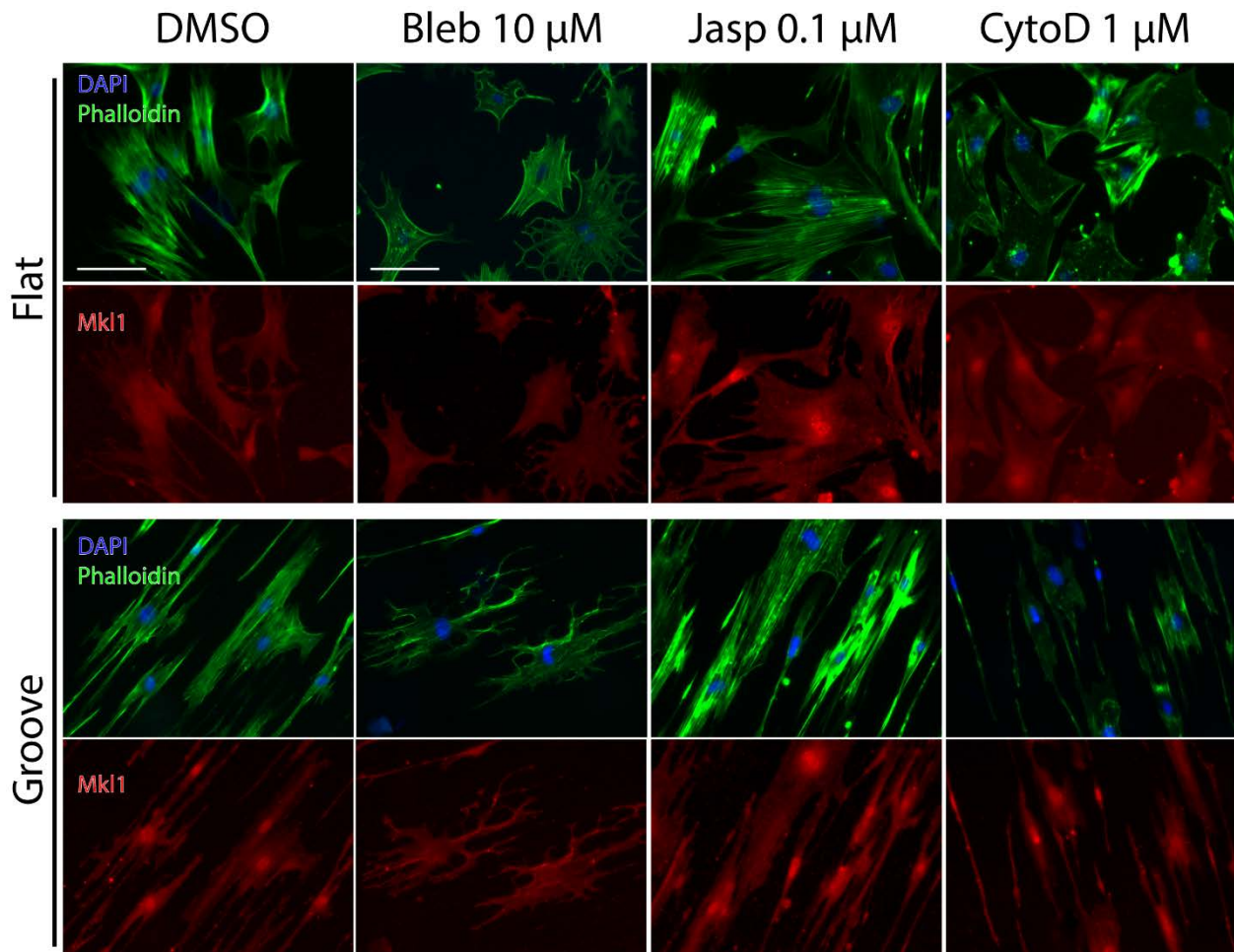
I therefore treated the reprogramming TTF seeded on grooved and flat surfaces with varying concentrations of Blebbistatin (Bleb), Jasplakinolide (Jasp) or Cytochalasin D (CytoD) and performed flow cytometry on day 10 to quantify GFP+ cells. Bleb inhibits the activity of myosin II[96]. Jasp promotes actin polymerization[97] whereas CytoD inhibits it[98]. The morphologies of the cells were distinctly different with the different drug treatments, and staining for filamentous actin (F-actin) with Phalloidin revealed that F-actin was perceptibly less in Bleb and CytoD, and more in Jasp treated cells (Fig 3.9). 50  $\mu$ M of Bleb, 0.5  $\mu$ M of Jasp and 5  $\mu$ M of CytoD all led to lower yields of GFP+ cells due to significant cytotoxic effects (data not shown). 10  $\mu$ M of Bleb reduced the yield of  $\alpha$ MHC-GFP+ cells on groove to that of flat surface (Fig 3.8), indicating that the activity of myosin II was necessary for the microtopography to take effect. Interestingly, although Jasp and CytoD have opposite effects on actin polymerization, both 0.1  $\mu$ M of Jasp and 1  $\mu$ M of CytoD improved the yield of GFP+ cells on flat surface to that of grooved surface (Fig 3.8). Explicitly, reprogramming yield was increased even though structural continuity of the actin network was compromised with CytoD treatment. This suggested that the actin cytoskeleton played an alternative role in the cells' response to the microtopography that was independent of that in transmitting mechanical signals. I therefore sought an alternative hypothesis to explain these results.



**Figure 3.8 Effect of actin cytoskeletal drugs on reprogramming efficiency.** Yield of GFP+ cells on day 10 under different drug treatments on flat and grooved surface. (\*p<0.05, \*\*p<0.001, compared to flat DMSO. #p<0.05, compared within bracket. All t-tests. n=3)

Mkl1, also known as Mal or Mrtf-A, is a mechanosensitive transcription factor that binds to and is sequestered by G-actin in the cytoplasm in its inactive state. Disruption of its binding to actin causes its translocation to the nucleus, where it acts as a transcriptional co-factor with serum response factor (SRF) to turn on gene expression[99,100]. Mkl1 has been implicated in reprogramming to cardiomyocytes before. One experiment showed that overexpression of SRF

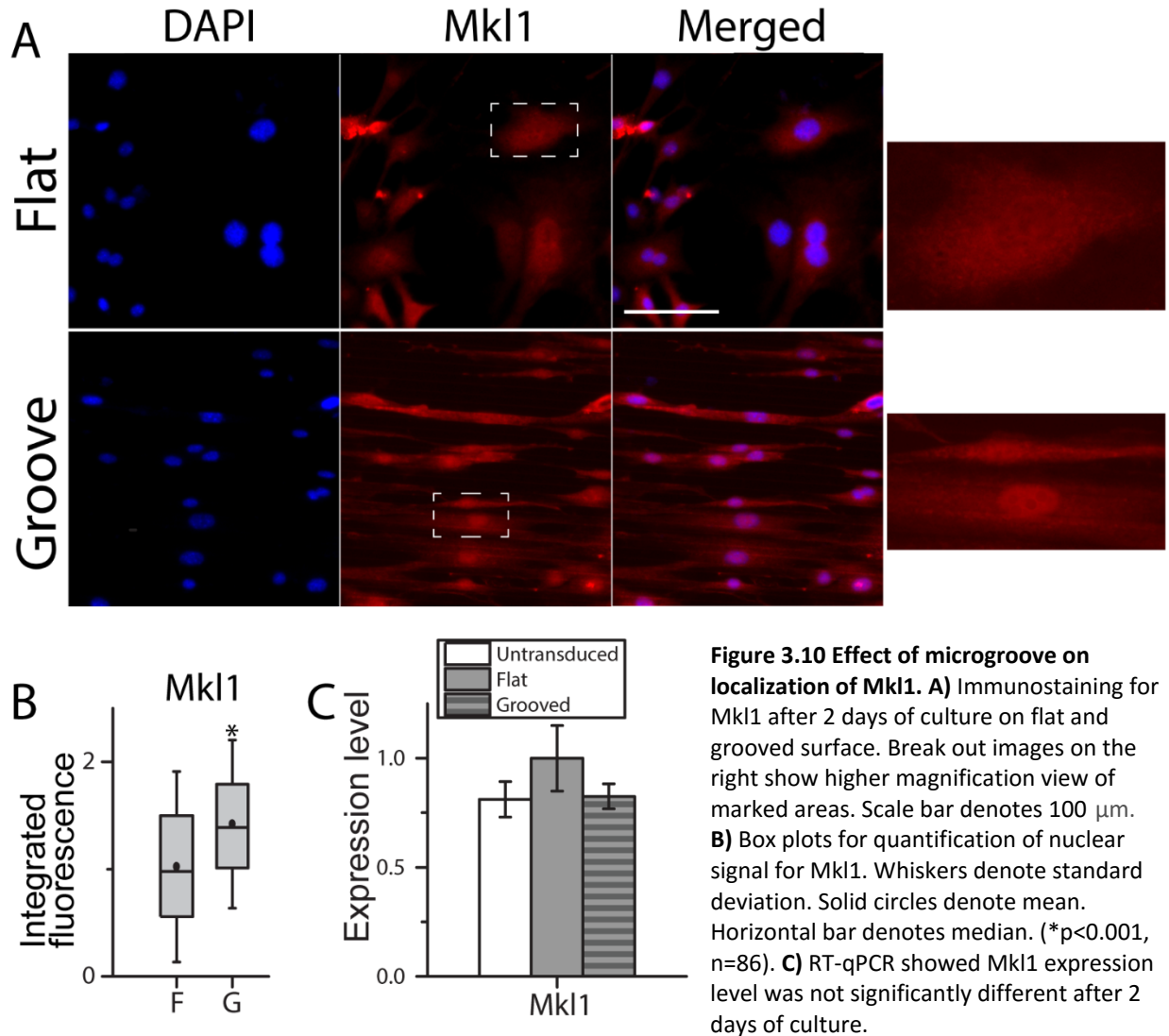
increased yield of reprogrammed cells from mouse embryonic fibroblasts[77], and the other showed that overexpression of Mkl1 increased yield from human fibroblasts[101]. The cytoskeletal drugs used in our experiments above have been shown to affect localization of Mkl1 by their effects on actin. Bleb has been shown to increase the sequestration of Mkl1 in the cytoplasm[102], whereas Jasp and CytoD have been shown to cause its translocation into the nucleus by disrupting its interaction with G-actin[99]. Immunostaining for Mkl1 indeed confirmed these effects in our GMT transduced TTF treated with the drugs (Fig 3.9). Although Mkl1 was distributed pan-cellularly in all samples, Jasp and CytoD samples showed perceptibly stronger and Bleb weaker nuclear signal for Mkl1 (Fig 3.9).



**Figure 3.9 Effect of cytoskeletal drugs on localization of Mkl1.** Wild type TTF was transduced with GMT, seeded on grooved and flat surfaces and cultured for 2 days in the various drugs before being stained for F-actin (green) and Mkl1 (red). Scale bar denotes 100 μm.

To reiterate, our results showed that on the grooved surface Bleb abolished the effect of microtopography and reduced the yield of GFP+ cells to that of flat surface. On the flat surface, Jasp and CytoD mimicked the effect of microtopography and improved yield to that of grooved surface treated with DMSO (Fig 3.8). These results therefore suggested that the effect of microgroove may be mediated by the sub-cellular localization and activity of Mkl1, and this effect was recapitulated by the drugs treatments. Comparing Mkl1 immunostaining for flat and

microgrooved surfaces, I indeed observed stronger nuclear signal for the latter after 2 days of culture (Fig 3.10A). Measurements of this signal showed that nuclear signal of Mkl1 was about half fold higher (Fig 3.10B) on microgrooved surface compared to flat. Interestingly, RT-qPCR showed that expression level of Mkl1 was not significantly different between grooved and flat surface (Fig 3.10C), thus suggesting that grooved surface only increased nuclear localization of Mkl1 but not its overall expression level. Like microgroove substrate, mechanical stretching also induced alignment of the cells (Fig 3.2A). Despite so, nuclear signal of Mkl1 was not different between static and stretched cells (Fig 3.11).



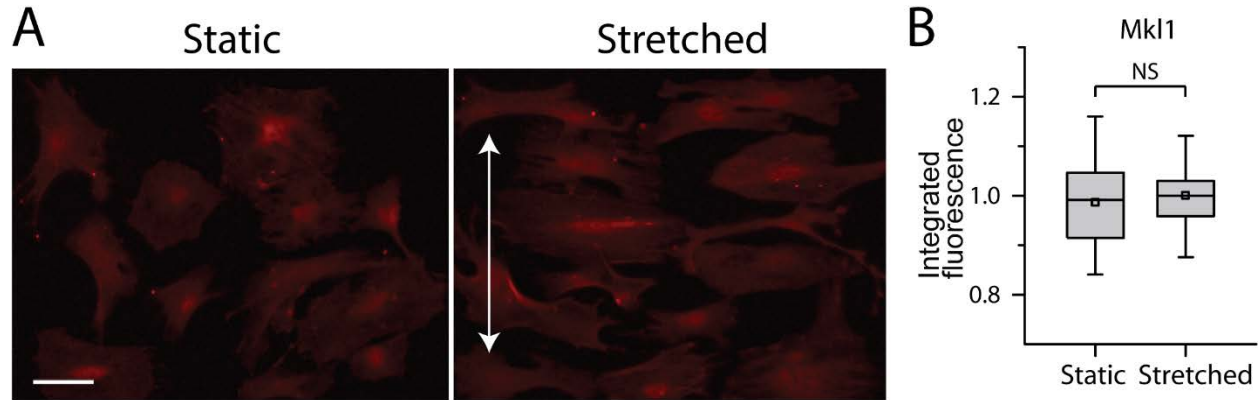


**Figure 3.11 Mkl1 localization for static and stretched reprogramming TTF. A)** Immunofluorescent staining for Mkl1 for static and stretched TTF transduced with GMT after 48 hours. Arrow indicates direction of stretch. **B)** Quantification of A). Not significantly different. ( $p=0.312$ .  $n=65$ .)

### 3.3.4 Overexpressing Mkl1 and treatment with valproic acid recapitulated the effect of microgroove in the early stage

Therefore, to attempt to recapitulate the effect of groove substrate I made a retroviral construct overexpressing murine Mkl1 and transduced TTF with it along with GMT. Immunostaining showed forcing the expression of Mkl1 with viral transduction successfully increased level of Mkl1 pan-cellularly and also within the nucleus (Fig 3.12A). I analyzed the transduced cells by RT-qPCR on day 2. Transduction of Mkl1 led to an increase in about 2.5 fold in its expression level. Concomitantly, some cardiomyocyte genes (Nk2.5, cTnT) were upregulated compared to GMT without Mkl1 (Fig 3.12B). These genes only form a subset of all the genes that were upregulated by groove (Fig 3.5C), suggesting that Mkl1 overexpression only partially recapitulated the effect of groove. Indeed, when I cultured GMT+Mkl1 transduced TTF on flat and grooved surface, the yield of  $\alpha$ MHC-GFP+ cells by day 10 was not increased to the same extent as groove (Fig 3.12D). Previous works have shown that microgroove could decrease histone deacetylase (HDAC) activity and increase acetylated Histone 3 (ACh3) level, thus promoting a more open chromatin structure and improving reprogramming efficiency[88,92]. Western blotting confirmed that microgroove increased the level of ACh3 in GMT transduced TTF (Fig 3.12C). I thus added 500  $\mu$ M valproic acid, a HDAC inhibitor, to TTF on flat surface to mimic this effect of microgroove and noticed a slight improvement in the yield of GFP+ cells (Fig 3.12D). Together, overexpression of Mkl1 and treatment with valproic acid fully recapitulated the effect of microgroove in the first 10 days (Fig 3.12D).

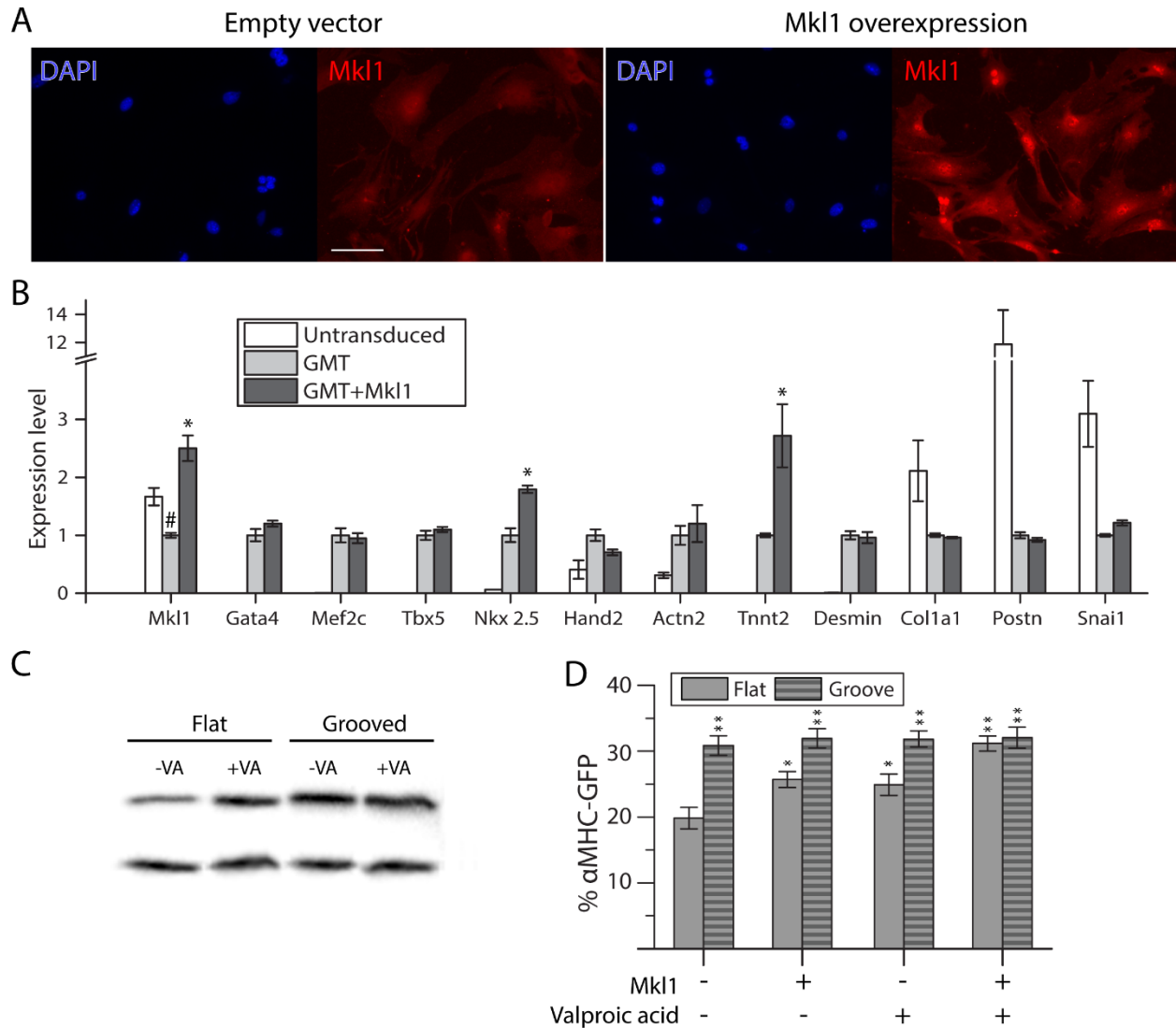


**Figure 3.12 Mkl1 overexpression and valproic acid treatment recapitulated the early effect of microgroove. A)** TTF was transduced with GMT plus empty vector or Mkl1, and immunostained on day 2. Scale bar denotes 100  $\mu\text{m}$ . **B)** TTF were transduced with GMT and GMT+Mkl1 and cultured for 2 days before being lysed for RT-qPCR. Expression levels normalized to flat surface. (# $p < 0.05$ , t-test, compared to untransduced TTF. \* $p < 0.05$ , t-test, compared to GMT transduced TTF.  $n = 3$ . **C)** GMT transduced TTF were cultured on flat and grooved substrate for 2 days before being lysed for Western blotting. Ach3 – Acetylated Histone 3, H3 - Histone 3, VA - Valproic acid. **D)** TTF was transduced with GMT or GMT+Mkl1 and treated with 500  $\mu\text{M}$  valproic acid. Yield of GFP+ cells quantified on day 10. (\* $p < 0.05$ , \*\* $p < 0.001$ , t-test, compared to flat without any treatments.  $n = 3$ )

To see if valproic acid and Mkl1 overexpression could recapitulate the effect of microgroove in the longer term, I transduced CF with GMT and Mkl1 and applied the optimized culture protocol described above (Fig 3.6A), with 500  $\mu$ M valproic acid added for the entire 4 weeks. With these treatments, the total number of cells with cTnT expression was improved to the same extent as cells cultured on microgroove, but the number of cells with striated pattern for cTnT was not improved significantly (Fig 3.13A). This indicates that microgroove has an additional effect in the later stage of reprogramming on the maturation and organization of sarcomeric structure that was not recapitulated by Mkl1 overexpression and valproic acid treatment. The number of beating cells for Mkl1 overexpression and valproic acid treatment was therefore significantly lower than that for microgroove culture (Fig 3.13B), since functional sarcomeres are needed for the cardiomyocytes' contractile activity.

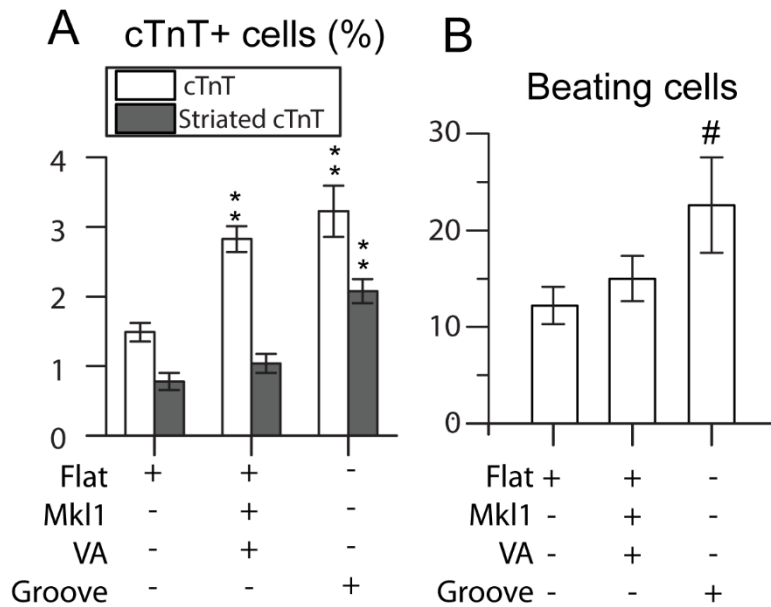


**Figure 3.13 Microgroove enhanced organization of sarcomeric structure.**

**A)** CF transduced with GMT and GMT+Mkl1, and subjected to the additional treatments. Samples were fixed and stained for cTnT after 4 weeks of optimized culture and counted for number of cells with cTnT expression and with cTnT that displayed striation. (\*\* $p < 0.001$ , Bonferroni test, compared to flat without any treatments within each group,  $n = 5$ .) **B)** Number of beating cardiomyocytes per well of a 12 well plate from. (#  $p < 0.005$ , Bonferroni test, compared to flat without any other treatments.)

### 3.4 Discussion

I chose the yield of  $\alpha$ MHC-GFP+ at day 10 as the criteria for determining the effect of mechanical stretch, substrate stiffness and microgroove on reprogramming under the assumption that what may affect reprogramming efficiency in the short term will also do so in the long term in order to expedite our initial screen. Therefore, while this approach saved time, the limitation was I have overlooked the possibility that while they do not increase the yield of GFP+ cells by day 10, cyclical stretch and substrate stiffness may enhance the maturation of partially reprogrammed cells in the later stage of reprogramming. In fact, existing work on the effects of cyclical stretch[83] and substrate stiffness[84,85] on the differentiation and maturation of cardiomyocyte support this possibility.

Although yield of  $\alpha$ MHC-GFP+ cells was enhanced by microgroove, no beating cells was observed by four weeks in DMEM/M199/FBS culture medium. Recently it has been reported that a serum free culture medium containing FGF2, FGF10 and VEGF could improve the

conversion of partially reprogrammed cardiomyocytes into functional iCMs at the late stage of reprogramming[81]. This culture protocol resulted in a one fold increase in beating cardiomyocytes when the starting population was cardiac fibroblasts (Fig 3.6D), but not tail tip fibroblasts. The inherent intractability of tail tip fibroblasts to being reprogrammed completely compared to cardiac fibroblasts has been reported before[4,81].

Previous works have demonstrated the positive effects of microgroove on reprogramming efficiency for induced pluripotent stem cells[92] and neurons[82]. The underlying mechanisms demonstrated were that microgroove inhibited the activity of HDAC and led to a higher Ach3 level, and promoted mesenchymal to epithelial transition. To identify other possible mediators of the cells' mechano-response to microgroove, I treated the cells with drugs targeting the actin cytoskeleton. I found that even though Jasplakinolide and Cytochalasin D have opposite effects on the polymerization of actin, both drugs improved the yield of GFP+ cells on flat surface at day 10 to that of cells on grooved surface (Fig 3.8B). Despite their opposite effects on actin polymerization, both drugs have the same effect on the activity of Mkl1[99], leading us to identify Mkl1 as a mediator of the effect of microtopographical cues on reprogramming to cardiomyocytes. Mkl1 has also been implicated in reprogramming to cardiomyocytes elsewhere [77,101]. In these experiments, overexpression of Mkl1 or its transcription cofactor, serum response factor (SRF), led to increased yield of reprogrammed cells.

I have thus shown here that microgroove could also affect reprogramming via another mechanism: increasing the nuclear translocation of Mkl1 and its activity. The underlying mechanism of how microgroove may increase the translocation and activity of Mkl1 is not clear at this point. It has been shown that forcing a cell to adopt a more elongated morphology through patterned fibronectin caused higher expression of a serum response element reporter[103]. Inasmuch as microgroove constrained cells to an elongated morphology, it could be acting along an analogous pathway, apart from possibly elucidating a mechano-response to the 3D topographical features.

Treatment with valproic acid, a HDAC inhibitor, together with Mkl1 overexpression fully recapitulated the effect of groove in the early stage of reprogramming (Fig 3.12D) but not in the longer term (Fig 3.13A-B). Although valproic acid and Mkl1 overexpression increased the yield of cells with cTnT expression to the same extent as microgroove, it did not increase the yield of cells with striated pattern for cTnT like microgroove did (Fig 3.13B). This indicated that although valproic acid treatment and Mkl1 overexpression could help improve the expression of sarcomeric proteins, it could not promote their organization into sarcomeric structures like microgroove could. The enhancing effect of microgrooved substrate on sarcomere formation has been observed in neonatal cardiomyocytes and cardiomyocytes differentiated from stem cells[86,88,104]. Therefore I conclude that the effect of microgrooved substrate is twofold: enhancing overall genetic reprogramming through regulating Mkl1 activity and Ach3 level, and enhancing the subsequent structural organization of sarcomeres.

A long term goal of cardiac reprogramming research is to obtain sufficiently large number of cardiomyocytes for therapeutic purposes for patients with cardiomyopathies. Our work and most of other existing approaches on enhancing reprogramming yields were demonstrated in murine systems. The natural next step will be to translate all these findings into improving human cardiac reprogramming. Existing genetic approaches to reprogram human fibroblasts into cardiomyocytes delivered very low yield of completely reprogrammed cardiomyocytes[105,106]. Majority of the cardiomyocyte-like cells that activated reporter constructs were not able to contract spontaneously. More recently, it has been demonstrated that a cocktail of 9 chemicals could convert human fibroblasts into mature cardiomyocytes[11]. It will be interesting to combine topographical cues and other methods with these human cardiac reprogramming approaches to see if further enhancement of yield can be achieved in human cardiac reprogramming.

In conclusion, microgroove improved the outcome of reprogramming from fibroblasts to cardiomyocytes by enhancing overall genetic conversion and the structural organization of sarcomeres. Passive topographical cues offers a simple and effective method to improve cardiomyocyte reprogramming without the need for biochemical manipulations.

## Chapter 4: Direct Reprogramming from Dermal Fibroblasts to Skeletal Muscle Cells

### 4.1 Introduction

Growth and repair of skeletal muscle fibers are mediated by a resident population of mononuclear myogenic precursors, the satellite cells. These cells, which are located between the sarcolemma and the basal lamina of the muscle fiber, divide at a slow rate to sustain both self-renewal and growth of skeletal muscle tissue. In response to muscle injury, satellite cells divide and fuse to repair or replace the damaged muscular fibers[107]. However, the self-renewal potential of adult satellite cells is limited and is compromised with aging, excessive trauma, or genetic defects as in certain muscular dystrophies such as Duchenne muscular dystrophy[108]. In such cases, external interventions are needed.

The delivery of muscle stem cells have been demonstrated to promote regeneration[107] and treatment of muscular diseases[109] in mouse models. Besides stem cells derived from muscles, other sources of myogenic cells for muscle repair have been found, including skin[110–112], bone marrow[113], umbilical cord blood[114], mesangioblasts[115], and iPSCs-derived muscle progenitors [116]. However, isolating myogenic stem cells from most of these sources is invasive and has low yield. Deriving muscle progenitors from iPSCs carries the risk of teratoma formation and requires lengthy differentiation process.

One clinically relevant approach is to use cell reprogramming approach to convert fibroblasts into myogenic cells. 5-azacytidine, a DNA methyltransferase inhibitor, was used to generate striated muscle from non-myoblast precursors[117]. However, this approach only worked for certain transformed cell lines, had comparatively low efficiency, and was non-specific in that adipocytes and chondrocytes were also produced[118]. Another method is to overexpress the transcriptional factor MyoD in non-muscle cells to convert them into muscle cells[119], but it requires genetic manipulation that might lead to tumorigenic phenotypes.

The use of only chemical compounds to achieve reprogramming, which obviates the need for direct genetic manipulation, has recently been highlighted by the discovery of chemically induced pluripotent stem cells[10,9] and other cell types[11–15]. Here, I reported the discovery of a cocktail of chemicals that, in combination with an optimized basal medium, could efficiently reprogram dermal fibroblasts into myogenic cells. By seeding the initial fibroblasts population on a substrate with microtopographical features, the reprogrammed cells could be easily isolated by selective detachment. The reprogrammed population consisted of both progenitors and differentiated myocytes, and could fuse into mature beating myotubes when cultured in differentiation medium and engrafted in vivo when injected into injured muscles. This non-viral approach of deriving myogenic cells from dermal fibroblasts could make autologous myogenic cells easily available for therapy, disease modeling and drug screening.

## 4.2 Materials and Methods

### 4.2.1 Cell culture and screening for candidates

1 day post-partum C57/B6 mice were sacrificed by decapitation with a pair of sharp scissors. The skin was peeled off and the underlying subcutaneous fats and panniculus carnosus were scrapped off. The skin was then floated on 0.05% freshly thawed trypsin overnight and the dermis was separated from the epidermis next day. The dermis was cut up and digested in 200U/ml collagenase II at 37 °C for 1 hour, and triturated vigorously by pipetting up and down to break up remaining tissue clumps. The mixture was mixed with fetal bovine serum (FBS) to quench the digestion enzyme activity and then spun down. The pellet was plated overnight in MEF medium (DMEM with 10% FBS and 1% penicillin/streptomycin). Thereafter, the culture was trypsinized, passed through a 40 µm filter and frozen down into aliquots in a medium containing 10% dimethyl sulfoxide (DMSO) and 90% FBS.

For screening for small molecules for reprogramming to skeletal muscle cells, dermal fibroblasts were seeded at 5000cells/cm<sup>2</sup> the night before in MEF medium. The next day, reprogramming medium (KnockOut DMEM (Invitrogen) 10% knockout serum replacement (Invitrogen), 10% fetal bovine serum (Hyclone), 2 mM GlutaMAX (Invitrogen), 1% nonessential amino acids (Invitrogen), 1% penicillin-streptomycin (Invitrogen) and 20 ng/ml bFGF (Peprotech)) containing the various small molecules were added. Medium was changed once every 2-3 days. Information on the small molecules are listed in table 4.1. All small molecules were purchased from Cayman Chemicals.

**Table 4.1** Information on small molecules

Small molecules	Concentration
Valproic acid	500 µM
Chir99021	20 µM
616452	10 µM
Tranyl	5 µM
Forskolin	10 µM
5-aza-2'deoxyctidine	5 µM

After the optimal cocktail of small molecules and their concentrations were found, I replaced the reprogramming medium with MEF medium and screened for additional candidates that could improve reprogramming efficiency. Information of these candidates are listed in table 4.2.

**Table 4.2** Information on candidate screen for enhancing efficiency

Candidates	Concentration	Company
Ascorbic acid	50 µg/ml	Sigma Aldrich
BMP4	20 ng/ml	Stemgent
Insulin	10 µg/ml	Stemgent
IGF-1	50 ng/ml	R&D Systems
PDGF	50 ng/ml	R&D Systems
bFGF	50 ng/ml	Peprotech

The optimized formulation, which is 20 $\mu$ M 616452 and 20 $\mu$ M Forskolin in MEF medium with 50  $\mu$ g/ml ascorbic acid and 50 ng/ml bFGF, is termed as 6F medium.

Primary murine myoblasts were generously gifted by Mike Conboy and maintained in F10 medium with 20% FBS, 1% penicillin-streptomycin and 10 ng/ml bFGF.

#### 4.2.2 Immunostaining, imaging and quantification

For immunostaining, cells were fixed in 4% paraformaldehyde and permeabilized with 0.5% Triton-X 100, both for 15 minutes. Cells were then incubated with primary antibodies overnight at 4°C. Secondary antibody (Alexafluor 488 or Alexafluor, 546 Thermofisher Scientific) were added overnight at 4°C before the nuclei were stained with Hoechst. Information on the primary antibodies are listed in table 4.3.

**Table 4.3** Information on antibodies used

Antibody	Concentration	Catalogue no	Company
Skeletal muscle myosin	1:200	M4276	Sigma Aldrich
Skeletal muscle troponin T	1:10	JLT12	DSHB
Pax7	1:10	Pax7	DSHB
MyoG	1:10	F5D	DSHB

For screening for reprogramming efficiency, cells were stained for skeletal muscle troponin T (TnnT) and imaged with ImageXpress Micro High-Content Analysis System (IXM, Molecular Devices) at 10X magnification. Images were analyzed with MetaXpress Software (Molecular Devices) to quantify number of nuclei co-localized with troponin T staining. Quantification of Pax7+ and MyoG+ cells was performed by similar way. Unless otherwise mentioned, microscope images were taken with a Zeiss AxioObserver epi-fluorescent microscope. Confocal images were taken with Prairie Confocal system (Bruker Corporation).

#### 4.2.3 Flow activated cell sorting

Fsp1-Cre (Stock no. 012641, Jackson Laboratory) mouse and ROSA26-tdTomato (Stock no. 7909, Jackson Laboratory) mouse were crossed to produce Fsp1-Cre/ROSA26-tdTomato offsprings. Dermal fibroblasts were isolated from these offsprings as per section 4.2.1, and mixed with FITC conjugated Sca-1 (1:50, 130-102-831, Miltenyi biotec) and Alexafluor 647 conjugated CD34 (1:100, 560233, BD Biosciences) in plain DMEM at 4°C or 30 minutes. Cells were washed with PBS twice before sorting with BD Bioscience Influx Sorter.

#### 4.2.4 Real time quantitative polymerase chain reaction

RT-qPCR was performed as per section 2.2.4, except that the PCR machine used was CFX96 Real-Time PCR Detection System (Biorad). Primers information are listed in table 4.4.

**Table 4.4** Primer information

	<b>Forward</b>	<b>Reverse</b>
Pax7	CGTAAGCAGGCAGGAGCTAA	ACTGTGCTGCCTCCATCTTG
Mrf5	AAGGCTCCTGTATCCCCTCAC	TGACCTTCTTCAGGCGTCTAC
Myod1	CTGCTCTGATGGCATGATGGA	CACTGTAGTAGGCGGTGTCG
Myomaker	TTCCTCCCGACAGTGAGCAT	GCACAGCACAGACAAACCAG
MyoG	GTGCCAGTGAATGCAACTC	CGAGCAAATGATCTCCTGGGT
Myh3	CTCTGTCACAGTCAGAGGTGT	TTCCGACTTGCGGAGGAAAG
Nanog	TCTTCTGGTCCCCACAGTTT	GCAAGAATAGTTCTCGGGATGAA
Oct4	GGCTTCAGACTTCGCCTCC	AACCTGAGGTCCACAGTATGC
Aggrecan	CCTGCTACTTCATCGACCCC	AGATGCTGTTGACTCGAACCT
Pparg	TCGCTGATGCACTGCCTATG	GAGAGGTCCACAGAGCTGATT
Runx2	AACGATCTGAGATTTGTGGGC	CCTGCGTGGGATTTCTTGTT
Hand2	CACCAGCTACATCGCCTACC	TCTCATTGAGCTCTTTCTTCTCT
B2M	CTCGGTGACCCTGGTCTTTC	TTGAGGGGTTTTCTGGATAGCA

#### 4.2.5 Microarray analysis

Dermal fibroblasts were treated with basal medium (MEF medium with 50µg/ml ascorbic acid and 50ng/ml bFGF) and 6F medium for 2 days. mRNA was extracted with RNeasy Micro Kit (Qiagen) and checked for RNA quality (RIN >7.5) with Bioanalyzer 2100 (Agilent) before linear amplification using Ovation Pico WTA System V2 (NuGEN). Biological triplicates were each hybridized to an Affymetrix Mouse Gene 1.0 ST Array and analyzed with GeneChip® Scanner 3000. CEL files were loaded into R and normalized with RMA method using *oligo* package[120]. Linear model was fitted to each gene and empirical Bayes statistics calculated with the *limma* package[121]. P-values for multiple testing were adjusted by the Benjamini-Hochberg method. Genes that were more than 2 fold different in expression level with adjusted P-values less than 0.05 were considered differentially expressed. Differentially expressed genes were submitted to DAVID [122] for gene ontology enrichment analysis.

#### 4.2.6 Skeletal muscle cells purification

Dermal fibroblasts were seeded on microgrooved substrate at 3000 cells/cm<sup>2</sup> prepared as per section 3.2.4. However, substrate was coated with 0.1% gelatin for 5 minutes instead of Matrigel before cell seeding. On day 10, reprogrammed cells were rinsed in PBS once and incubated in 100U/ml Collagenase II dissolved in DMEM for 10 minutes at 37 °C . The culture plates were knocked on the side a few times to dislodge the colonies of skeletal muscle cells, which were triturated into single cells before being spun down and plated.

#### 4.2.7 In vivo transplantation

10 µl (0.03 mg/ml) of *Naja mossambica mossambica* cardiotoxin (Sigma) was injected in the tibialis anterior (TA) muscle of anesthetized BALB/c SCID mice 1 day before cell transplantation. The next day, 10<sup>5</sup> skeletal muscle cells were injected directly into these preinjured muscles in 20 µl Matrigel solution (5mg/ml). The contralateral TA was injected with Matrigel solution as a negative control. All transplanted cells were previously transduced with

Dsred retrovirus for tracing. Injected muscles were harvested 1 week after cell transplantation and analyzed by dissection microscope and confocal microscope.

#### 4.2.8 Statistical analysis

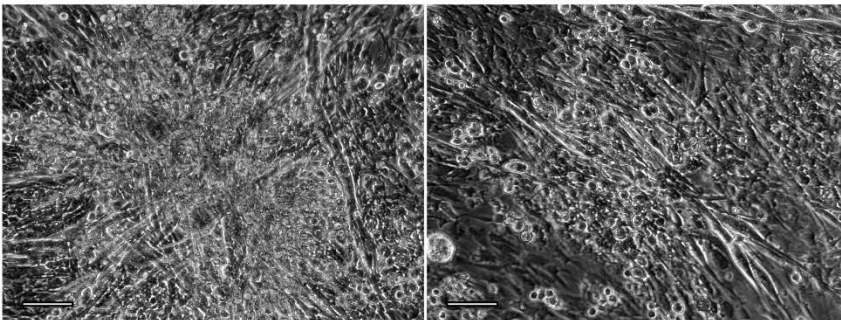
All statistical analysis were performed using Holm-Sidak t-tests.

### 4.3 Results

#### 4.3.1 Induction of skeletal muscle cells by chemical cocktail

Hou *et al.* discovered a method to reprogram fibroblasts into iPSCs using only small molecules[10]. Following their protocol, I treated neonatal murine dermal fibroblasts with a similar cocktail of chemicals, acronymed VC6TF (V – Valproic acid, C – Chir99021, 6 – 616452, T – Tranylcypramine, F – Forskolin), and noticed the emergence of colonies of cells as early as day 6 onwards. By day 10, some of the cells in the colonies exhibited elongated morphologies and also contracted spontaneously, reminiscent of myotubes (Fig 4.1A). I performed immunostaining of the chemically treated culture at different time points for skeletal muscle myosin heavy chain (MHC) and observed MHC+ cells present by day 4 which expanded into noticeable clusters by day 10 (Fig 4.1B).

A



B

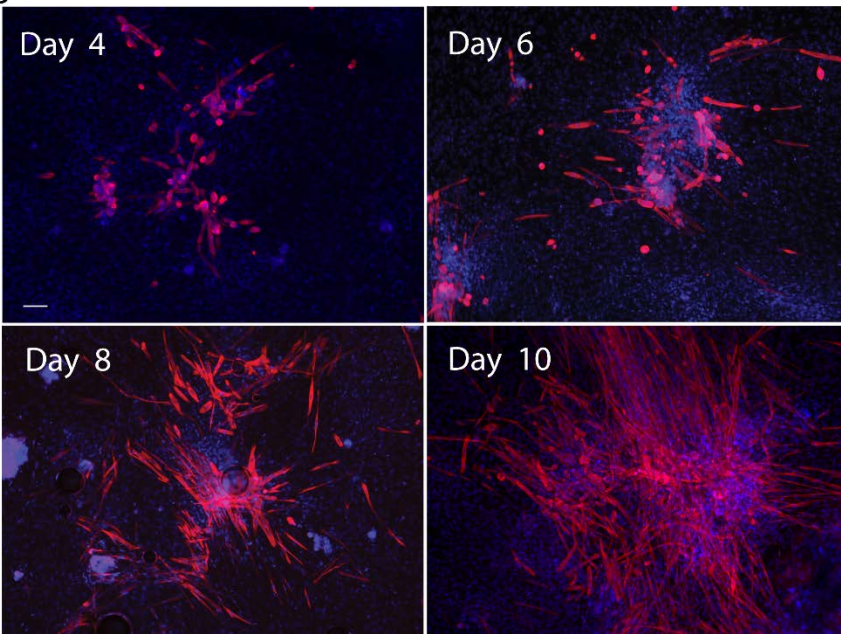


**Figure 4.1 Emergence of clusters of skeletal muscle cells. A)**

Representative phase contrast images of skeletal muscle cell clusters observed on day 10 after treatment with VC6TF cocktail. **B)** Skeletal muscle cell clusters stained for myosin heavy chain at the indicated days after treatment with VC6TF cocktail. All scale bars denote 100µm

I hypothesized that a subset of the cocktail was sufficient to induce the appearance of myogenic cells, and examined the effect of serially removing individual chemicals from the original pool of 5 chemicals. I observed that removing either 6 or F greatly reduced the induction of skeletal muscle cells (Fig 4.2A). I next screened for all combinations involving both 6 and F, and just 6 and F alone. I also tested the demethylating agent 5-aza-2′deoxycytidine (5 Aza). I found that the combination of only 6 and F (I refer to this combination as 6F for brevity from now on) induced the appearance of myogenic cells at the highest efficiency (Fig 4.2B). I then tested for the optimal concentration of the chemicals, and found that 20  $\mu$ M of 6 and F gave the highest yield (Fig 4.2C).

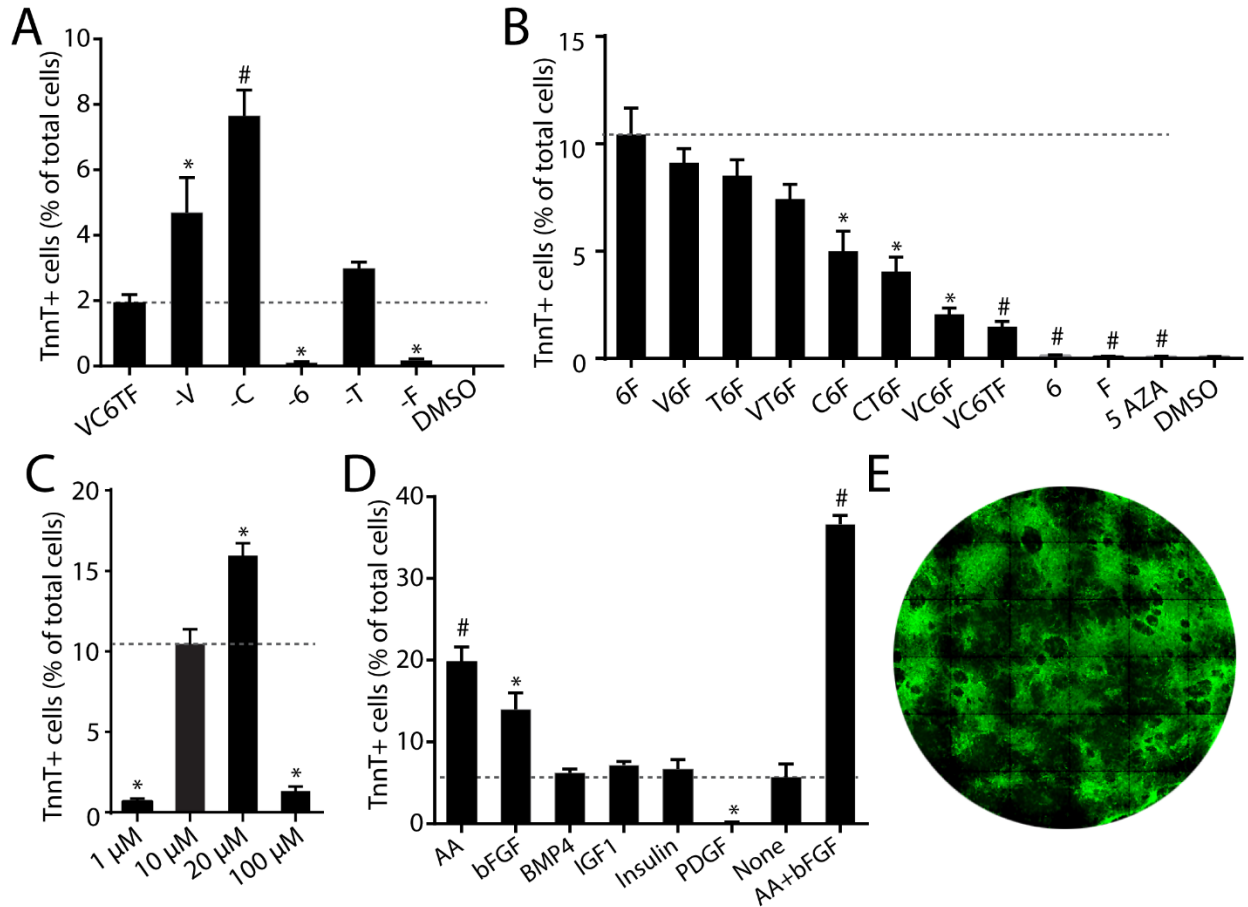


**Figure 4.2 Screening for optimal small molecule combinations and basal medium. A)** Yield of TnnT+ cells at day 10 as a result of serially removing 1 chemical. **B)** Yield of TnnT+ cells at day 10 for all combinations of chemicals that included 6 and F. **C)** Yield of TnnT+ cells for different concentrations of 6 and F at day 10. **D)** Yield of TnnT+ cells at day 10 for 20  $\mu$ M 6F in MEF medium with each of the listed candidates added. (\* $p < 0.05$ , # $p < 0.0001$ ,  $n = 3$ . Compared against the conditions in level with dashed line) **E)** Whole well image for TnnT+ cells derived from dermal fibroblasts treated with 20  $\mu$ M 6 and 20  $\mu$ M F in MEF medium containing 50  $\mu$ g/ml of ascorbic acid and 50 ng/ml of bFGF after 10 days.

Up to this point, I have used the same formulation of reprogramming medium as Hou et. al[10]. This formulation might not be optimal for inducing myogenic cells, so I sought to optimize it. I used MEF medium as the basal medium and tested adding candidates that have been implicated in enhancing direct cell reprogramming or skeletal muscle development, and found that 50 ng/ml of bFGF and 50  $\mu$ g/ml of ascorbic acid each significantly enhanced the

induction of skeletal muscle cells by 6F (Fig 4.2D). Together, bFGF and AA synergistically enhanced the induction to about 37% of the total cell population (Fig 4.2D-E). Normalizing by the initial number of cells seeded gave a yield of about 2.5 skeletal muscle cells per fibroblast seeded. This optimized formulation, which is 20 $\mu$ M 616452 and 20 $\mu$ M Forskolin in MEF medium with 50  $\mu$ g/ml ascorbic acid and 50 ng/ml bFGF, is termed as 6F medium.

#### 4.3.2 Skeletal muscle cells were directly reprogrammed and did not pass through a pluripotent state

Dermal fibroblasts were treated with 6F medium and lysed for RNA extraction every 2 days. RT-qPCR revealed that some myogenic genes were significantly upregulated by day 4 onwards (Fig 4.3A). In contrast, expression of pluripotency genes Nanog and Oct4 remained consistently low throughout the 12 days of treatment with 6F medium (Fig 4.3B), indicating that the cells did not pass through a pluripotent state. I also measured expression of key markers for other mesodermal cell types and found that markers for cardiomyocytes (Hand2), chondrocytes (Aggrecan) and osteoblasts (Runx2) were not significantly upregulated overall.

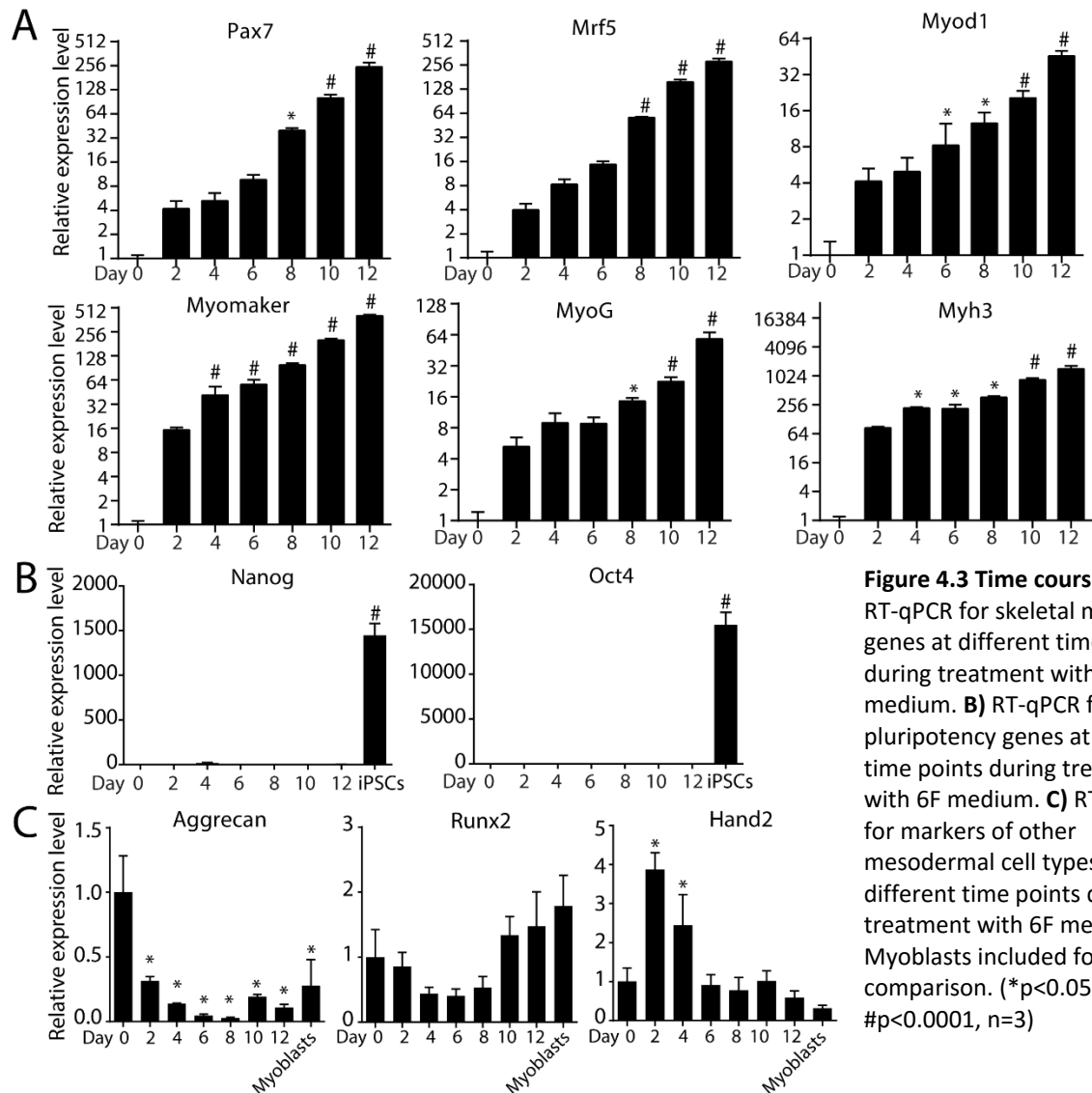


**Figure 4.3 Time course PCR. A)** RT-qPCR for skeletal muscle genes at different time points during treatment with 6F medium. **B)** RT-qPCR for pluripotency genes at different time points during treatment with 6F medium. **C)** RT-qPCR for markers of other mesodermal cell types at different time points during treatment with 6F medium. Myoblasts included for comparison. (\*p<0.05, #p<0.0001, n=3)

The global gene expression of dermal fibroblasts cultured in only basal medium and in 6F medium for 2 days was analyzed with mRNA microarray. 385 genes and 378 genes were upregulated and downregulated respectively (>2 fold, FDR-adj p<0.05) in cells cultured in 6F medium (Fig 4.4A). Genes upregulated for 6F medium cultured cells were significantly enriched for biological processes related to development, while those downregulated were enriched for processes related to cytoskeleton organization and cell adhesion (Fig 4.4B).

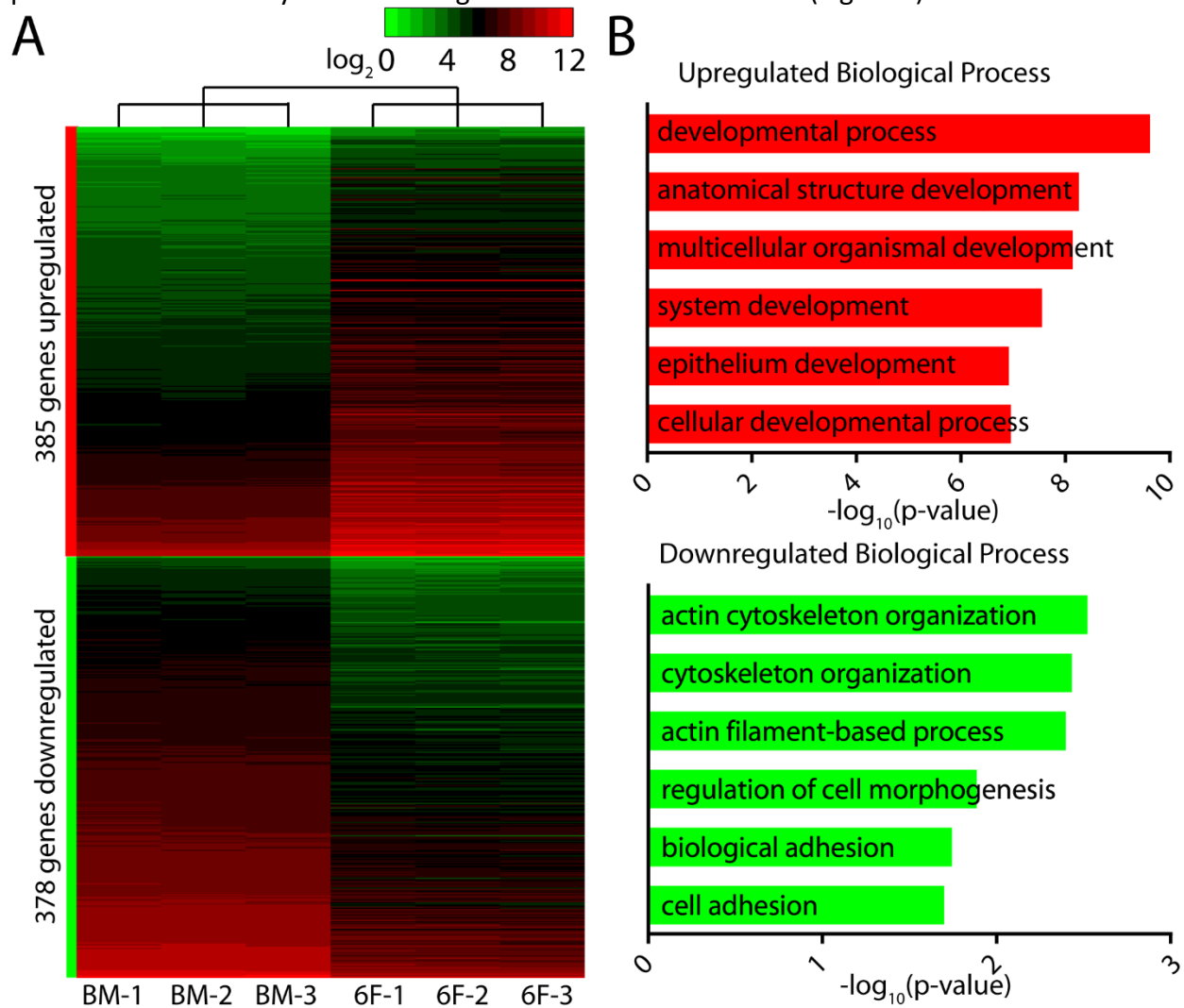
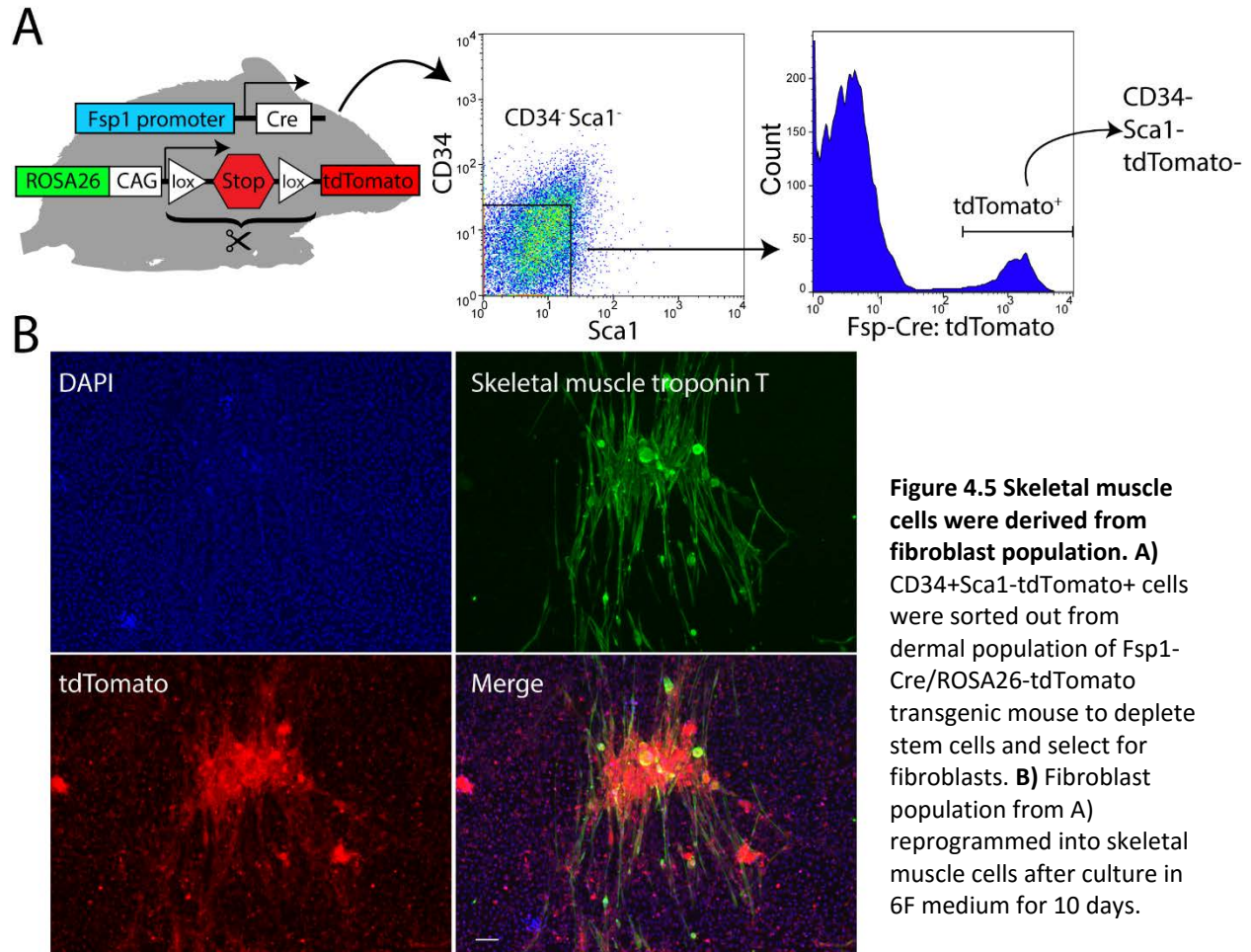


**Figure 4.4 mRNA microarray analysis on fibroblasts in 6F medium on day 2. A)** Heatmap of upregulated and downregulated genes (>2 fold, FDR-adj p<0.05). **B)** Enriched gene ontology terms for upregulated and downregulated biological processes.

### 4.3.3 Lineage tracing indicated that skeletal muscle cells were reprogrammed from fibroblasts

Other than fibroblasts, the starting population could also contain stem cells within the dermal layer or muscle progenitor cells from the Panniculus Carnosus. I next sought to establish that the chemically derived skeletal muscle cells were reprogrammed from fibroblasts and not differentiated from stem cells. To this end I employed a gating strategy that would remove known stem cell populations residing in the skin while selecting for fibroblasts. Fsp1 is a fibroblast marker[123], and has been used as a marker to trace fibroblast origins[7,80]. In Fsp1-

Cre/ROSA26-tdTomato mouse, Cre recombinase expressed under the control of Fsp1 promoter will remove a floxed STOP cassette preceding tdTomato to permanently label fibroblasts with the red fluorescent protein. I isolated dermal fibroblast from Fsp1-Cre/ROSA26-tdTomato neonates and stained them for the surface markers CD34 and Sca1. CD34 would label keratinocyte[124], bulge stem cells[125] and muscle progenitors [126], while Sca-1 would mark pre-adipocytes[127] and multipotent skin-derived precursor cells[128]. I then sorted for CD34-/Sca1-/tdTomato+ population (Fig 4.5A). Treatment with 6F medium caused skeletal muscle cell colonies to emerge from this sorted starting population (Fig 4.5B), indicating that these skeletal muscle cells were reprogrammed from fibroblasts and not differentiated from stem cells.



It has been reported that addition of only Forskolin could significantly enhance the proliferation of myoblasts[129]. Since our chemical cocktail contained Forskolin, I sought to rule out the possibility that the cocktail was merely inducing the proliferation of muscle progenitors that might have existed in the starting population. I first tested the effect of 6 and F, both individually and combined, on the proliferation of primary murine myoblast in the optimized basal medium. Results showed that although F alone enhanced proliferation of myoblasts in comparison to basal medium after 8 days of culture, 6F together did not (Fig 4.6A-B). Since I did not observe skeletal muscle cell clusters in fibroblasts treated with basal medium, these results indicated that skeletal muscle clusters derived from 6F treatment were not expanded from

muscle progenitors that could have existed in the starting population. I also treated unsorted dermal fibroblasts with 6 and F and performed RT-qPCR. Together, 6 and F dramatically upregulated the expression of skeletal muscle genes, compared to their individual effects (Fig 4.6C). The combined effects of 6 and F were therefore critical for inducing reprogramming, and F alone was not capable of inducing expansion of muscle progenitors that might exist in the unsorted dermal population.

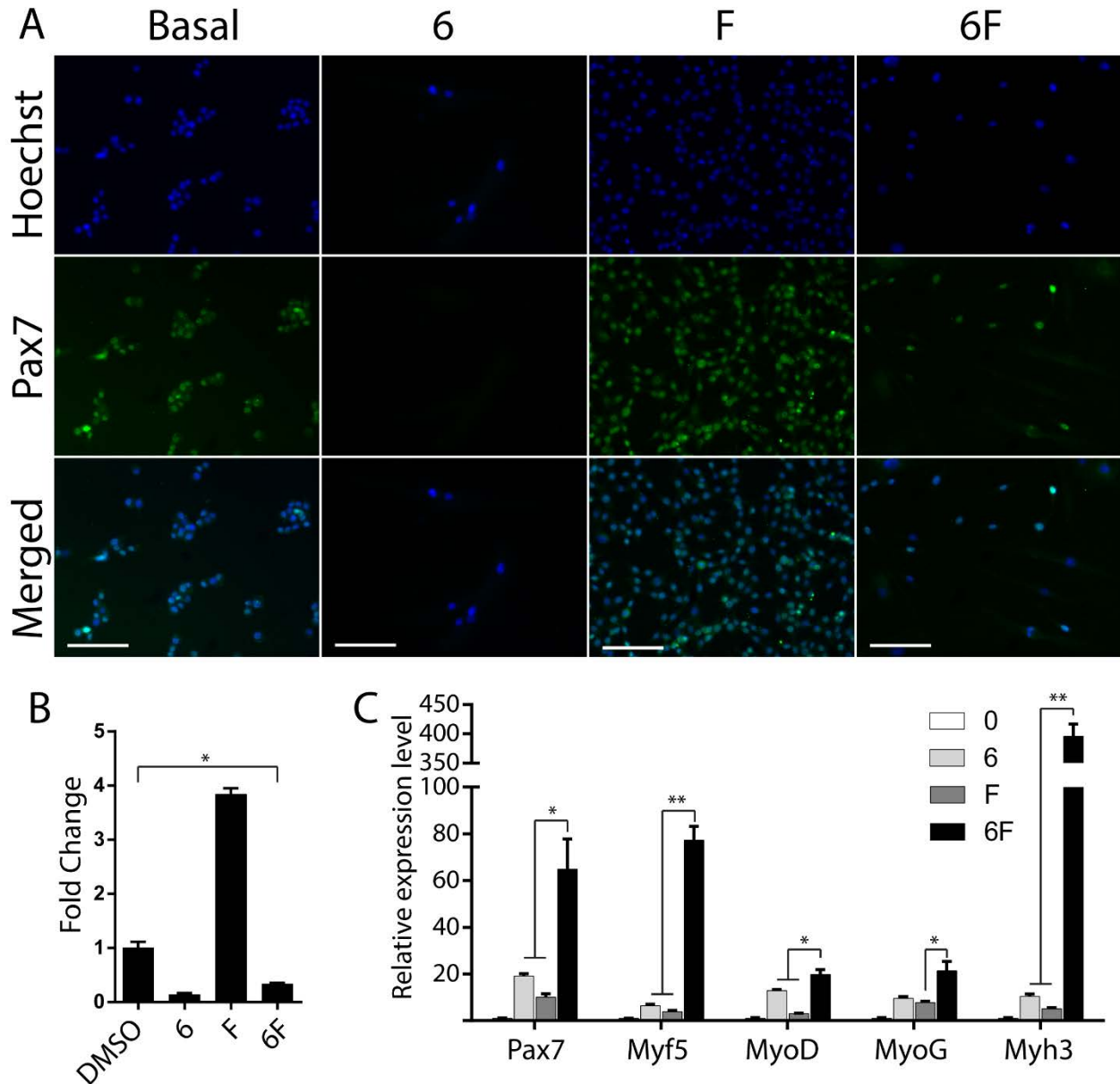


**Figure 4.6 Myoblasts and dermal fibroblasts treated with 6, F and 6F together.** **A)** Myoblasts were cultured in basal medium (MEF medium with 50µg/ml ascorbic acid and 50ng/ml bFGF), 6, F and 6F combined for 8 days and stained for Pax7. **B)** Quantification of A). **C)** Unsorted dermal fibroblasts were treated similarly to A) and subjected to RT-qPCR after 8 days. (\*p<0.05, \*\*p<0.01, n=3)

#### **4.3.4 Microgrooved substrate allowed easy purification of skeletal muscle cells**

I noticed that the skeletal muscle cells emerged in clusters. I next sought a convenient way to isolate the reprogrammed skeletal muscle cells. I noticed that the skeletal muscle cell colonies sometimes contracted into spheres as they became very dense and myocytes within the colonies pulled the surrounding cells inwards. I hypothesized that culturing the reprogramming cells on microgrooved substrate would promote this phenomenon by aligning the myocytes within the colonies in the same direction. As expected, many more spherical colonies were observed on microgrooved than flat substrate on day 10. Staining for Pax7 revealed presence of progenitor cells within the colonies (Fig 4.7A). After 10 minutes of collagenase treatment, gentle knocking on the culture plates detached the colonies cleanly (Fig 4.7B). Spherical colonies on flat substrate could not be detached cleanly with this method, suggesting that the microgroove played a role in weakening the attachment of the colonies to the substrate to allow easier detachment. If initial population was seeded at a sufficiently low density, incubating the culture in  $\text{Ca}^{2+}/\text{Mg}^{2+}$  free PBS was sufficient to detach the colonies and collagenase treatment was not necessary.

I analyzed the makeup of the cells in the colonies. I disaggregated the detached colonies, plated the single cells and stained them for Pax7 and MyoG. 23%, and 62% of the disaggregated cells were positive for each of these markers respectively (Fig 4.7C), indicating the 6F medium derived population contained a mixture of progenitors and differentiated skeletal muscle cells.

#### **4.3.5 Reprogrammed skeletal muscle cells engrafted in vivo**

I cultured the isolated skeletal muscle cells in MEF medium for 2 weeks and observed formation of long myotubes that contracted spontaneously (Fig 4.8A). Many of the myotubes displayed striated patterns, an indication of formation of mature sarcomeres (Fig 4.8B).

I next tested if the reprogrammed skeletal muscle cells could engraft in injured muscle and contribute to regeneration. I labelled the starting population with Dsred using retrovirus, and reprogrammed the cells on microgrooved substrate. I isolated and disaggregated the colonies after 10 days and injected the cells into the tibialis anterior muscle of Balb/c SCID mouse that had been preinjured by cardiotoxin injection 24 hr before transplantation. The contralateral muscles of recipient mice were injured but injected with Matrigel solution only. 1 week after transplantation muscles were harvested. Dsred positive cells were clearly observed at the site of injection. Confocal microscopy revealed these cells had morphology resembling myofibres (Fig 4.8C). By contrast, site injected with Matrigel solution did not have any Dsred positive cells. Therefore, reprogrammed skeletal muscle cells derived from 6F medium could engraft in injured muscles.

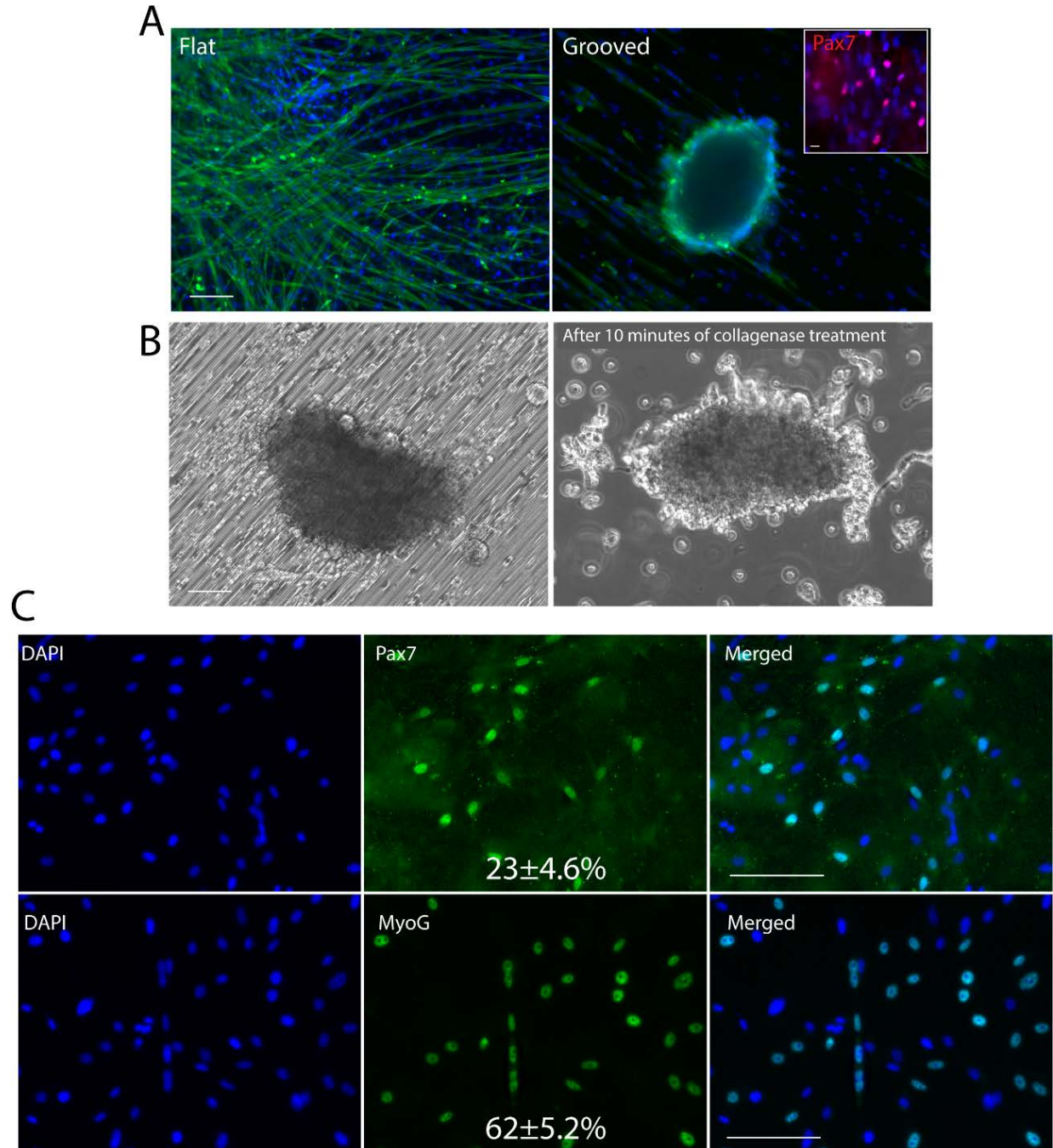


**Figure 4.7 Purification of skeletal muscle cells with microgrooved substrate.** **A)** Dermal fibroblasts on flat (left) and grooved (right) substrate treated with 6F medium for 10 days and stained for skeletal muscle troponin T. Skeletal muscle cells contracted into spherical colony on grooved substrate. Scale bar denotes 100 $\mu$ m. Insert: Confocal image of Pax7 positive cells within spherical colony. Scale bar of insert denotes 10 $\mu$ m. **B)** Skeletal muscle cell colonies detached after 10 minutes of collagenase treatment. Scale bar denotes 100 $\mu$ m. **C)** Disaggregated skeletal muscle colonies stained and quantified for Pax7 and MyoG positive cells. Scale bar denotes 100 $\mu$ m.

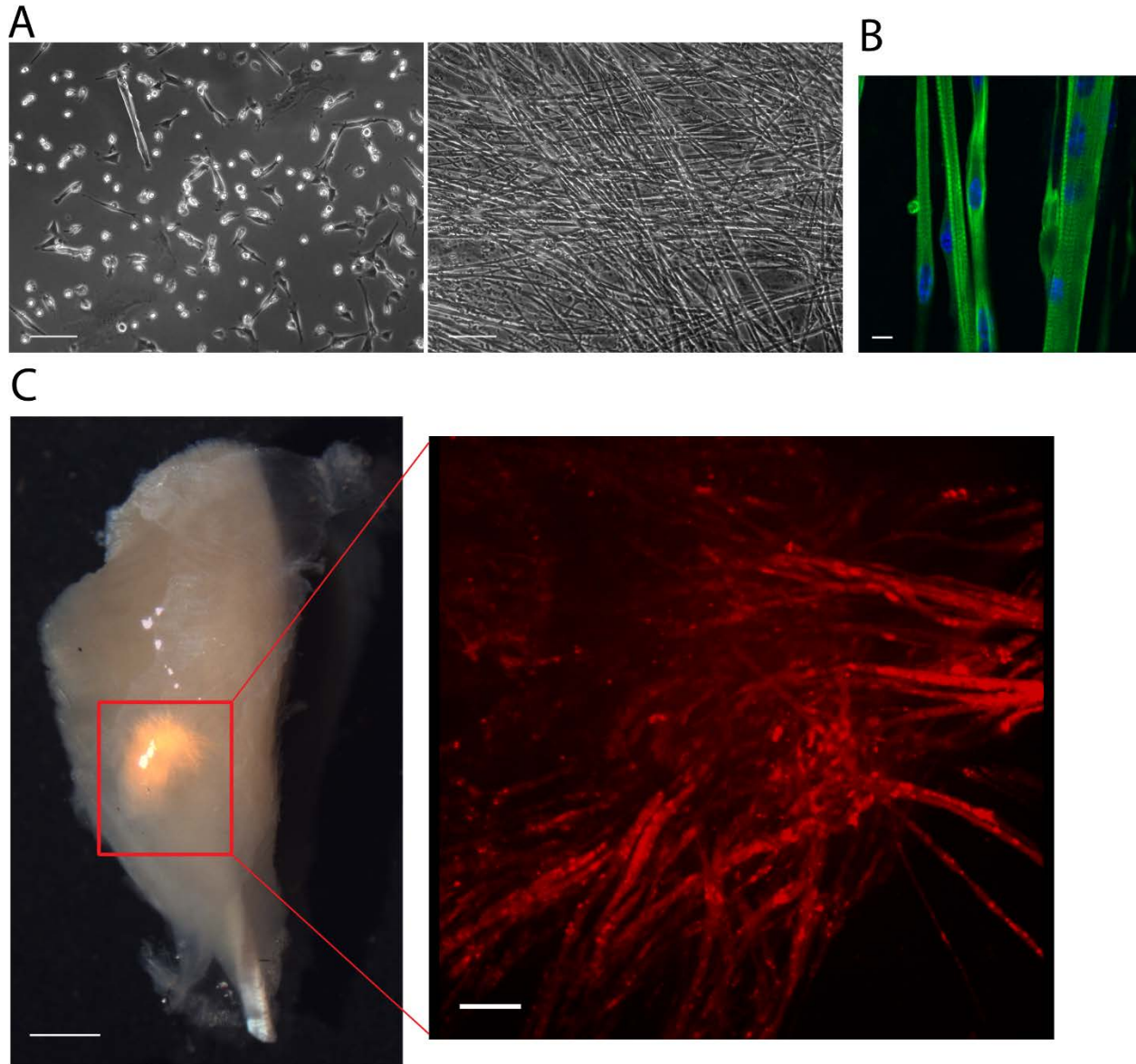


**Figure 4.8 Maturation and engraftment potential of reprogrammed skeletal muscle cells.** **A)** Purified skeletal muscle cells cultured in MEF medium for 2 weeks formed long myotubes that beat spontaneously. Scale bar denotes 100 $\mu$ m. **B)** Staining for skeletal muscle troponin T revealed clear striated pattern. Scale bar denotes 10 $\mu$ m. **C)** Purified skeletal muscle cells injected into cardiotoxin-injured tibialis anterior engrafted after 1 week. Scale bar denotes 1mm. Insert: Confocal image of engrafted skeletal muscle cells. Scale bar denotes 10 $\mu$ m.

#### 4.4 Discussion

Previous works have demonstrated using skin derived cells as a source of myogenic cells. One of the earlier work directly transplanted dermal fibroblasts into irradiated mdx mouse muscle and subsequently showed presence of dystrophin positive fibers as a proof of engraftment[130]. Subsequently, it was shown that dermal fibroblasts could be induced to convert into a MyoD positive cells when co-cultured with myoblasts[131]. I could convert dermal fibroblasts into Pax7 positive cells with our chemical cocktail. It would be interesting to study if co-culture with myoblasts and chemical cocktail treatment induced lineage conversion

via similar mechanisms, and that the 6F chemical cocktail mimicked certain soluble factors secreted by myoblasts that were key to inducing lineage conversion.

Toma et. al. have identified a population of multipotent stem cells that could be isolated from the dermal layer, termed skin derived precursors (SKP)[132]. Subsequent works showed that expanded SKPs could be induced to differentiate into skeletal muscle cells[110,133]. However, since SKP expressed Sca-1, I have excluded this population from our starting population by FACs. Interestingly, it was shown that Sca-1 negative population from the dermal layer could also differentiate into skeletal muscle cells after an initial aggregation in suspension and subsequent plating onto collagen coated surface[111]. In our case, I need not aggregate our starting population nor coat our culture surface with collagen.

Montanaro et. al. have shown that side population cells from the epidermis could differentiate into skeletal muscle cells when transplanted into mdx mouse muscle[112]. Our work excluded the participation of this population since I separated the epidermal layer.

In addition to dermal fibroblasts, I have tried unsuccessfully to reprogram fibroblasts from the ear, tail tip and skeletal muscle. Dermal fibroblasts originated from the dermatome, and skeletal muscle from the myotome. Both dermatome and myotome originated from the somitic dermomyotome[131]. Thus, a lower epigenetic barrier as a result of their shared developmental origin could help explain why only dermal fibroblasts could be reprogrammed into skeletal muscle cells with the 6F cocktail.

I observed that the skeletal muscle cells usually emerged in clusters. This could be because the fibroblast was reprogrammed into a skeletal muscle progenitor first, which proliferated and differentiated to form the cluster of myocytes. Some of the daughter cells might have remained in the progenitor state, thus explaining the presence of Pax7+ cells in the clusters. Such asymmetrical division of muscle progenitor cells has been observed before[136]. The use of a Pax7 reporter mouse to track the appearance of any Pax7 positive cells in the reprogramming culture would be useful to verify this hypothesis.

I have treated human foreskin-derived dermal fibroblasts with our reprogramming medium but failed to observe any myocyte clusters emerging after up to 3 weeks. Future work will screen for additional chemicals to achieve reprogramming with human dermal fibroblasts.

For the first time I have shown that a cocktail of two small molecules can efficiently reprogram dermal fibroblasts into skeletal muscle cells. The short duration required, high yield, differentiation and engraftment potential of the resulting cells will offer significant advantages in advancing muscle regeneration.

## Conclusion and Future Directions

In chapter 2 and 3, I described simple physical methods to improve efficiency of reprogramming into iPSCs and cardiomyocytes respectively. These results further revealed a physical dimension to approaches for affecting cellular reprogramming efficiency. While I have provided some insights into the underlying mechanisms, large scale profiling methods such as microarray, bisulfite seq and CHIP seq may reveal other pathways on a transcriptomic and epigenetic level that are perturbed by these physical cues. I also have not established if these methods work for human cells, and it will be imperative to do so in future work.

In chapter 4, I described a cocktail of 2 chemicals that could efficiently reprogram murine dermal fibroblasts into skeletal muscle cells. I showed that the reprogrammed cells engrafted into injured muscle after 1 week, but samples from longer time points need to be examined as well to determine if this engraftment is temporary or permanent. Behavioral tests could be performed to demonstrate that engraftment is indeed beneficial for functional recovery. Histological examination should be performed to determine if engrafted cells home in and take up satellite cell niches in either the endogenous or donor-derived myofibers. Apart from regenerating injured muscle, another important application of this chemical reprogramming method is the treatment of muscular dystrophy. As a proof of concept, donor dermal fibroblasts from mdx mutant mouse can be genetically corrected by expressing mini-dystrophin or correcting the endogenous gene locus. The corrected cells can then be reprogrammed with 6F medium, injected back into the donor's muscle and subsequently analyzed for expression of dystrophin. Ultimately, I need to translate these findings into human cells, so more screens need to be performed to identify additional small molecules to augment our 6F cocktail to reprogram human fibroblasts into skeletal muscle cells.

I have demonstrated how to influence cell fate decisions with physical and chemical cues, and hope that these findings can contribute to establishing direct cell reprogramming as a viable approach for regenerative medicine.

## References

- [1] R.L. Davis, H. Weintraub, A.B. Lassar, Expression of a single transfected cDNA converts fibroblasts to myoblasts, *Cell*. 51 (1987) 987–1000. doi:10.1016/0092-8674(87)90585-X.
- [2] H. Xie, M. Ye, R. Feng, T. Graf, Stepwise Reprogramming of B Cells into Macrophages, *Cell*. 117 (2004) 663–676. doi:10.1016/S0092-8674(04)00419-2.
- [3] K. Takahashi, S. Yamanaka, Induction of pluripotent stem cells from mouse embryonic and adult fibroblast cultures by defined factors, *Cell*. 126 (2006) 663–676.
- [4] M. Ieda, J.-D. Fu, P. Delgado-Olguin, V. Vedantham, Y. Hayashi, B.G. Bruneau, D. Srivastava, Direct Reprogramming of Fibroblasts into Functional Cardiomyocytes by Defined Factors, *Cell*. 142 (2010) 375–386. doi:10.1016/j.cell.2010.07.002.
- [5] T. Vierbuchen, A. Ostermeier, Z.P. Pang, Y. Kokubu, T.C. Südhof, M. Wernig, Direct conversion of fibroblasts to functional neurons by defined factors, *Nature*. 463 (2010) 1035–1041. doi:10.1038/nature08797.
- [6] S. Sekiya, A. Suzuki, Direct conversion of mouse fibroblasts to hepatocyte-like cells by defined factors, *Nature*. 475 (2011) 390–393. doi:10.1038/nature10263.
- [7] L. Qian, Y. Huang, C.I. Spencer, A. Foley, V. Vedantham, L. Liu, S.J. Conway, J. Fu, D. Srivastava, In vivo reprogramming of murine cardiac fibroblasts into induced cardiomyocytes, *Nature*. 485 (2012) 593–598. doi:10.1038/nature11044.
- [8] Z. Guo, L. Zhang, Z. Wu, Y. Chen, F. Wang, G. Chen, In Vivo Direct Reprogramming of Reactive Glial Cells into Functional Neurons after Brain Injury and in an Alzheimer’s Disease Model, *Cell Stem Cell*. 14 (2014) 188–202. doi:10.1016/j.stem.2013.12.001.
- [9] A XEN-like State Bridges Somatic Cells to Pluripotency during Chemical Reprogramming: *Cell*, (n.d.). [http://www.cell.com/cell/abstract/S0092-8674\(15\)01497-X](http://www.cell.com/cell/abstract/S0092-8674(15)01497-X) (accessed July 17, 2016).
- [10] P. Hou, Y. Li, X. Zhang, C. Liu, J. Guan, H. Li, T. Zhao, J. Ye, W. Yang, K. Liu, J. Ge, J. Xu, Q. Zhang, Y. Zhao, H. Deng, Pluripotent Stem Cells Induced from Mouse Somatic Cells by Small-Molecule Compounds, *Science*. 341 (2013) 651–654. doi:10.1126/science.1239278.
- [11] N. Cao, Y. Huang, J. Zheng, C.I. Spencer, Y. Zhang, J.-D. Fu, B. Nie, M. Xie, M. Zhang, H. Wang, T. Ma, T. Xu, G. Shi, D. Srivastava, S. Ding, Conversion of human fibroblasts into functional cardiomyocytes by small molecules, *Science*. (2016) aaf1502. doi:10.1126/science.aaf1502.
- [12] Y. Fu, C. Huang, X. Xu, H. Gu, Y. Ye, C. Jiang, Z. Qiu, X. Xie, Direct reprogramming of mouse fibroblasts into cardiomyocytes with chemical cocktails, *Cell Res*. 25 (2015) 1013–1024. doi:10.1038/cr.2015.99.
- [13] X. Li, X. Zuo, J. Jing, Y. Ma, J. Wang, D. Liu, J. Zhu, X. Du, L. Xiong, Y. Du, J. Xu, X. Xiao, J. Wang, Z. Chai, Y. Zhao, H. Deng, Small-Molecule-Driven Direct Reprogramming of Mouse Fibroblasts into Functional Neurons, *Cell Stem Cell*. 17 (2015) 195–203. doi:10.1016/j.stem.2015.06.003.
- [14] E. Tian, G. Sun, G. Sun, J. Chao, P. Ye, C. Warden, A.D. Riggs, Y. Shi, Small-Molecule-Based Lineage Reprogramming Creates Functional Astrocytes, *Cell Rep*. 0 (2016). doi:10.1016/j.celrep.2016.06.042.
- [15] M. Zhang, Y.-H. Lin, Y.J. Sun, S. Zhu, J. Zheng, K. Liu, N. Cao, K. Li, Y. Huang, S. Ding, Pharmacological Reprogramming of Fibroblasts into Neural Stem Cells by Signaling-

- Directed Transcriptional Activation, *Cell Stem Cell*. 18 (2016) 653–667.  
doi:10.1016/j.stem.2016.03.020.
- [16] M. Wernig, A. Meissner, R. Foreman, T. Brambrink, M. Ku, K. Hochedlinger, B.E. Bernstein, R. Jaenisch, In vitro reprogramming of fibroblasts into a pluripotent ES-cell-like state, *Nature*. 448 (2007) 318–324.
- [17] C. Hu, L. Li, Current reprogramming systems in regenerative medicine: from somatic cells to induced pluripotent stem cells, *Regen. Med.* 11 (2015) 105–32. doi:10.2217/rme.15.79.
- [18] M. Stadtfeld, N. Maherali, M. Borkent, K. Hochedlinger, A reprogrammable mouse strain from gene-targeted embryonic stem cells, *Nat. Methods*. 7 (2010) 53–55.  
doi:10.1038/nmeth.1409.
- [19] B.W. Carey, S. Markoulaki, C. Beard, J. Hanna, R. Jaenisch, Single-gene transgenic mouse strains for reprogramming adult somatic cells, *Nat. Methods*. 7 (2010) 56–59.
- [20] M. Stadtfeld, K. Hochedlinger, Induced pluripotency: history, mechanisms, and applications, *Genes Dev.* 24 (2010) 2239–2263.
- [21] H. Li, M. Collado, A. Villasante, K. Strati, S. Ortega, M. Cañamero, M.A. Blasco, M. Serrano, The Ink4/Arf locus is a barrier for iPS cell reprogramming, *Nature*. 460 (2009) 1136–1139.
- [22] Y. Rais, A. Zviran, S. Geula, O. Gafni, E. Chomsky, S. Viukov, A.A. Mansour, I. Caspi, V. Krupalnik, M. Zerbib, Deterministic direct reprogramming of somatic cells to pluripotency, *Nature*. 502 (2013) 65–70.
- [23] H. Hong, K. Takahashi, T. Ichisaka, T. Aoi, O. Kanagawa, M. Nakagawa, K. Okita, S. Yamanaka, Suppression of induced pluripotent stem cell generation by the p53–p21 pathway, *Nature*. 460 (2009) 1132–1135.
- [24] B. di Stefano, S. Collombet, T. Graf, C/EBPalpha poises B cells for rapid reprogramming into induced pluripotent stem cells, *Nature*. 1 (2013) 8.
- [25] Y. Rais, A. Zviran, S. Geula, O. Gafni, E. Chomsky, S. Viukov, A.A. Mansour, I. Caspi, V. Krupalnik, M. Zerbib, Deterministic direct reprogramming of somatic cells to pluripotency, *Nature*. 502 (2013) 65–70.
- [26] H. Hong, K. Takahashi, T. Ichisaka, T. Aoi, O. Kanagawa, M. Nakagawa, K. Okita, S. Yamanaka, Suppression of induced pluripotent stem cell generation by the p53–p21 pathway, *Nature*. 460 (2009) 1132–1135.
- [27] O. Bar-Nur, J. Brumbaugh, C. Verheul, E. Apostolou, I. Pruteanu-Malinici, R.M. Walsh, S. Ramaswamy, K. Hochedlinger, Small molecules facilitate rapid and synchronous iPSC generation, *Nat. Methods*. 11 (2014) 1170–1176.
- [28] M.A. Esteban, T. Wang, B. Qin, J. Yang, D. Qin, J. Cai, W. Li, Z. Weng, J. Chen, S. Ni, Vitamin C enhances the generation of mouse and human induced pluripotent stem cells, *Cell Stem Cell*. 6 (2010) 71–79.
- [29] D. Huangfu, R. Maehr, W. Guo, A. Eijkelenboom, M. Snitow, A.E. Chen, D.A. Melton, Induction of pluripotent stem cells by defined factors is greatly improved by small-molecule compounds, *Nat. Biotechnol.* 26 (2008) 795–797.
- [30] J.K. Ichida, J. Blanchard, K. Lam, E.Y. Son, J.E. Chung, D. Egli, K.M. Loh, A.C. Carter, F.P. Di Giorgio, K. Koszka, A small-molecule inhibitor of Tgf- $\beta$  signaling replaces Sox2 in reprogramming by inducing Nanog, *Cell Stem Cell*. 5 (2009) 491–503.

- [31] S.E. Vidal, B. Amlani, T. Chen, A. Tsigirigos, M. Stadtfeld, Combinatorial modulation of signaling pathways reveals cell-type-specific requirements for highly efficient and synchronous iPSC reprogramming, *Stem Cell Rep.* 3 (2014) 574–584.
- [32] D. Huangfu, R. Maehr, W. Guo, A. Eijkelenboom, M. Snitow, A.E. Chen, D.A. Melton, Induction of pluripotent stem cells by defined factors is greatly improved by small-molecule compounds, *Nat. Biotechnol.* 26 (2008) 795–797. doi:10.1038/nbt1418.
- [33] M.A. Esteban, T. Wang, B. Qin, J. Yang, D. Qin, J. Cai, W. Li, Z. Weng, J. Chen, S. Ni, Vitamin C enhances the generation of mouse and human induced pluripotent stem cells, *Cell Stem Cell.* 6 (2010) 71–79.
- [34] T.L. Downing, J. Soto, C. Morez, T. Houssin, A. Fritz, F. Yuan, J. Chu, S. Patel, D. V Schaffer, S. Li, Biophysical regulation of epigenetic state and cell reprogramming, *Nat. Mater.* 12 (2013) 1154–1162.
- [35] Y. Yoshida, K. Takahashi, K. Okita, T. Ichisaka, S. Yamanaka, Hypoxia enhances the generation of induced pluripotent stem cells, *Cell Stem Cell.* 5 (2009) 237–241.
- [36] D.A. Fluri, P.D. Tonge, H. Song, R.P. Baptista, N. Shakiba, S. Shukla, G. Clarke, A. Nagy, P.W. Zandstra, Derivation, expansion and differentiation of induced pluripotent stem cells in continuous suspension cultures, *Nat. Methods.* 9 (2012) 509–516.
- [37] B. Choi, K. Park, J. Kim, K. Ko, J. Kim, D.K. Han, S. Lee, Stiffness of Hydrogels Regulates Cellular Reprogramming Efficiency Through Mesenchymal-to-Epithelial Transition and Stemness Markers, *Macromol. Biosci.* (2015).
- [38] B.W. Carey, S. Markoulaki, C. Beard, J. Hanna, R. Jaenisch, Single-gene transgenic mouse strains for reprogramming adult somatic cells, *Nat. Methods.* 7 (2010) 56–59.
- [39] J.M.D. Thomas, A. Chakraborty, M.K. Sharp, R.E. Berson, Spatial and temporal resolution of shear in an orbiting petri dish., *Biotechnol. Prog.* 27 (2011) 460–5. doi:10.1002/btpr.507.
- [40] E.P. Rogakou, D.R. Pilch, A.H. Orr, V.S. Ivanova, W.M. Bonner, DNA Double-stranded Breaks Induce Histone H2AX Phosphorylation on Serine 139, *J. Biol. Chem.* 273 (1998) 5858–5868. doi:10.1074/jbc.273.10.5858.
- [41] V. Turinetto, L. Orlando, Y. Sanchez-Ripoll, B. Kumpfmüller, M.P. Storm, P. Porcedda, V. Minieri, S. Saviozzi, L. Accomasso, E. Cibrario Rocchietti, K. Moorwood, P. Circosta, A. Cignetti, M.J. Welham, C. Giachino, High basal  $\gamma$ H2AX levels sustain self-renewal of mouse embryonic and induced pluripotent stem cells, *Stem Cells Dayt. Ohio.* 30 (2012) 1414–1423. doi:10.1002/stem.1133.
- [42] T. Chen, D. Yuan, B. Wei, J. Jiang, J. Kang, K. Ling, Y. Gu, J. Li, L. Xiao, G. Pei, E-Cadherin-Mediated Cell–Cell Contact Is Critical for Induced Pluripotent Stem Cell Generation, *Stem Cells.* 28 (2010) 1315–1325.
- [43] I. Lian, J. Kim, H. Okazawa, J. Zhao, B. Zhao, J. Yu, A. Chinnaiyan, M. a Israel, L.S.B. Goldstein, R. Abujarour, S. Ding, K.-L. Guan, The role of YAP transcription coactivator in regulating stem cell self-renewal and differentiation., *Genes Dev.* 24 (2010) 1106–18. doi:10.1101/gad.1903310.
- [44] M. Aragona, T. Panciera, A. Manfrin, S. Giullitti, F. Michielin, N. Elvassore, S. Dupont, S. Piccolo, A mechanical checkpoint controls multicellular growth through YAP/TAZ regulation by actin-processing factors, *Cell.* 154 (2013) 1047–1059.

- [45] R. Ho, B. Papp, J.A. Hoffman, B.J. Merrill, K. Plath, Stage-specific regulation of reprogramming to induced pluripotent stem cells by Wnt signaling and T cell factor proteins, *Cell Rep.* 3 (2013) 2113–2126.
- [46] F. Aulicino, I. Theka, L. Ombrato, F. Lluís, M.P. Cosma, Temporal perturbation of the Wnt signaling pathway in the control of cell reprogramming is modulated by TCF1, *Stem Cell Rep.* 2 (2014) 707–720.
- [47] Y. Kuo, T. Chang, W. Hsu, J. Zhou, H. Lee, J. Hui-Chun Ho, S. Chien, O. Kuang-Sheng, Oscillatory Shear Stress Mediates Directional Reorganization of Actin Cytoskeleton and Alters Differentiation Propensity of Mesenchymal Stem Cells, *STEM CELLS.* 33 (2015) 429–442.
- [48] B. Zhao, X. Wei, W. Li, R.S. Udan, Q. Yang, J. Kim, J. Xie, T. Ikenoue, J. Yu, L. Li, Inactivation of YAP oncoprotein by the Hippo pathway is involved in cell contact inhibition and tissue growth control, *Genes Dev.* 21 (2007) 2747–2761.
- [49] C. Dietrich, J. Scherwat, D. Faust, F. Oesch, Subcellular localization of  $\beta$ -catenin is regulated by cell density, *Biochem. Biophys. Res. Commun.* 292 (2002) 195–199.
- [50] K. Orford, C.C. Orford, S.W. Byers, Exogenous expression of  $\beta$ -catenin regulates contact inhibition, anchorage-independent growth, anoikis, and radiation-induced cell cycle arrest, *J. Cell Biol.* 146 (1999) 855–868.
- [51] J. Hanna, K. Saha, B. Pando, J. Van Zon, C.J. Lengner, M.P. Creighton, A. van Oudenaarden, R. Jaenisch, Direct cell reprogramming is a stochastic process amenable to acceleration, *Nature.* 462 (2009) 595–601.
- [52] M.G.P. Stoker, H. Rubin, Density dependent inhibition of cell growth in culture, (1967).
- [53] M. Stadtfeld, N. Maherali, D.T. Breault, K. Hochedlinger, Defining molecular cornerstones during fibroblast to iPS cell reprogramming in mouse, *Cell Stem Cell.* 2 (2008) 230–240.
- [54] Y. Zhang, W. Li, T. Laurent, S. Ding, Small molecules, big roles -- the chemical manipulation of stem cell fate and somatic cell reprogramming, *J. Cell Sci.* 125 (2012) 5609–5620. doi:10.1242/jcs.096032.
- [55] Y. Zhai, X. Chen, D. Yu, T. Li, J. Cui, G. Wang, J.-F. Hu, W. Li, Histone deacetylase inhibitor valproic acid promotes the induction of pluripotency in mouse fibroblasts by suppressing reprogramming-induced senescence stress, *Exp. Cell Res.* 337 (2015) 61–67. doi:10.1016/j.yexcr.2015.06.003.
- [56] N. Maherali, K. Hochedlinger, Tgf $\beta$  Signal Inhibition Cooperates in the Induction of iPSCs and Replaces Sox2 and cMyc, *Curr. Biol.* 19 (2009) 1718–1723. doi:10.1016/j.cub.2009.08.025.
- [57] D. Huangfu, R. Maehr, W. Guo, A. Eijkelenboom, M. Snitow, A.E. Chen, D.A. Melton, Induction of pluripotent stem cells by defined factors is greatly improved by small-molecule compounds, *Nat. Biotechnol.* 26 (2008) 795–797. doi:10.1038/nbt1418.
- [58] A. Banito, S.T. Rashid, J.C. Acosta, S. Li, C.F. Pereira, I. Geti, S. Pinho, J.C. Silva, V. Azuara, M. Walsh, Senescence impairs successful reprogramming to pluripotent stem cells, *Genes Dev.* 23 (2009) 2134–2139.
- [59] R.P. Koche, Z.D. Smith, M. Adli, H. Gu, M. Ku, A. Gnirke, B.E. Bernstein, A. Meissner, Reprogramming factor expression initiates widespread targeted chromatin remodeling, *Cell Stem Cell.* 8 (2011) 96–105.

- [60] S. Ruiz, A.D. Panopoulos, A. Herrerías, K.-D. Bissig, M. Lutz, W.T. Berggren, I.M. Verma, J.C.I. Belmonte, A high proliferation rate is required for cell reprogramming and maintenance of human embryonic stem cell identity, *Curr. Biol.* 21 (2011) 45–52.
- [61] D.M. Gilbert, Cell fate transitions and the replication timing decision point, *J. Cell Biol.* 191 (2010) 899–903.
- [62] A.P. Wolffe, Implications of DNA replication for eukaryotic gene expression., *J. Cell Sci.* 99 (1991) 201–206.
- [63] J.M. Polo, E. Anderssen, R.M. Walsh, B.A. Schwarz, C.M. Nefzger, S.M. Lim, M. Borkent, E. Apostolou, S. Alaei, J. Cloutier, A molecular roadmap of reprogramming somatic cells into iPS cells, *Cell.* 151 (2012) 1617–1632.
- [64] S. Guo, X. Zi, V.P. Schulz, J. Cheng, M. Zhong, S.H.J. Koochaki, C.M. Megyola, X. Pan, K. Heydari, S.M. Weissman, Nonstochastic reprogramming from a privileged somatic cell state, *Cell.* 156 (2014) 649–662.
- [65] M. Pour, I. Pilzer, R. Rosner, Z.D. Smith, A. Meissner, I. Nachman, Epigenetic predisposition to reprogramming fates in somatic cells, *EMBO Rep.* (2015) e201439264.
- [66] N.-G. Kim, E. Koh, X. Chen, B.M. Gumbiner, E-cadherin mediates contact inhibition of proliferation through Hippo signaling-pathway components, *Proc. Natl. Acad. Sci.* 108 (2011) 11930–11935.
- [67] T. Alkasalias, E. Flaberg, V. Kashuba, A. Alexeyenko, T. Pavlova, A. Savchenko, L. Szekely, G. Klein, H. Guven, Inhibition of tumor cell proliferation and motility by fibroblasts is both contact and soluble factor dependent, *Proc. Natl. Acad. Sci.* 111 (2014) 17188–17193.
- [68] M.H. Lee, I. Reynisdóttir, J. Massagué, Cloning of p57KIP2, a cyclin-dependent kinase inhibitor with unique domain structure and tissue distribution., *Genes Dev.* 9 (1995) 639–649. doi:10.1101/gad.9.6.639.
- [69] M. Serrano, H.-W. Lee, L. Chin, C. Cordon-Cardo, D. Beach, R.A. DePinho, Role of the INK4a Locus in Tumor Suppression and Cell Mortality, *Cell.* 85 (1996) 27–37. doi:10.1016/S0092-8674(00)81079-X.
- [70] Y. Xiong, G.J. Hannon, H. Zhang, D. Casso, R. Kobayashi, D. Beach, p21 is a universal inhibitor of cyclin kinases, *Nature.* 366 (1993) 701–704. doi:10.1038/366701a0.
- [71] T. Sadahiro, S. Yamanaka, M. Ieda, Direct Cardiac Reprogramming Progress and Challenges in Basic Biology and Clinical Applications, *Circ. Res.* 116 (2015) 1378–1391. doi:10.1161/CIRCRESAHA.116.305374.
- [72] T.M. Jayawardena, B. Egemnazarov, E.A. Finch, L. Zhang, J.A. Payne, K. Pandya, Z. Zhang, P. Rosenberg, M. Mirotsov, V.J. Dzau, MicroRNA-mediated in vitro and in vivo direct reprogramming of cardiac fibroblasts to cardiomyocytes, *Circ. Res.* 110 (2012) 1465–1473. doi:10.1161/CIRCRESAHA.112.269035.
- [73] N. Muraoka, H. Yamakawa, K. Miyamoto, T. Sadahiro, T. Umei, M. Isomi, H. Nakashima, M. Akiyama, R. Wada, K. Inagawa, T. Nishiyama, R. Kaneda, T. Fukuda, S. Takeda, S. Tohyama, H. Hashimoto, Y. Kawamura, N. Goshima, R. Aeba, H. Yamagishi, K. Fukuda, M. Ieda, MiR-133 promotes cardiac reprogramming by directly repressing Snai1 and silencing fibroblast signatures, *EMBO J.* 33 (2014) 1565–1581. doi:10.15252/emj.201387605.
- [74] Y. Zhao, P. Londono, Y. Cao, E.J. Sharpe, C. Proenza, R. O'Rourke, K.L. Jones, M.Y. Jeong, L.A. Walker, P.M. Buttrick, T.A. McKinsey, K. Song, High-efficiency reprogramming of

- fibroblasts into cardiomyocytes requires suppression of pro-fibrotic signalling, *Nat. Commun.* 6 (2015). doi:10.1038/ncomms9243.
- [75] J.L. Ifkovits, R.C. Addis, J.A. Epstein, J.D. Gearhart, Inhibition of TGF $\beta$  Signaling Increases Direct Conversion of Fibroblasts to Induced Cardiomyocytes, *PLoS ONE*. 9 (2014) e89678. doi:10.1371/journal.pone.0089678.
- [76] H. Zhou, M.E. Dickson, M.S. Kim, R. Bassel-Duby, E.N. Olson, Akt1/protein kinase B enhances transcriptional reprogramming of fibroblasts to functional cardiomyocytes, *Proc. Natl. Acad. Sci.* 112 (2015) 11864–11869. doi:10.1073/pnas.1516237112.
- [77] N. Christoforou, M. Chellappan, A.F. Adler, R.D. Kirkton, T. Wu, R.C. Addis, N. Bursac, K.W. Leong, Transcription factors MYOCD, SRF, Mesp1 and SMARCD3 enhance the cardio-inducing effect of GATA4, TBX5, and MEF2C during direct cellular reprogramming, (2013). <http://dx.plos.org/10.1371/journal.pone.0063577> (accessed January 29, 2016).
- [78] H. Hirai, N. Katoku-Kikyo, S.A. Keirstead, N. Kikyo, Accelerated direct reprogramming of fibroblasts into cardiomyocyte-like cells with the MyoD transactivation domain, *Cardiovasc. Res.* 100 (2013) 105–113. doi:10.1093/cvr/cvt167.
- [79] L. Wang, Z. Liu, C. Yin, H. Asfour, O. Chen, Y. Li, N. Bursac, J. Liu, L. Qian, Stoichiometry of Gata4, Mef2c, and Tbx5 Influences the Efficiency and Quality of Induced Cardiac Myocyte Reprogramming, *Circ. Res.* 116 (2015) 237–244. doi:10.1161/CIRCRESAHA.116.305547.
- [80] K. Song, Y.-J. Nam, X. Luo, X. Qi, W. Tan, G.N. Huang, A. Acharya, C.L. Smith, M.D. Tallquist, E.G. Neilson, J.A. Hill, R. Bassel-Duby, E.N. Olson, Heart repair by reprogramming non-myocytes with cardiac transcription factors, *Nature*. 485 (2012) 599–604. doi:10.1038/nature11139.
- [81] H. Yamakawa, N. Muraoka, K. Miyamoto, T. Sadahiro, M. Isomi, S. Haginiwa, H. Kojima, T. Umei, M. Akiyama, Y. Kuishi, J. Kurokawa, T. Furukawa, K. Fukuda, M. Ieda, Fibroblast Growth Factors and Vascular Endothelial Growth Factor Promote Cardiac Reprogramming under Defined Conditions, *Stem Cell Rep.* 5 (2015) 1128–1142. doi:10.1016/j.stemcr.2015.10.019.
- [82] K. Kulangara, A.F. Adler, H. Wang, M. Chellappan, E. Hammett, R. Yasuda, K.W. Leong, The effect of substrate topography on direct reprogramming of fibroblasts to induced neurons, *Biomaterials*. 35 (2014) 5327–5336. doi:10.1016/j.biomaterials.2014.03.034.
- [83] M. Govoni, C. Muscari, C. Guarnieri, E. Giordano, Mechanostimulation Protocols for Cardiac Tissue Engineering, *BioMed Res. Int.* 2013 (2013) e918640. doi:10.1155/2013/918640.
- [84] J.G. Jacot, A.D. McCulloch, J.H. Omens, Substrate Stiffness Affects the Functional Maturation of Neonatal Rat Ventricular Myocytes, *Biophys. J.* 95 (2008) 3479–3487. doi:10.1529/biophysj.107.124545.
- [85] G. Forte, S. Pagliari, M. Ebara, K. Uto, J.K.V. Tam, S. Romanazzo, C. Escobedo-Lucea, E. Romano, P. Di Nardo, E. Traversa, T. Aoyagi, Substrate Stiffness Modulates Gene Expression and Phenotype in Neonatal Cardiomyocytes In Vitro, *Tissue Eng. Part A*. 18 (2012) 1837–1848. doi:10.1089/ten.tea.2011.0707.
- [86] C. Rao, T. Prodromakis, L. Kolker, U.A.R. Chaudhry, T. Trantidou, A. Sridhar, C. Weekes, P. Camelliti, S.E. Harding, A. Darzi, M.H. Yacoub, T. Athanasiou, C.M. Terracciano, The effect of microgrooved culture substrates on calcium cycling of cardiac myocytes derived from

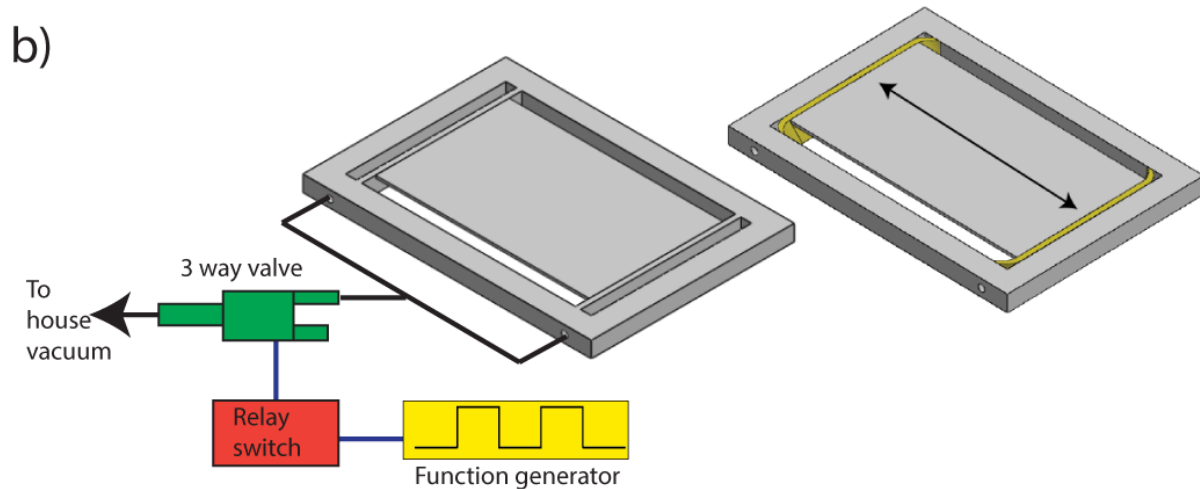
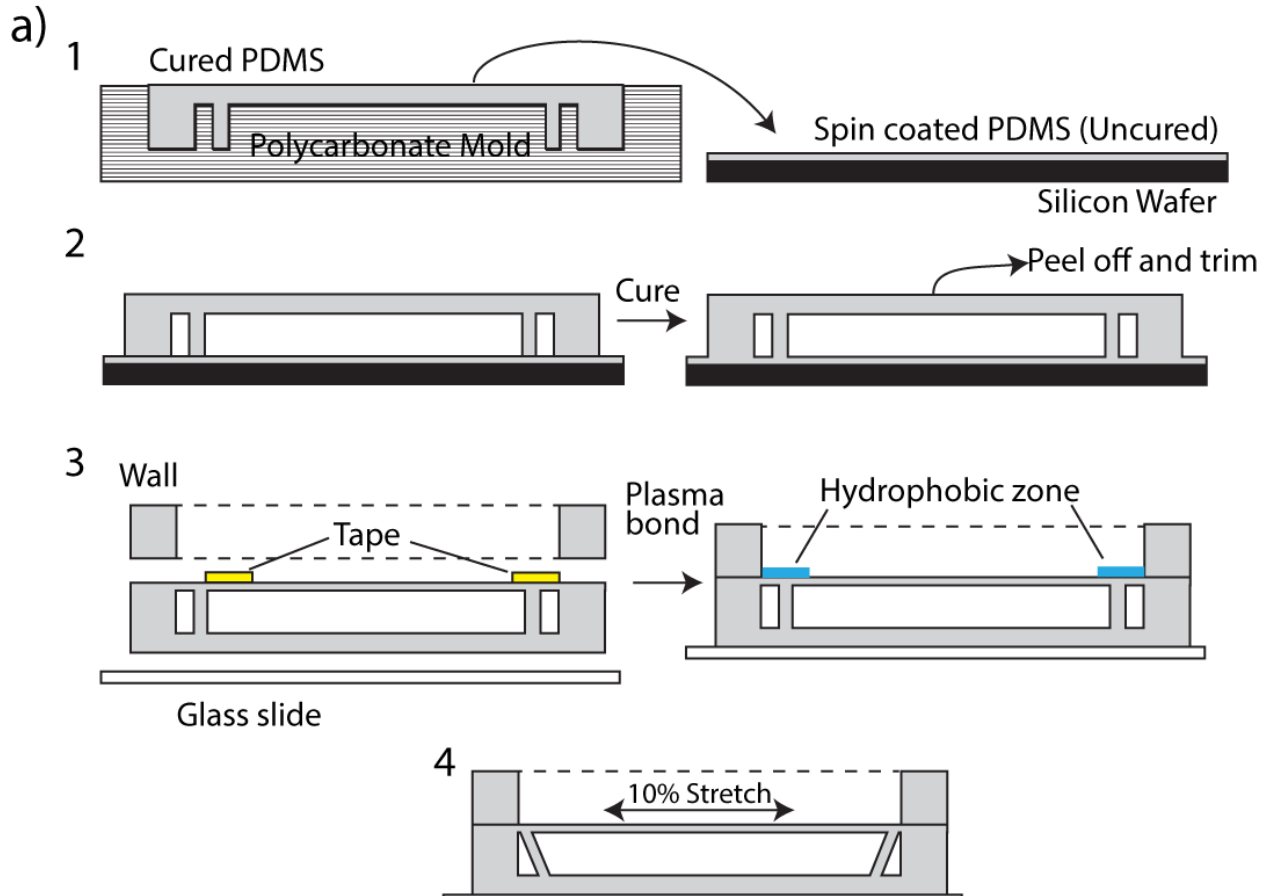
- human induced pluripotent stem cells, *Biomaterials*. 34 (2013) 2399–2411. doi:10.1016/j.biomaterials.2012.11.055.
- [87] C.Y. Tay, H. Yu, M. Pal, W.S. Leong, N.S. Tan, K.W. Ng, D.T. Leong, L.P. Tan, Micropatterned matrix directs differentiation of human mesenchymal stem cells towards myocardial lineage, *Exp. Cell Res.* 316 (2010) 1159–1168. doi:10.1016/j.yexcr.2010.02.010.
- [88] C. Morez, M. Nosedá, M.A. Paiva, E. Belian, M.D. Schneider, M.M. Stevens, Enhanced efficiency of genetic programming toward cardiomyocyte creation through topographical cues, *Biomaterials*. 70 (2015) 94–104. doi:10.1016/j.biomaterials.2015.07.063.
- [89] A.K. Yip, K. Iwasaki, C. Ursekar, H. Machiyama, M. Saxena, H. Chen, I. Harada, K.-H. Chiam, Y. Sawada, Cellular Response to Substrate Rigidity Is Governed by Either Stress or Strain, *Biophys. J.* 104 (2013) 19–29. doi:10.1016/j.bpj.2012.11.3805.
- [90] A.E. Carpenter, T.R. Jones, M.R. Lamprecht, C. Clarke, I.H. Kang, O. Friman, D.A. Guertin, J.H. Chang, R.A. Lindquist, J. Moffat, P. Golland, D.M. Sabatini, CellProfiler: image analysis software for identifying and quantifying cell phenotypes, *Genome Biol.* 7 (2006) R100. doi:10.1186/gb-2006-7-10-r100.
- [91] S.J. Kattman, T.L. Huber, G.M. Keller, Multipotent flk-1+ cardiovascular progenitor cells give rise to the cardiomyocyte, endothelial, and vascular smooth muscle lineages, *Dev. Cell.* 11 (2006) 723–732. doi:10.1016/j.devcel.2006.10.002.
- [92] T.L. Downing, J. Soto, C. Morez, T. Houssin, A. Fritz, F. Yuan, J. Chu, S. Patel, D.V. Schaffer, S. Li, Biophysical regulation of epigenetic state and cell reprogramming, *Nat. Mater.* 12 (2013) 1154–1162. doi:10.1038/nmat3777.
- [93] J. Kang, K.M. Puskar, R.S. Schwartz, P.R. LeDuc, Modeling Mechanotransduction Signaling through Actin Filament Network Deformation Linked to Biochemical Response, *Biophys. J.* 104 (2013) 317a–318a.
- [94] U.S. Schwarz, M.L. Gardel, United I stand—integrating the actin cytoskeleton and cell–matrix adhesions in cellular mechanotransduction, *J. Cell Sci.* 125 (2012) 3051–3060.
- [95] N. Wang, J.P. Butler, D.E. Ingber, Mechanotransduction across the cell surface and through the cytoskeleton, *Science*. 260 (1993) 1124–1127.
- [96] M. Kovács, J. Tóth, C. Hetényi, A. Málnási-Csizmadia, J.R. Sellers, Mechanism of Blebbistatin Inhibition of Myosin II, *J. Biol. Chem.* 279 (2004) 35557–35563. doi:10.1074/jbc.M405319200.
- [97] A. Holzinger, Jasplakinolide: an actin-specific reagent that promotes actin polymerization, *Methods Mol. Biol. Clifton NJ.* 586 (2009) 71–87. doi:10.1007/978-1-60761-376-3\_4.
- [98] S.N. Rubtsova, R.V. Kondratov, P.B. Kopnin, P.M. Chumakov, B.P. Kopnin, J.M. Vasiliev, Disruption of actin microfilaments by cytochalasin D leads to activation of p53, *FEBS Lett.* 430 (1998) 353–357. doi:10.1016/S0014-5793(98)00692-9.
- [99] E.N. Olson, A. Nordheim, Linking actin dynamics and gene transcription to drive cellular motile functions, *Nat. Rev. Mol. Cell Biol.* 11 (2010) 353–365. doi:10.1038/nrm2890.
- [100] S. Guettler, M.K. Vartiainen, F. Miralles, B. Larijani, R. Treisman, RPEL Motifs Link the Serum Response Factor Cofactor MAL but Not Myocardin to Rho Signaling via Actin Binding, *Mol. Cell. Biol.* 28 (2008) 732–742. doi:10.1128/MCB.01623-07.
- [101] Y.-J. Nam, K. Song, X. Luo, E. Daniel, K. Lambeth, K. West, J.A. Hill, J.M. DiMaio, L.A. Baker, R. Bassel-Duby, E.N. Olson, Reprogramming of human fibroblasts toward a cardiac fate, *Proc. Natl. Acad. Sci.* 110 (2013) 5588–5593. doi:10.1073/pnas.1301019110.

- [102] N. Gjorevski, A. S. Piotrowski, V.D. Varner, C.M. Nelson, Dynamic tensile forces drive collective cell migration through three-dimensional extracellular matrices, *Sci. Rep.* 5 (2015) 11458. doi:10.1038/srep11458.
- [103] N. Jain, K.V. Iyer, A. Kumar, G.V. Shivashankar, Cell geometric constraints induce modular gene-expression patterns via redistribution of HDAC3 regulated by actomyosin contractility, *Proc. Natl. Acad. Sci.* 110 (2013) 11349–11354. doi:10.1073/pnas.1300801110.
- [104] H.T.H. Au, B. Cui, Z.E. Chu, T. Veres, M. Radisic, Cell culture chips for simultaneous application of topographical and electrical cues enhance phenotype of cardiomyocytes, *Lab. Chip.* 9 (2009) 564–575. doi:10.1039/B810034A.
- [105] J.-D. Fu, N.R. Stone, L. Liu, C.I. Spencer, L. Qian, Y. Hayashi, P. Delgado-Olguin, S. Ding, B.G. Bruneau, D. Srivastava, Direct Reprogramming of Human Fibroblasts toward a Cardiomyocyte-like State, *Stem Cell Rep.* 1 (2013) 235–247. doi:10.1016/j.stemcr.2013.07.005.
- [106] R. Wada, N. Muraoka, K. Inagawa, H. Yamakawa, K. Miyamoto, T. Sadahiro, T. Umei, R. Kaneda, T. Suzuki, K. Kamiya, S. Tohyama, S. Yuasa, K. Kokaji, R. Aeba, R. Yozu, H. Yamagishi, T. Kitamura, K. Fukuda, M. Ieda, Induction of human cardiomyocyte-like cells from fibroblasts by defined factors, *Proc. Natl. Acad. Sci.* 110 (2013) 12667–12672. doi:10.1073/pnas.1304053110.
- [107] A. Sacco, R. Doyonnas, P. Kraft, S. Vitorovic, H.M. Blau, Self-renewal and expansion of single transplanted muscle stem cells, *Nature.* 456 (2008) 502–506. doi:10.1038/nature07384.
- [108] F. Relaix, P.S. Zammit, Satellite cells are essential for skeletal muscle regeneration: the cell on the edge returns centre stage, *Development.* 139 (2012) 2845–2856. doi:10.1242/dev.069088.
- [109] M. Cerletti, S. Jurga, C.A. Witczak, M.F. Hirshman, J.L. Shadrach, L.J. Goodyear, A.J. Wagers, Highly efficient, functional engraftment of skeletal muscle stem cells in dystrophic muscles, *Cell.* 134 (2008) 37–47. doi:10.1016/j.cell.2008.05.049.
- [110] Z. Qiu, C. Miao, J. Li, X. Lei, S. Liu, W. Guo, Y. Cao, E.-K. Duan, Skeletal Myogenic Potential of Mouse Skin-Derived Precursors, *Stem Cells Dev.* 19 (2009) 259–268. doi:10.1089/scd.2009.0058.
- [111] M. Wakabayashi, Y. Ito, T.S. Hamazaki, H. Okochi, Efficient Myogenic Differentiation of Murine Dermal Sca-1 (–) Cells via Initial Aggregation Culture, *Tissue Eng. Part A.* 16 (2010) 3251–3259. doi:10.1089/ten.tea.2009.0678.
- [112] F. Montanaro, K. Liadaki, J. Volinski, A. Flint, L.M. Kunkel, Skeletal muscle engraftment potential of adult mouse skin side population cells, *Proc. Natl. Acad. Sci.* 100 (2003) 9336–9341. doi:10.1073/pnas.1133179100.
- [113] G. Ferrari, G. Cusella-De Angelis, M. Coletta, E. Paolucci, A. Stornaiuolo, G. Cossu, F. Mavilio, Muscle regeneration by bone marrow-derived myogenic progenitors, *Science.* 279 (1998) 1528–1530.
- [114] E.J. Gang, J.A. Jeong, S.H. Hong, S.H. Hwang, S.W. Kim, I.H. Yang, C. Ahn, H. Han, H. Kim, Skeletal myogenic differentiation of mesenchymal stem cells isolated from human umbilical cord blood, *Stem Cells Dayt. Ohio.* 22 (2004) 617–624. doi:10.1634/stemcells.22-4-617.

- [115] M. Sampaolesi, Y. Torrente, A. Innocenzi, R. Tonlorenzi, G. D'Antona, M.A. Pellegrino, R. Barresi, N. Bresolin, M.G.C.D. Angelis, K.P. Campbell, R. Bottinelli, G. Cossu, Cell Therapy of  $\alpha$ -Sarcoglycan Null Dystrophic Mice Through Intra-Arterial Delivery of Mesoangioblasts, *Science*. 301 (2003) 487–492. doi:10.1126/science.1082254.
- [116] J. Chal, M. Oginuma, Z. Al Tanoury, B. Gobert, O. Sumara, A. Hick, F. Bousson, Y. Zidouni, C. Mursch, P. Moncuquet, O. Tassy, S. Vincent, A. Miyanari, A. Bera, J.-M. Garnier, G. Guevara, M. Hestin, L. Kennedy, S. Hayashi, B. Drayton, T. Cherrier, B. Gayraud-Morel, E. Gussoni, F. Relaix, S. Tajbakhsh, O. Pourquié, Differentiation of pluripotent stem cells to muscle fiber to model Duchenne muscular dystrophy, *Nat. Biotechnol.* 33 (2015) 962–969. doi:10.1038/nbt.3297.
- [117] P.G. Constantinides, P.A. Jones, W. Gevers, Functional striated muscle cells from non-myoblast precursors following 5-azacytidine treatment, *Nature*. 267 (1977) 364–366. doi:10.1038/267364a0.
- [118] D.F. Pinney, C.P. Emerson, 10T1/2 cells: an in vitro model for molecular genetic analysis of mesodermal determination and differentiation., *Environ. Health Perspect.* 80 (1989) 221–227.
- [119] L.A. Muir, Q.G. Nguyen, S.D. Hauschka, J.S. Chamberlain, Engraftment potential of dermal fibroblasts following in vivo myogenic conversion in immunocompetent dystrophic skeletal muscle, *Mol. Ther. — Methods Clin. Dev.* 1 (2014) 14025. doi:10.1038/mtm.2014.25.
- [120] B.S. Carvalho, R.A. Irizarry, A framework for oligonucleotide microarray preprocessing, *Bioinforma. Oxf. Engl.* 26 (2010) 2363–2367. doi:10.1093/bioinformatics/btq431.
- [121] M.E. Ritchie, B. Phipson, D. Wu, Y. Hu, C.W. Law, W. Shi, G.K. Smyth, limma powers differential expression analyses for RNA-sequencing and microarray studies, *Nucleic Acids Res.* (2015) gkv007. doi:10.1093/nar/gkv007.
- [122] D.W. Huang, B.T. Sherman, R.A. Lempicki, Systematic and integrative analysis of large gene lists using DAVID bioinformatics resources, *Nat. Protoc.* 4 (2008) 44–57. doi:10.1038/nprot.2008.211.
- [123] F. Strutz, H. Okada, C.W. Lo, T. Danoff, R.L. Carone, J.E. Tomaszewski, E.G. Neilson, Identification and characterization of a fibroblast marker: FSP1., *J. Cell Biol.* 130 (1995) 393–405. doi:10.1083/jcb.130.2.393.
- [124] C.S. Trempus, R.J. Morris, C.D. Bortner, G. Cotsarelis, R.S. Faircloth, J.M. Reece, R.W. Tennant, Enrichment for living murine keratinocytes from the hair follicle bulge with the cell surface marker CD34, *J. Invest. Dermatol.* 120 (2003) 501–511. doi:10.1046/j.1523-1747.2003.12088.x.
- [125] T. Schepeler, M.E. Page, K.B. Jensen, Heterogeneity and plasticity of epidermal stem cells, *Development*. 141 (2014) 2559–2567. doi:10.1242/dev.104588.
- [126] R.I. Sherwood, J.L. Christensen, I.M. Conboy, M.J. Conboy, T.A. Rando, I.L. Weissman, A.J. Wagers, Isolation of Adult Mouse Myogenic Progenitors, *Cell*. 119 (2004) 543–554. doi:10.1016/j.cell.2004.10.021.
- [127] A. Wolnicka-Glubisz, W. King, F.P. Noonan, SCA-1+ Cells with an Adipocyte Phenotype in Neonatal Mouse Skin, *J. Gen. Intern. Med.* 20 (2005) 383–385. doi:10.1111/j.0022-202X.2005.23781.x.

- [128] K.J.L. Fernandes, I.A. McKenzie, P. Mill, K.M. Smith, M. Akhavan, F. Barnabé-Heider, J. Biernaskie, A. Junek, N.R. Kobayashi, J.G. Toma, D.R. Kaplan, P.A. Labosky, V. Rafuse, C.-C. Hui, F.D. Miller, A dermal niche for multipotent adult skin-derived precursor cells, *Nat. Cell Biol.* 6 (2004) 1082–1093. doi:10.1038/ncb1181.
- [129] C. Xu, M. Tabebordbar, S. Iovino, C. Ciarlo, J. Liu, A. Castiglioni, E. Price, M. Liu, E.R. Barton, C.R. Kahn, A.J. Wagers, L.I. Zon, A Zebrafish Embryo Culture System Defines Factors that Promote Vertebrate Myogenesis across Species, *Cell.* 155 (2013) 909–921. doi:10.1016/j.cell.2013.10.023.
- [130] A.J. Gibson, J. Karasinski, J. Relvas, J. Moss, T.G. Sherratt, P.N. Strong, D.J. Watt, Dermal fibroblasts convert to a myogenic lineage in mdx mouse muscle, *J. Cell Sci.* 108 (1995) 207–214.
- [131] C.J. Wise, D.J. Watt, G.E. Jones, Conversion of dermal fibroblasts to a myogenic lineage is induced by a soluble factor derived from myoblasts, *J. Cell. Biochem.* 61 (1996) 363–374. doi:10.1002/(SICI)1097-4644(19960601)61:3<363::AID-JCB4>3.0.CO;2-R.
- [132] J.G. Toma, M. Akhavan, K.J. Fernandes, F. Barnabé-Heider, A. Sadikot, D.R. Kaplan, F.D. Miller, Isolation of multipotent adult stem cells from the dermis of mammalian skin, *Nat. Cell Biol.* 3 (2001) 778–784. doi:10.1038/ncb0901-778.
- [133] P. García-Parra, N. Naldaiz-Gastesi, M. Maroto, J.F. Padín, M. Goicoechea, A. Aiastui, J.C. Fernández-Morales, P. García-Belda, J. Lacalle, J.I. Álava, J.M. García-Verdugo, A.G. García, A. Izeta, A. López de Munain, Murine Muscle Engineered from Dermal Precursors: An In Vitro Model for Skeletal Muscle Generation, Degeneration, and Fatty Infiltration, *Tissue Eng. Part C Methods.* 20 (2014) 28–41. doi:10.1089/ten.tec.2013.0146.
- [134] G. Shefer, M. Wleklinski-Lee, Z. Yablonka-Reuveni, Skeletal muscle satellite cells can spontaneously enter an alternative mesenchymal pathway, *J. Cell Sci.* 117 (2004) 5393–5404. doi:10.1242/jcs.01419.
- [135] A. Asakura, M.A. Rudnicki, M. Komaki, Muscle satellite cells are multipotential stem cells that exhibit myogenic, osteogenic, and adipogenic differentiation, *Differentiation.* 68 (2001) 245–253. doi:10.1046/j.1432-0436.2001.680412.x.
- [136] J.R. Beauchamp, L. Heslop, D.S. Yu, S. Tajbakhsh, R.G. Kelly, A. Wernig, M.E. Buckingham, T.A. Partridge, P.S. Zammit, Expression of CD34 and Myf5 defines the majority of quiescent adult skeletal muscle satellite cells, *J. Cell Biol.* 151 (2000) 1221–1234.

## Appendix A



a) 1. The main structure was made by casting and curing PDMS in a mold fabricated out of polycarbonate using a mill. The PDMS was removed and place on a thin layer of uncured PDMS spin coated on a silicon wafer. This thin layer would ultimately become the membrane for stretching the cells. 2. The PDMS was cured in an oven at 80°C for 1 hour. The excess

membrane was subsequently trimmed off. 3. The wall (also made of PDMS) for holding the media and glass slide for making the device sturdy were bonded to the main structure by plasma treatment. The surfaces were exposed to oxygen plasma and quickly pressed together. The assembled device was then baked at 80°C overnight. Oxygen plasma treatment rendered the otherwise hydrophobic PDMS surface hydrophilic. To preserve hydrophobic zones at the edges of the membrane so as to prevent cell suspension from flowing off during the initial cell seeding, tapes were placed to block out the oxygen plasma. 4. Upon application of vacuum, device could attain about 10% stretch. The membrane surface was coated with 0.25 mg/ml Matrigel for 30 mins before cell seeding. For static condition, cells were also seeded on a stretching device but no stretching was applied. **b)** Cyclical stretch was applied by applying house vacuum to the device periodically. To apply vacuum periodically, a function generator was used to control a relay switch, which in turn opened and closed a three way valve connecting the house vacuum to the device.

## Appendix B

### Formulas for polyacrylamide gel substrate

Acrylamide (%)	Bis Acrylamide (%)	Elastic Modulus (kPa)
4	0.08	1.2
4	0.17	4.3
4.9	0.21	15.5
5	0.3	21.3
6.5	0.28	30.9
8	0.4	62.1
10.5	0.45	108.6

Polyacrylamide gels were fabricated on 25 mm radius circular coverslips as described in Methods and Materials, without activation with EDC and NHS. The gels were soaked in PBS at 37 °C overnight. The next day, oscillatory shear measurements were performed on a rheometer (MCR300, Anton Paar, Ashland, VA) with a 25-mm radius parallel plate. Gap between plate and base was first zeroed with a clean coverslip in between to account for the thickness of the coverslip. A humidity chamber was placed around the sample to prevent dehydration. The temperature of the base was set to 37°C, and frequency sweep from 0.001–10 Hz at 5% strain was performed. The elastic modulus,  $E'$ , was estimated as  $E' = 2G'(1 + \nu)$ , where  $G'$  is the complex storage modulus at 1 Hz as measured by the rheometer and  $\nu$  is the Poisson's ratio, assumed to be 0.5.

Formulas highlighted in grey were subsequently used for our experiments.